AD-766 141

RESEARCH ON THE PROPERTIES OF AMORPHOUS SEMICONDUCTORS AT HIGH TEMPERATURES

ENERGY CONVERSION DEVICES, INC.

PREPARED FOR
ADVANCED RESEARCH PROJECTS AGENCY

JUNE 1973

FINAL TECHNICAL REPORT

Contract DAHC15-70-C-0187

RESEARCH ON THE PROPERTIES OF AMORPHOUS SEMICONDUCTORS AT HIGH TEMPERATURES

Prepared by: Energy Conversion Devices, Inc.
1675 W. Maple Road
Troy, Michigan 48084

For: Advanced Research Projects Agency
[Order No. 1570; Program Code 0D10]

Contract Period: 18 May 1970 to 18 May 1973

Total Contract Price: $976,786

J. P. deNeufville
Program Technical Manager
313-549-7300

Copy No. 7

Hoff

Unclassified

Security Classification

i

DOCUMENT CONTROL DATA - R&D

(Security classification of title, body of abstract and indexing annotation must be entered when the overall report is classified)

1 ORIGINATING ACTIVITY (Corporate author) Energy Conversion Devices, Inc., 1675 West Maple Road, Troy, Michigan 48084	2a. REPORT SECURITY CLASSIFICATION Unclassified 2b GROUP N/A

3. REPORT TITLE

RESEARCH ON THE PROPERTIES OF AMORPHOUS SEMICONDUCTORS AT HIGH TEMPERATURES

4 DESCRIPTIVE NOTES (Type of report and inclusive dates)

Final Technical Report - 18 May 1970 to 18 May 1973

5 AUTHOR(S) (Last name, first name, initial)

deNeufville, John P.

6. REPORT DATE 18 June 1973	7a. TOTAL NO. OF PAGES ~~115~~ 2 68	7b. NO. OF REFS 70
8a. CONTRACT OR GRANT NO. DAHC15-70-C-0187 b. PROJECT NO. 1601/36 c. d.	9a. ORIGINATOR'S REPORT NUMBER(S) 516-6 9b. OTHER REPORT NO(S) (Any other numbers that may be assigned this report) None	

10 AVAILABILITY/LIMITATION NOTICES

The distribution of this report is unlimited

11. SUPPLEMENTARY NOTES	12 SPONSORING MILITARY ACTIVITY Advanced Research Projects Agency Arlington, Virginia 22209

13 ABSTRACT

In the course of these investigations we have prepared over 460 amorphous semiconducting alloys. The thermal, optical and transport properties of many of these alloys have been investigated in great detail. Special emphasis has been placed on the preparation and examination of amorphous phases which cannot be prepared by conventional glass-forming methods. This approach has enabled us to determine many of the general relationships between structure (chemical bonding) and properties (thermal, optical and transport) within the entire family of covalently bonded amorphous semiconducting (A.S.) alloys. This was our major goal.

A second major accomplishment was the recognition that the average number $\bar{N}$ of outer electrons per atom or network connectedness C, defined as $C = 8 - \bar{N}$, governs the thermal stability of A.S. alloys. Covalently bonded A. S. glasses can be formed for $2 \leq C \leq 4$, and within this range of C T_g increases with C for fixed covalent bond strength or optical band gap. However, as $C \rightarrow 4$, the ease of glass formation is drastically reduced, so that fabrication of large samples of the most stable high temperature glasses is impeded. For chalcogenide systems, the practical limit of C for which easy glass-formation is possible appears to be $C = 3$, but in the Cd-Ge-As system bulk $C = 4$ glasses can be formed.[1]

In order to reproducibly prepare thin films of multicomponent amorphous

(continued...)

DD FORM 1 JAN 64 1473

Unclassified

Security Classification

14. KEY WORDS	LINK A		LINK B		LINK C	
	ROLE	WT	ROLE	WT	ROLE	WT
Amorphous Semiconductors Amorphous Materials Chalcogenide Materials High temperature device materials						

alloys, we utilized the r.f. sputtering technique. Many deposition variables must be controlled in this process, so that extensive studies were performed to characterize the various effects of these deposition variables. In particular, substrate temperature and dc substrate bias were extensively examined. The effect of substrate bias and temperature on film stoichiometry and the effect of substrate bias on argon content were monitored.

While the alloys with $C \rightarrow 4$ appear to have the highest thermal stabilities, we have found that the most interesting electronic and structural transformations occur for alloys with $C \approx 2 - 2.66$. These studies relate to the application of A.S. layers for information storage and as active electronic devices such as Ovshinsky threshold switches. The chalcogen lone pair electrons which constitute the valence band for this subgroup of A.S. alloys[2] play a significant role in producing the electronic excitation involved in threshold switching, and the bond-switching involved in photostructural transformations.[3] These excitations occur under conditions which do not permit the major structural rearrangements which would be required for crystallization to occur. In contrast to those subtle changes, crystallization of Te accompanies electronic switching[4] intense optical pulsing[5], and electron beam exposure of Te-rich memory alloys.

References

1. L. A. Cervinka et al., J. Non-Crystalline Solids 4 (1970) 258.

2. M. Kastner, Phys. Rev. Letters 28 (1972) 355.

3. S. R. Ovshinsky and K. Sapru, Fifth Intl. Conf. on Amorphous and Liquid Semiconductors, Garmisch-Partenkirchen, September 1973.

4. R. G. Neale and J. A. Aseltine, IEEE Trans. Electron Devices ED-20 195 (1973); M. H. Cohen, R. G. Neale and A. Paskin, J. Non-Crystalline Solids 8-10 (1972) 885.

5. J. Feinleib, J. P. deNeufville, S. C. Moss and S. R. Ovshinsky, Appl. Phys. Letters 18 (1971) 254; J. Feinleib, S. Iwasa, S. C. Moss, J. P. deNeufville and S. R. Ovshinsky, J. Non-Crystalline Solids 8-10 (1972) 909.

TABLE OF CONTENTS

1. INTRODUCTION AND SUMMARY OF MAJOR ACCOMPLISHMENTS

1.1 Introduction

This research program has addressed the factors which control the behavior of chalcogenide amorphous semiconducting (A.S.) alloys at elevated temperatures. While primary emphasis has been placed on achieving a fundamental understanding of the structure-property relationships which govern high temperature behavior, technological considerations have guided to some extent the choice of topics. A.S. alloys have been used for electrical switching[1] and memory[2] applications, optical recording[3], optical lenses, windows[4] and filters, and a wide variety of additional applications. Thus we have related alloy structure to technologically relevant properties such as optical absorption and electronic transport behavior, including switching. Furthermore, inasmuch as most of these technological applications require thin films, we have prepared many of our samples as thin films, using both rf sputtering and thermal evaporation techniques. These deposition techniques introduce a wide variety of new variables which must be specified, and a significant portion of our research effort has been directed towards the relationship between deposition parameters and film structure and properties.[5,6] Finally, information storage applications of A.S. films, whether the information is introduced electrically,[2] optically,[3] by electron-beam, or in other fashion, involves structural transformations and utilizes the property differences thereby produced for read-out. Thus the thermal crystallization

kinetics and the structure-property relationship of A.S. "memory" alloys fall within the scope of the present Research Program, and several such examples have been carefully characterized in these respects.[9] Other transitions, including the electronic transformation involved in threshold switching[7,8] and the photostructural transformations which have been studied in two alloy systems,[10] occur without involving any crystallization.

Our research on the Properties of Amorphous Semiconductors at Elevated Temperatures ~~can therefore~~ be organized into three broad topics: (1) Glassy alloy studies, including both survey studies and detailed composition-property studies in a few selected systesm. Much emphasis in these studies has been placed on the correlation of thermal, electrical, and optical data in understanding chemical bonding and the associated band level structure in amorphous chalcogenide alloy systems; (2) The role of deposition techniques in controlling thin film composition, structure and properties with special emphasis on the roles of argon entrapment and substrate bias during the r.f. sputter deposition of amorphous chalcogenide alloys; (3) Studies of controlled changes in conductivity, refractive index, or absorption, produced electrically, optically or thermally in Ovonic threshold and memory alloys. Subtopics of emphasis within this broad topic include various studies of the mechanism of threshold switching, studies of the thermally induced crystallization of electrical memory alloys and studies of the photostructural changes in amorphous holographic media.

All of these topics have been introduced in the five earlier Semi-Annual Technical Reports under this Contract, and each has already been covered by one or more publications. This report contains in Appendix I the entire list of publications and anticipated publications which have resulted from this research program. In Appendix II are reproduced five of these manuscripts which have not yet been published. The main body of the present report contains some additional unpublished results concerning Topic (1), glassy alloy studies, and also includes an extensive overview of the structure-property relationships for A.S. alloys.

1.2 Summary of Major Accomplishments

In the course of these investigations we have prepared over 460 amorphous semiconducting alloys. The thermal, optical and transport properties of many of these alloys have been investigated in great detail. Special emphasis has been placed on the preparation and examination of amorphous phases which cannot be prepared by conventional glass-forming methods. This approach has enabled us to determine many of the general relationships between structure (chemical bonding) and properties (thermal, optical and transport) within the entire family of covalently bonded amorphous semiconducting (A.S.) alloys. This was our major goal.

A second major accomplishment was the recognition that the average number $\overline{N}$ of outer electrons per atom or network connectedness C, defined as $C = 8 - \overline{N}$, governs the thermal stability of A. S. Alloys. Covalently bonded A.S. glasses can be formed for $2 \leq C \leq 4$, and within this range of C Tg increases with C for fixed covalent bond strength or optical band gap. However, as $C \rightarrow 4$, the ease of glass formation is drastically reduced, so that fabrication of large samples of the most stable high temperature glasses is impeded. For chalcogenide systems, the practical limit of C for which easy glass formation is possible appears to be $C = 3$, but in the Cd-Ge-As system bulk $C = 4$ glasses can be formed.[27]

In order to reproducibly prepare thin films of multicomponent amorphous alloys, we utilized the r.f. sputtering technique. Many deposition variables must be controlled in this process, so that extensive studies

were performed to characterize the various effects of these deposition variables. In particular, substrate tmperature and dc substrate bias were extensively examined. The effect of substrate bias and temperature on film stoichiometry and the effect of substrate bias on argon content were monitored.

While the alloys with $C \rightarrow 4$ appear to have the highest thermal stabilities, we have found that the most interesting electronic and structural transformations occur for alloys with $C \approx 2 - 2.66$. These studies relate to the application of A.S. layers for information storage and as active electronic devices such as Ovshinsky threshold switches. The chalcogen lone pair electrons which constitute the valence band for this subgroup of A.S. alloys[42] play a significant role in producing the electronic excitation involved in threshold switching, and the bond-switching involved in photostructural transformations.[57] These excitations occur under conditions which do not permit the major structural rearrangements which would be required for crystallization to occur. In contrast to those subtle changes, crystallization of Te accompanies electronic switching,[2] intense optical pulsing,[3] and electron beam exposure of Te-rich memory alloys.

2. GLASSY ALLOY STUDIES

2.1 Introduction

Studies of glassy alloys represent the primary emphasis in this Research Program, and thus dominate the Final Report. In studies described in earlier Technical Reports or listed in Appendix II as preprints in the present report, we have taken alloy composition as the primary experimental variable, monitoring the changes in thermal, electrical and optical properties as composition is changed in some systematic fashion. The goal of this approach has been to assess the role of all the conceivable experimental parameters which determine the structural state of an amorphous phase by manipulating these parameters indirectly via the composition, and then to establish predictive principles in correlating the known structural state with its measured properties. These alloys are for the most part covalently bonded, so that the concept of covalency satisfaction[11] has been useful in establishing structural models which can then be tested by noting how properties vary with composition.

2.1.1 Summary and Structural Concepts

The basic structural chemical information which one requires is the concentration of possible covalent chemical bond types, and the spatial distribution of these bond types. This information more or less establishes the short range structural order and determines whether the amorphous phase is homogeneous or phase separated. Various additional structural parameters must also be specified, such as the concentration of nonequilibrium atomic

defects (vacancies, "dislocations", voids, bond strains, etc.), the molecular constituency (polymer-monomer ratio, polymer chain length) and the concentration of nonequilibrium electronic defects (broken bonds, trapped charges). We have used the concept of chemical ordering as a constant reference point throughout these studies, having anticipated such ordering effects in multicomponent chalcogenide alloys in our initial proposal.[12] The discovery of such ordering tendencies[13] substantially reduced the complexity of examining and analyzing these alloy systems, and permitted the identification of a handful of structural prototypes which serve as the conceptual basis for analyzing very complex systems. In a very real sense, every homogeneous covalent glass is a chemical compound with a structure which, at least in principle, can be established with relative precision. In order to analyze the general case we need to have in mind a series of structural prototypes to which we can refer an unknown structure for comparison. The glassy compounds we have chosen to represent these structures are relatively well characterized, at least in the sense that all the prototypes have a single covalent chemical bond type and thus are demonstrably single-phase and chemically ordered. In this sequence of prototype alloys we span the entire range of covalently bonded inorganic polymers from the viewpoint of connectedness, C, which is defined as the average number of network connections per atom.

Connectedness of a polymeric network can vary from 2 to 4. The lower limit of two is given by the requirement that an infinitely extendable structure

must have two connections for each unit member: a chain is the minimally connected network. The 8-N rule, where N is the number of valence electrons, establishes the coordination number, which for covalent networks correspond to the connectedness. Thus the chalcogens, S, Se, and Te with N = 6 have the minimum connectedness of 2 and can form one-dimensional polymer chains. S and Se tend to have an equilibrium fraction of S_8 or Se_8 monomer rings in the amorphous state, and thus are not maximally polymerized. We shall therefore use Te as the prototype of a 2-connected A.S. polymer.

The upper limit of connectedness of a covalent network is set a 4 because the 4 pairs of electrons per atom thereby produced fill the entire 8 s and p valence states per atom. By the 8-N rule this gives N = 4 for C = 4, corresponding to column IV of the periodic table. Si and Ge are well known to form this maximally connected network, and this limiting structural prototype has been well characterized experimentally[14] and theoretically.[15] The entire sequence of structural prototypes and the connectedness which they describe is listed below:

C	N	Materials	Comments and Reference
2	6	Te	1 dim. chain polymer[16]
2.4	5.6	As_2S_3	2-connected S and 3-connected As[17]
2.666	5.333	GeS_2	2-connected S and 4-connected Ge[18]
3	5	As	(Krebs and Steffen)[19]
4	4	Ge	(Schevcik)[20]

The C = 2 structure is so intuitively analogous to the myriad carbon-based polymers as to require little further elaboration in terms of structural description. While the structural details, such as chain length and inter-chain bonding configurations, may be poorly established, the topology of intertwined chains is familiar. The chalcogens apparently form copolymer chains, at least in the Te-Se system, but the introduction of much Se or S adds the possibility of copolymer rings to complicate the structure.[21]

The C = 2.666 structure for GeS_2 is probably the next most familiar, occuring for vitreous SiO_2 and having been modeled and studied in that manifestation for over 40 years.[22] This simple structure has C = 8/3, because one third of the atoms are four-connected (Ge) and one third are two-connected (S). The topology of the 4-connected Ge structure can be directly obtained from the topology of the 2.666 connected GeS_2 structure by removing the S atoms and reconnecting the Ge atoms to each other. It turns out that this is exactly the topological relationship between the familiar SiO_2 (or GeS_2) "random network" structure and the Ge "Polk-Turnbull" model for describing the structure of tetrahedrally connected Ge and Si, and that, in these two cases, the experimentally determined RDF's are in excellent agreement with the model predictions.

The C = 3 structure prototype, arsenic, has been much less well characterized than the C = 2, C = 2.66 and C = 4 structures, perhaps because of the difficulty of constructing a three-dimensional model of a structure which is locally <u>two</u>-dimensional. The RDF analysis[19] indicates for arsenic three

nearest neighbors at the covalent distance, and a next-neighbor shell at approximately a van der Waals distance. However, the topological relationship which connects these local environments together to create the "long-range order" which actually specifies all the non-local features of the RDF is not yet known.

By analogy to the relationship between GeS_2 and Ge, there exists in principal a one-to-one relationship between the C = 3 structure and the C = 2.4 structure, whereby S atoms can be introduced between each pair of covalently bonded As atoms without affecting the relative topology of the As atoms. Of course As remains 3-connected, which is experimentally demonstrable in a number of ways in As_2S_3, while S is demonstrably 2-connected.[17] Since detailed models exist for neither structure, it is not clear whether this geometrical transformation correctly describes the relationship between these two structural types, but at this stage of analysis it must certainly be taken as the least complicated hypothesis.

Our five prototype amorphous covalent network structures obey several simple rules which can be summarized for clarity at this point before we proceed to analyze more complicated alloys in terms of these structures:

1. They are either elemental (Te, As, Ge) or perfectly ordered chemically (GeS_2, As_2S_3) and thus each can be constructed using a single covalent bond type.

2. They are covalently bonded in the sense that each atom has a full shell of electrons, and thus each chemical bond contains a pair of electrons.

3. The coordination number for each atom is given by the 8-N rule for that atom, i.e., the covalent bonds are classical in the sense that (for these five structures) they are all constructed with a pair of shared electrons, one electron originating from each partner of the covalent bond.

The domination of the third rule above leads in certain alloy systems to a very simple interpretation of the structure as a function of composition. For example, in the As-Se and Ge-Se systems, if we ignore the Se_8 ring component, the role of As and Ge as each is added to pure Se involves the introduction of chain branching points (As) or chain cross-linking points (Ge). Since the chemical ordering tendency which is complete at $GeSe_2$ and As_2Se_3 is already present for dilute As or Ge alloys, one need not consider the possibility of As-As bonds or Ge-Ge bonds in these concentration limits. Thus the progression from C = 2 to C = 2.4 (Se-As_2Se_3) or from C = 2 to C = 2.666 (Se-$GeSe_2$) is well characterized in terms of a gradation from one structure prototype to the other. While this analysis ignores the long range topological considerations and the possibility of such alloy sequences separating, under certain circumstances, into two phases which may approach the structural prototype end members in composition, it certainly provides a first level of understanding of the structure-composition relationship for such systems.

However, the applicability of the foregoing rule 3 to other more complex alloy systems is clearly limited, and an alternative rule involving the average value of N, $\bar{N}$, where $\bar{N} = \Sigma X_i N_i$ and X_i is the fraction of i atoms, can be shown to apply in certain circumstances. Borrowing now from the much more extensive

experience with crystalline materials,[23] and focusing attention on alloys which have $\bar{N} = 4$, we find many examples where the connectedness or coordination number is given by $C = 8-\bar{N}$ rather than $C = 8-N$ for each individual atom. Examples of such behavior abound: ZnS, CdTe, GaAs, ZnO, $CdGeAs_2$ etc.[24]

A few of these $\bar{N} = 4$ structures have been studied in the amorphous phase (GaAs,[25] CuAsSe alloys,[26] $CdGeAs_2$[27] etc.) and all appear to retain the short range order of their respective crystals, i.e., $C = 8-\bar{N}$ rather than $C = 8-N$. The bonding in these materials can be viewed as a generalized form of covalent bonding in the sense that each bonded atom contains a full shell of valence electrons, obtained in part by sharing adjacent electrons, and that each chemical bond contains a pair of electrons. However, the parentage of these shared electron pairs does not obey the classical rule for covalent bonding, for the electron-rich atoms such as the chalcogens supply more than their classical share of shared electrons. Of course all of the final electron wave-functions are hybridized to yield the appropriate geometrical distribution, so that the parentage for a particular bonding electron is meaningless. But in these maximally connected covalent structures all the valence electrons are shared (there are no lone pairs), so that on the average each atom contributes $N/4$ electrons to each bond, where N is its number of valence electrons in the atomic state.

The question which now arises in examining the structure-composition relationship for any complex A.S. alloy system is whether the $8-N$ or the

$8-\bar{N}$ rule determines the local coordination environment for an individual atom. This central question has been discussed with respect to many of the binary and ternary alloys we have examined, especially in the case of GeTe, which has $\bar{N} = 5$, like As, but which may have the C = 3 arsenic structure or a mixture on a local scale of the C = 2.666 $GeTe_2$ structure and the C = 4 Ge structure.

Although the structure-composition relationship lies at the heart of any composition-property relationship, other categories of structural information are required to complete the description of the structural state of an amorphous alloy, as enumerated below:

1. The role of chemical ordering. The recognition of chemical ordering effects extends the covalency satisfaction model of Mott,[11] by analysing the relative concentrations of possible covalent bond types which are established by short-range chemical ordering effects. Such ordering is nearly complete at certain stoichiometrics (e.g., $GeTe_2$,[13] $GeSe_2$,[28] As_2Se_3,[17] As_2S_3[29]) for well annealed amorphous phases. Chemical ordering is a universal feature of the $8-\bar{N}$ = C = 4 group of crystalline alloys, and thus, by inference, must be essential for the analogous amorphous alloys as well. All the examples cited previously contained equal concentrations of electropositive and electronegative elements, i.e., GaAs, $CdGeAs_2$, etc., permitting complete chemical ordering of the more positive and the more negative elements on separate lattices, and enhancing the ionic contribution to bonding. While compounds like $CdAs_2$ which have $\bar{N} = 4$ must

form bonds between like atoms (As-As) to have C = 4, such compounds are less common due to the diminished ionic stabilization of the structure. An important question regarding the structure of the amorphous analogues of the ordered crystalline $\bar{N} = 4$ alloy concerns the degree to which the chemical order can be preserved as long range atomic order is lost. For example it is not possible to completely order Ga and As in the Polk-Turnbull model due to the presence of 5-membered rings.[25]

2. The role of phase separation. This question involves the distribution of the chemical bonds. Of course if chemical ordering causes only a single bond type to occur as in the case of GeS_2, As_2S_3, or, perhaps, GaAs, then the possibility of phase separation is clearly excluded. On the other hand if chemical ordering tends to favor the formation of certain sets of chemical bonds and the exclusion of others, this may prohibit attainment of homogeneity, as exemplified by the $GeSe_2$-Te alloys considered in the Fourth Semi-Annual Technical Report. The obvious rule for creating an amorphous covalently bonded multi-component homogeneous alloy (an amorphous compound by previous definition) is to equalize the bonding tendency between all pairs of atoms, so that one type of bond is not favored above all others. This is of course the same criterion for the formation of multi-component crystalline compounds, a rule which can be expressed in terms of the electronegativities of the component atoms.[30] We shall see in later discussions some examples where amorphous alloy formation is restricted by the application of this rule.

Phase separation which is based on chemical ordering has been termed "primary phase separation" in the Fourth Semi-Annual Technical Report (ref. 32, p.6), because it is a topological consequence of the requirement for formation of the lowest energy set of covalent bonds. However, many real cases of phase separation which we have observed cannot be accounted for on this basis, because the concentration of bond types in the separated alloy is the same as could be obtained in a homogeneous version of the same composition. An example of this effect is the As_2S_3-As_2Te_3 pseudobinary system. Here the two bond types, As-S and As-Te which are predicted on the basis of chemical ordering effects can coexist with each other in any concentration and yet the two end-member phases tend to separate from each other in nearly the entire concentration range. This effect wich we shall term "secondary phase separation", is analogous to the size effect rule for metallic alloy solid solutions. A positive heat of mixing is introduced if the geometries of the species to be mixed together (As-Te and As-S bonds, in this case) are sufficiently dissimilar.

3. <u>The role of molecularity versus network connectedness</u>. Here we are concerned with a question which is independent of the connectedness per atom or the concentration of bond types, but is very relevant for understanding the complete structure of the amorphous alloy. For example, pure Se contains rings and chains, and its properties very much reflect the presence of both.[21] However, its RDF is relatively insensitive to this structural distinction, because the nearest (Se-Se covalent bonds) and

next-nearest (van der Waals bonds) neighbors are fixed by chemical considerations which apply equally to both molecular species (rings and chains), and the RDF technique is relatively insensitive to the long range topological parameters which would distinguish a pure ring glass from a pure chain glass.

It is often convenient to ignore this problem, and assume that it is confined to Se-rich and S-rich glasses. However, we have shown[31] that these effects can be very important in controlling the properties of films evaporated under certain conditions from a vapor stream containing molecular entities, such as As_4S_6 molecules. A metastable molecular glass can be so produced whose structure and properties differ completely from the more stable fully cross-linked (i.e., fully polymerized) glass. Here the concept of connectedness loses its usefulness, because the As_4S_6 molecular glass has the same (C = 2.4) connectedness per atom as the fully polymerized version of the same composition. We shall refer to "network-connectedness" to describe the topology of the fully polymerized version of a given alloy, recognizing that under some conditions (equilibrium or otherwise) the topology of the actual glassy structure may be less connected than expected.

4. <u>The role of defects</u>. This is a particularly important topic in understanding the properties of amorphous films. Two cases have been observed and described by us in the course of these studies.

1. Alloys which are deposited near T_g, (e.g., the low T_g electrical

memory alloy $Te_{81}Ge_{15}Sb_2S_2$, Se, etc.) or can be annealed to T_g without causing crystallization (Te-rich Ge-Te alloys up to $GeTe_2$, Ge-Se alloys between Se and GeSe, etc.). These alloys can be fully annealed to achieve properties which are usually indistinguishable from those measured on alloys of the same composition produced by other techniques, including cooling of the liquid.

2. Alloys for which $T_g > T_x$, and which thus crystallize below T_g. For these alloys, including the Ge and the Ge-rich portions of the Ge-Te and Ge-Se systems, T_g is not an observable quantity, and it is not possible to ensure that a given annealing treatment below T_x achieves metastable homogeneous equilibrium at that temperature.

These defect effects include many structural effects listed under classes 1-3 of structural parameters described above, such as "wrong" chemical bonds, homogeneity and even molecularity, since all of these properties can be affected by the annealing near T_g of an amorphous film deposited well below T_g (i.e., more than $75^{\circ}C$ below T_g). Annealing near T_g is presumably sufficient to assure attainment of metastable homogeneous equilibrium at the annealing temperature, so that the properties of glasses so annealed depends only on the subsequent thermal history. Thus annealing, in principle, wipes out all memory of the deposition conditions. An alloy which normally phase separates upon cooling from the liquid can be prepared as a

homogeneous amorphous film by rf sputter deposition, e.g., $Ge_{20}Se_{40}Te_{40}$ as described previously.[32] Also, "wrong" bonds may be largely responsible for the properties of unannealed rf sputtered $GeSe_2$-$GeTe_2$ films as described by reference 4 in Appendix II to this Report. And, finally, the thermally induced structural changes of evaporated As_2S_3 and As_2Se_3 films[31] involve, in the same sense, the removal of structural defects, if the molecular constituents present in these films can be regarded as defects.

2.1.2. Summary of Properties Studied: Definitions and Relevance

All of the properties which were systematically examined for a large number of amorphous chalcogenide alloys under this program can be classified into two groups: 1. Thermal properties, including glass transition temperature, T_g, and crystallization temperature, T_x, and 2. Optical and transport properties, including optical absorption, α, electrical conductivity, σ, versus temperature, and thermoelectric power, S, versus temperature. Many other properties in these two broad categories were measured for specific alloys, including density, thermal conductivity, enthalpy photoconductivity, optical absorption versus temperature and pressure, etc. In this section appear references to the definitions and experimental determination of these five most studied properties, T_g, T_x, α, σ and S, and of the various parameters which are derived from them. In addition each of these key properties is examined in terms of its physical and practical significance.

2.1.2.1. Thermal Properties

The key thermal properties which we have investigated in a wide variety of bulk and thin film amorphous semiconducting alloys are the glass transition temperature, T_g, and the thermal crystallization temperature, T_x. Both properties were measured only by differential scanning calorimetry (D.S.C.) at a scanning rate of 20 deg min^{-1}. T_g is the temperature at which the calorimeter output, which is proportional to C_p, attains the value half-way between the glassy value below T_g and the liquid value above T_g as the temperature is scanned through T_g at 20 deg min^{-1}. Lower

scan rates result in lower values for T_g, because of thermal lag effects associated with scanning, and, in some cases, because the value of T_g itself is sensitive to the time scale of the measurement. The former effect depends only on sample size and thermal conductivity, and tends to raise the measured value of T_g 5-10°C with respect to the actual value for typical materials and sample sizes. The latter effect, which is also sensitive to prior heat treatments, can introduce an additional 5-10°C correction term.

T_x is the temperature at which the calorimeter output begins to deviate in an exothermic manner from the steady-state glass or liquid value. For materials which have $T_x > T_g$, the identification of T_x is usually unambiguous, because crystallization occurs relatively suddenly and involves a large exothermic effect. Occasionally T_x approaches T_L, the beginning of melting or solidus temperature, which can reduce the crystallization tendency to the point where T_x is poorly defined. In the limit, of course, T_x is undefined because an alloy can be heated throughout the entire region of liquid metastability from T_g to T_L, the end of melting or liquidus temperature, without nucleating any crystals.

For materials which have $T_x < T_g$, crystallization preceeds any glass transition as the amorphous sample is heated. Such amorphous materials can only be prepared by evaporation, sputtering or other thin-film deposition process, and thus tend to undergo exothermic reactions upon heating which are associated with the removal or redistribution of various defects, and

which preceed crystallization. The onset of the crystallization exotherm occurs during the defect removal exotherm, so T_x is identified by a break in the slope of the calorimeter output rather than by the beginning of the exotherm itself.

T_g is a fundamental parameter which defines the onset of diffusive motions in amorphous solids. These motions, in turn, lead to the increased values of fluidity, heat capacity and thermal expansion which serve to characterize the liquid state. Because crystallization of an amorphous alloy usually involves diffusion, T_g for such alloys sets a lower limit on the possible values for T_x.[33] Conversely, it would appear that crystallization must occur without diffusion for those alloys for which $T_x < T_g$. Further study of this class of alloys will be required to verify this inference

From a practical standpoint, T_g and T_x, taken together, provide an index of the thermal stability of amorphous alloys at elevated temperatures. Other factors can limit thermal stability, such as chemical reactivity, sublimation, "cold flow" below T_g, etc. Therefore, the suitability of a particular alloy for use at elevated temperatures is dependent on many properties in addition to T_g and T_x. Furthermore, some high temperature applications for amorphous semiconductors permit[34] or even require[35] the material to be above T_g. Nonetheless, T_g and T_x, measured at a fixed temperature scanning rate, provide an easily attainable and extremely useful preliminary index of thermal stability.

2.1.2.2 Optical and Transport Properties

An excellent review of the behavior and significance of the optical constant α and the transport parameter σ and S for amorphous semiconductor materials is contained in the Mott and Davis text.[36] A brief summary of some salient features of these properties is provided below.

Knowledge of the optical constants as a function of photon energy provide a wealth of information concerning the electronic band structure and the optical phonon spectrum. Most optical studies of amorphous semiconductos have emphasized the dependence of the absorption coefficient α upon photon energy $\hbar\omega$ in the vicinity of the optical absorption edge, and only a few complete determinations of both, ϵ_1 and ϵ_2 over an extended range of photon energy[37,38] have been performed.

Near the absorption edge itself, where we have performed the majority of our studies, the two important experimental variables are the position and the shape of the edge. We arbitrarily define the optical gap E_{O4} as the energy E_{O4} at which $\alpha = 10^4 cm^{-1}$. E_{O4} is of universal interest in these studies because it characterizes the energy gap at a joint density of states corresponding roughly to the C.F.O[39] mobility gap,[40,41] and thus can be closely related to the transport parameters σ and S. Since the density of states pseudogap is also closely related to the chemical bonding through the separation between valence band non-bonding (lone pair) or bonding states and conduction band antibonding states,[42] the value of E_{O4} is also a scaling parameter for covalent bond strength. Covalent bond strengths can also be calculated from thermochemical data if the atomic coordination

is established, so that a close connection exists between E_{O4} and the thermodynamic properties of amorphous semiconductor elements, compounds and alloys. We have therefore emphasized E_{O4} as a useful optical parameter, easily measurable on the 1-5 μm sputtered films used for σ and S characterization.

The shape of the edge can be expressed either as A, the slope of log α vs $\hbar\omega$ which is usually constant for log $\alpha \leq 3$, or as B, the slope of $\sqrt{\alpha\hbar\omega}$ vs $h\omega$ which is usually constant for $3 \leq \log \alpha \leq 5.5$. A and B vary little with composition or annealing history for most chalcogenide glasses,[36] whereas the amorphous tetrahedral elements[43] and alloys[44] can have values of A which are exceedingly sensitive to preparation method[45] and annealing history.[46] A becomes interesting for specific chalcogenide systems such as Ge-Te[47] and $GeSe_2$-$GeTe_2$[48] where its compositional dependence hints at changes in the shape of the pseudogap.

The transport properties which we have emphasized are the dc conductivity σ and the Seebeck coefficient S, both of which have been extensively measured as a function of temperature in these studies. Most amorphous chalcogenide alloys including sputtered films have nearly linear log σ vs 1/T plots both in the unannealed state and after annealing to an elevated temperature just below T_x. To the extent that the conductivity obeys this simple relationship:

$$\sigma = \sigma_o \exp(-\Delta E_o/kT)$$

we generally consider that conduction is occurring in the extended states in the vicinity of one mobility shoulder with a relatively constant mobility contained in σ_o. This picture is confirmed when the slope of eS/k vs 1/T closely approximates ΔE_o. The sign of S under these conditions which is positive for tellurium-rich alloys and can be negative for As or Se-rich alloys indicates which mobility shoulder lies closer to the Fermi level E_F.

Exceptions to this general behavior can occur when the Fermi level is so situated that valence and conduction bands make roughly comparable contributions to the conductivity, or when the density of localized states at the Fermi level is so great that conduction takes place primarily by hopping. Both situations lead to a thermopower which is small in magnitude and whose temperature dependence is less than the apparent activation energy ΔE_o.[49] Additionally, the former situation can give rise to a thermopower which varies continuously through zero with heat treatment.

Other transport parameters, in particular the a.c. conductivity[50] and the photoconductivity,[51] provide further information concerning the density of states and mobility functions. These parameters have been carefully analyzed[52,53] and utilized to expand the knowledge of electronic transport in a few selected cases.

2.1.3 Emphasis and Summary of Experimental Results.

The emphasis of the glassy alloy studies has been directed on the one hand to the preparation and preliminary characterization of a wide range of amorphous semiconducting alloys and on the other hand to the thorough characterization of a much more restricted range of carefully chosen prototypical compounds, alloys, and systems. The procedure for thorough characterization involved in addition to the standard T_g and T_x thermal measurements, the measurement of optical absorption, α, electrical conductivity, σ, and thermoelectric power, S. σ and S were measured versus temperature throughout the experimentally accessible temperature range, which was limited at the lower end by the tolerable source impedance of our instrumentation and at the upper end by crystallization or by mechanical failure of the thin-film sample.

The summary of alloys investigated under this program is contained in Section 2.2 and tends, at first examination, to emphasize the preliminary survey studies due to the numerical predominance of alloys in this category. However the "Properties Measured" column in Table 2.1 serves to identify all of those alloys examined in detail, which, though numerous, constitute a relatively small proportion of the total number of alloys synthesized in the course of the program.

The preliminary results of the thermal, optical and transport investigations of the specifically selected prototype compounds, alloys and systems have been presented in the first four Semi-Annual Technical Reports,

most especially in the Third and Fourth of these Reports. More of these results are included in Section 2.3 of the present report. The complete list of publications and publications in preparation concerning this topic is given in Appendix I of this report.

2.2 Summary of Alloys Investigated Under this Program

This section briefly describes the overall strategy of this program from a materials point of view. We began with a largely empirical perspective, bearing in mind the role of chemical ordering in determining short range order in complex alloys but without attempting to describe in complete detail the atomic and electronic structure as a function of composition. We certainly believed that most A.S. alloys could not be produced by normal or even rapid spray-quenching[54] of the liquid, so that an integral component of our approach to the subject was to develop reproducible techniques for fabricating a wide range of alloy compositions in the amorphous state via rf sputter deposition.

As these studies progressed it emerged that a good measure of structural information could be determined indirectly by the various thermal, optical and electronic property measurements we were making. We therefore chose to examine in detail a few selected simple binary and ternary systems, establishing structure-property relationships for them as a guide to other systems. We also selected a few binary and ternary alloy compositions representing well known or potentially analyzable structural prototypes, and measured this thermal, optical and electronic properties in order to draw some preliminary conclusions regarding structure-property relationship in their parent binary or ternary systems.

Thus, rather than continue the composition-property measurements on the many alloy systems which we began as the first stage of this materials investigation, we chose instead to characterize the thermal, optical and electronic properties of prototypical alloy compositions (As_2S_3, As_2Se_3, GeSeAs, GeTeAs, etc.) binary systems (Ge-Te, Ge-Se), pseudobinary systems ($GeTe_2$-$GeSe_2$, GeAsTe-GeAsSe) and ternary systems (Ge-Se-Te) which typified, to a first approximation, the range of behavior observable in the multicomponent alloys. One surely must depart from the elemental and compound A.S. materials in order to witness many of the interesting and useful complexities of these alloys such as phase separation, optimum memory and threshold switching behavior etc. However, the excursions into three and four-component space must be judiciously selected in order to achieve describable and intelligible results.

The entire list of alloys fabricated under this program is listed in Table 2.1. We have grouped these alloys into eleven categories which attempt to reflect the various purposes which motivated the selections of compositions to be studied. Of the 460 or so alloys prepared, many were merely fabricated and stored after making certain visual observations of the melt or the ingot itself. Since we were concerned with amorphous phases, the alloys which were not at least partially glassy had to be sputtered to yield any useful samples, a process which is very time consuming in terms of cathode fabri-

TABLE 2.1

List of materials and index of measurements for all alloys investigated under this research program. Tg = glass transition temperature; Tx = beginning of crystallization exotherm, both measured at 20°C/min by differential scanning calorimetry. Other properties measured include: σ, electrical conductivity versus temperature; s, thermoelectric power versus temperature; α, optical absorption versus photon energy; x, x-ray diffraction pattern; k, thermal conductivity. Where no bulk Tg value is reported, (a) indicates that a portion of the ingot appeared glassy, while (b) indicates that no bulk glass was obtained. The categories 1 - 11 refer to the classification of materials investigations which is described in Section 2 of the text.

Table 2.1

TABULATION OF MATERIALS AND MEASUREMENTS

			Form and Properties Measured					
			Bulk			Sputtered Film		
Category	Number	Composition	T_g, °C	T_x, °C	other properties	T_g, °C	T_x, °C	other properties
1	2000	$As_{20}Bi_{20}Se_{30}Te_{30}$	133	155				
1	2001	$As_{24}Bi_{16}Se_{24}Te_{36}$	130	140				
1	2002	$As_{28}Bi_{12}Se_{18}Te_{42}$	125	135				
1	2003	$As_{32}Bi_{8}Se_{12}Te_{48}$	125	155				
1	2004	$As_{36}Bi_{4}Se_{6}Te_{54}$	119	131				
1	2005	$As_{20}Ge_{16.67}Se_{33.33}Te_{30}$	205					σ, α
1	2006	$As_{24}Ge_{13.33}Se_{26.67}Te_{36}$	185					σ, α
1	2007	$As_{28}Ge_{10}Se_{20}Te_{42}$	153			195	235	σ, α
1	2008	$As_{32}Ge_{6.67}Se_{13.33}Te_{48}$	145	270		178	196	σ, α
1	2009	$As_{36}Ge_{3.33}Se_{6.67}Te_{54}$	a			145	165	σ, α
1	2010	$Sn_{16.67}As_{20}Se_{33.33}Te_{30}$	140	163				
1	2011	$Sn_{13.33}As_{24}Se_{26.67}Te_{36}$	130	172				

Category	Number	Composition	Form and Properties Measured					
			Bulk			Sputtered Film		
			T_g, °C	T_x, °C	other properties	T_g, °C	T_x, °C	other properties
1	2012	$Sn_{10}As_{28}Se_{20}Te_{42}$	130	165				
1	2013	$Sn_{6.67}As_{32}Se_{13.33}Te_{48}$	130	155				
1	2014	$Sn_{3.33}As_{36}Se_{6.67}Te_{54}$	125	148				
1	2015	$Sn_{16.67}As_{20}S_{33.33}Te_{30}$	b					
1	2016	$Sn_{33.33}As_{24}S_{6.67}Te_{36}$	108	144				
1	2017	$Sn_{10}As_{28}S_{20}Te_{42}$	112	130				
1	2018	$Sn_{6.67}As_{32}S_{13.33}Te_{48}$	120	155				
1	2019	$Sn_{3.33}As_{36}S_{6.67}Te_{54}$	128	164				
1	2020	$As_{20}Bi_{20}S_{30}Te_{30}$	b					
1	2021	$As_{24}Bi_{16}S_{24}Te_{36}$	b					
1	2022	$As_{28}Bi_{12}S_{18}Te_{42}$	b					
1	2023	$As_{32}Bi_{8}S_{12}Te_{48}$	b					
1	2024	$As_{36}Bi_{4}S_{6}Te_{54}$	b					
1	2025	$As_{20}Sb_{20}Se_{30}Te_{30}$	147	170				
1	2026	$As_{24}Sb_{16}Se_{24}Te_{36}$	145	170				
1	2027	$As_{28}Sb_{12}Se_{18}Te_{42}$	b					
1	2028	$As_{32}Sb_{8}Se_{12}Te_{48}$	134	160				

Category	Number	Composition	Form and Properties Measured					
			Bulk			Sputtered Film		
			T_g, °C	T_x, °C	other properties	T_g, °C	T_x, °C	other properties
1	2029	$As_{36}Sb_4Se_6Te_{54}$	130	156				
2	2030	$In_{20}As_{20}Se_{30}Te_{30}$	b					
2	2031	$In_{16}As_{24}Se_{24}Te_{36}$	b					
2	2032	$In_{12}As_{28}Se_{18}Te_{42}$	b					
2	2033	$In_8As_{32}Se_{12}Te_{48}$	b					
2	2034	$In_4As_{36}Se_6Te_{54}$	b					
2	2035	$Ga_{20}As_{20}Se_{30}Te_{30}$	b					
2	2036	$Ga_{16}As_{24}Se_{24}Te_{36}$	b					
2	2037	$Ga_{12}As_{28}Se_{18}Te_{42}$	b					
2	2038	$Ga_8As_{32}Se_{12}Te_{48}$	b					
2	2039	$Ga_4As_{36}Se_6Te_{54}$	b					
1	2040	$As_{36}Sb_4S_6Te_{54}$	130	177				
1	2041	$As_{32}Sb_8S_{12}Te_{48}$	133	165				
1	2042	$As_{28}Sb_{12}S_{18}Te_{42}$	143	160				
1	2043	$As_{24}Sb_{16}S_{24}Te_{36}$	145	185				
1	2044	$As_{20}Sb_{20}S_{30}Te_{30}$	165					
2	2045	$In_{20}As_{20}S_{30}Te_{30}$	125	155				

Category	Number	Composition	Form and Properties Measured: Bulk T_g, °C	Bulk T_x, °C	Bulk other properties	Sputtered Film T_g, °C	Sputtered Film T_x, °C	Sputtered Film other properties
2	2046	$In_{16}As_{24}S_{24}Te_{36}$	125	158				
2	2047	$In_{12}As_{28}S_{18}Te_{42}$	123	152				
2	2048	$In_{8}As_{32}S_{12}Te_{48}$	125	158				
2	2049	$In_{4}As_{36}S_{6}Te_{54}$	121	146				
2	2050	$Ga_{4}As_{36}S_{6}Te_{54}$	b					
2	2051	$Ga_{8}As_{32}S_{12}Te_{48}$	b					
2	2052	$Ga_{12}As_{28}S_{18}Te_{42}$	b					
2	2053	$Ga_{16}As_{24}S_{24}Te_{36}$	b					
2	2054	$Ga_{20}As_{20}S_{30}Te_{30}$	b					
1	2055	$As_{40}S_{6}Te_{54}$	125	178				σ, α
1	2056	$As_{40}S_{12}Te_{48}$	a			118	165	σ, α
1	2057	$As_{40}S_{18}Te_{42}$	Bulk samples of 2057 - 2063 are grossly phase separated					σ, α
1	2058	$As_{40}S_{24}Te_{36}$						α
1	2059	$As_{40}S_{30}Te_{30}$						α
1	2060	$As_{40}S_{36}Te_{24}$						α
1	2061	$As_{40}S_{42}Te_{18}$						α
1	2062	$As_{40}S_{48}Te_{12}$						α

Category	Number	Composition	Form and Properties Measured: Bulk T_g, °C	Bulk T_x, °C	Bulk other properties	Sputtered Film T_g, °C	Sputtered Film T_x, °C	Sputtered Film other properties
1	2063	$As_{40}S_{54}Te_6$						σ, α
1	2064	$As_{40}S_{60}$	216					α
1	2065	$As_{40}Se_{30}Te_{30}$	144	269				
1	2066	$As_{40}Se_{24}Te_{36}$	138	247				
1	2067	$As_{40}Se_{18}Te_{42}$	138	210				
1	2068	$As_{40}Se_{12}Te_{48}$	133	203				
1	2069	$As_{40}Se_6Te_{54}$	127	185				
3	2070	$In_{10}Te_{90}$	b					
3	2071	$In_{15}Te85$	b			96	108	
3	2072	$In_{20}Te_{80}$	b					
3	2073	$In_{25}Te_{75}$	b			157	166	
3	2074	$In_{30}Te_{70}$	148	157				
3	2075	$Ga_{10}Te_{90}$	b					
3	2076	$Ga_{15}Te_{85}$	b			113	118	
3	2077	$Ga_{20}Te_{80}$	150	207				
3	2078	$Ga_{25}Te_{75}$	b			200	230	
3	2079	$Ga_{30}Te_{70}$	195	210				

Category	Number	Composition	Form and Properties Measured: Bulk T_g, °C	Bulk T_x, °C	Bulk other properties	Sputtered Film T_g, °C	Sputtered Film T_x, °C	Sputtered Film other properties
1	2080	$Ge_{3.33}As_{36}S_{6.67}Te_{54}$	128	186				
1	2081	$Ge_{6.67}As_{32}S_{13.33}Te_{48}$	Bulk samples of 2081 - 2084 are grossly phase separated.					
1	2082	$Ge_{10}As_{28}S_{20}Te_{42}$						
1	2083	$Ge_{13.33}As_{24}S_{26.67}Te_{36}$						
1	2084	$Ge_{16.67}As_{20}S_{33.33}Te_{30}$						
1	2085	$Si_{1.67}As_{38}Te_{60.33}$	a					σ
1	2086	$Si_{3.33}As_{36}Te_{60.67}$	a					σ, α
1	2087	$Si_{5}As_{34}Te_{61}$	141	220				σ, α
1	2088	$Si_{6.67}As_{32}Te_{61.33}$	147	248				σ, α
1	2089	$Si_{8.33}As_{30}Te_{61.67}$	b					σ, α
1	2090	$Ge_{3.33}As_{36}Te_{60.67}$	b					σ, α
1	2091	$Ge_{6.67}As_{32}Te_{61.33}$	b					σ, α
1	2092	$Ge_{10}As_{28}Te_{62}$	b					σ, α
1	2093	$Ge_{13.33}As_{24}Te_{62.67}$	b					σ, α
1	2094	$Ge_{16.67}As_{20}Te_{63.33}$	b					α
1	2095	$Ge_{1.67}As_{38}Se_{3.33}Te_{57}$	b					
1	2096	$Ge_{5}As_{34}Se_{10}Te_{51}$	a					

Category	Number	Composition	Form and Properties Measured: Bulk T_g, °C	Bulk T_x, °C	Bulk other properties	Sputtered Film T_g, °C	Sputtered Film T_x, °C	Sputtered Film other properties
1	2097	$Ge_{8.33}As_{30}Se_{16.67}Te_{45}$	a					
1	2098	$Ge_{11.67}As_{26}Se_{23.33}Te_{39}$	a					
1	2099	$Ge_{15}As_{22}Se_{30}Te_{33}$	a					
1	2100	$Ge_{1.67}As_{38}S_{3.33}Te_{57}$	a					
1	2101	$As_{40}S_{3}Te_{57}$	a					
2	2102	$Ga_{20}As_{20}Te_{60}$	b					
2	2104	$Ga_{22.5}As_{22.5}Te_{55}$	b					
2	2105	$Ga_{17.5}As_{17.5}Te_{65}$	b					
2	2106	$Ga_{15}As_{15}Te_{70}$	b					
2	2107	$Ga_{10}As_{10}Te_{80}$	b					
1	2108	$Si_{.83}As_{39}S_{1.67}Te_{58.5}$	b					
1	2109	$Si_{1.67}As_{38}S_{3.33}Te_{57}$	b					
1	2110	$Si_{2.5}As_{37}S_{5}Te_{55.5}$	b					
1	2111	$Si_{3.33}As_{36}S_{6.67}Te_{54}$	b					
1	2112	$Si_{4.17}As_{35}S_{8.33}Te_{52.5}$	b					
1	2113	$Si_{1.67}As_{38}Se_{3.33}Te_{57}$	b					
1	2114	$Si_{3.33}As_{36}Se_{6.67}Te_{54}$	b					

Category	Number	Composition	Form and Properties Measured					
			Bulk			Sputtered Film		
			T_g, °C	T_x, °C	other properties	T_g, °C	T_x, °C	other properties
1	2115	$Si_5As_{34}Se_{10}Te_{51}$	b					
1	2116	$Si_{6.67}As_{32}Se_{13.33}Te_{48}$	b					
1	2117	$Si_{8.33}As_{30}Se_{16.67}Te_{45}$	b					
3	2120	$As_{30}S_{60}Te_{10}$	a					
3	2121	$As_{30}S_{50}Te_{20}$	a					
3	2122	$As_{30}S_{40}Te_{30}$	a					
3	2123	$As_{30}S_{30}Te_{40}$	a					
3	2124	$As_{30}S_{20}Te_{50}$	a					
3	2125	$As_{30}S_{10}Te_{60}$	a					
3	2126	$As_{20}S_{70}Te_{10}$	a					
3	2127	$As_{20}S_{60}Te_{20}$	a					
3	2128	$As_{20}S_{50}Te_{30}$	a					
3	2129	$As_{20}S_{40}Te_{40}$	a					
3	2130	$As_{20}S_{30}Te_{50}$	a					
3	2131	$As_{20}S_{20}Te_{60}$	a					
3	2132	$As_{20}S_{10}Te_{70}$	a					

Category	Number	Composition	Form and Properties Measured					
			Bulk			Sputtered Film		
			T_g, °C	T_x, °C	other properties	T_g, °C	T_x, °C	other properties
1	2134	$As_{30}S_{69}Te_1$	a					
4	2135	$Cd_{20}Ge_{10}As_{60}Te_{10}$	b					
4	2136	$Cd_{15}Ge_{10}As_{60}Te_{15}$	b					
4	2137	$Cd_{10}Ge_{10}As_{60}Te_{20}$	b					
4	2138	$Cd_5Ge_{10}As_{60}Te_{25}$	b					
5	2139	$Cd_{23.5}Ge_{11.5}As_{65}$	344	430				
5	2140	$Cd_{60}As_{40}$	b					
5	2141	$Cd_{33.33}As_{66.67}$	b					
5	2142	$Cd_{30}Ge_{15}As_{55}$	367	410				
5	2143	$Cd_{33.5}Ge_{16.5}As_{50}$	b					
4	2144	$Cd_{25}Ge_{10}As_{60}Te_5$	b					
5	2145	$Cd_{26.8}Ge_{13.2}As_{60}$	b					
5	2147	$Cd_{32.26}Ge_{3.23}As_{64.52}$	b					
5	2148	$Cd_{30.30}Ge_{9.09}As_{60.60}$	342	403				
5	2149	$Cd_{28.57}Ge_{14.29}As_{57.14}$	362	430				
5	2150	$Cd_{27.03}Ge_{18.92}As_{54.05}$	b					
5	2151	$Cd_{25.64}Ge_{23.08}As_{51.28}$	393	440				

Category	Number	Composition	Form and Properties Measured: Bulk T_g, °C	Bulk T_x, °C	Bulk other properties	Sputtered Film T_g, °C	Sputtered Film T_x, °C	Sputtered Film other properties
5	2152	$Cd_{24.39}Ge_{26.83}As_{48.78}$	a	500				
5	2153	$Cd_{23.26}Ge_{30.23}As_{46.51}$	b					
5	2154	$Si_{10}As_{50}Te_{40}$	225					
5	2155	$Si_{15}As_{45}Te_{40}$	255					
5	2156	$Si_{20}As_{40}Te_{40}$	290					
5	2157	$Si_{25}As_{35}Te_{40}$	328					
5	2158	$Si_{30}As_{30}Te_{40}$	365					
5	2159	$Si_{35}As_{25}Te_{40}$	435					
5	2160	$Si_{40}As_{20}Te_{40}$	438					
5	2161	$Si_{45}As_{15}Te_{40}$	a					
5	2162	$Si_{50}As_{10}Te_{40}$	400					
5	2163	$Si_{10}As_{60}Te_{30}$	236					
5	2164	$Si_{15}As_{55}Te_{30}$	294					
5	2165	$Si_{20}As_{50}Te_{30}$	310					
5	2166	$Si_{25}As_{45}Te_{30}$	352					
5	2167	$Si_{30}As_{40}Te_{30}$	382					
5	2168	$Si_{35}As_{35}Te_{30}$	428					

Category	Number	Composition	Form and Properties Measured: Bulk T_g, °C	Bulk T_x, °C	Bulk other properties	Sputtered Film T_g, °C	Sputtered Film T_x, °C	Sputtered Film other properties
5	2169	$Si_{40}As_{30}Te_{30}$	386					
5	2170	$Si_{45}As_{25}Te_{30}$	a					
5	2171	$Si_{50}As_{20}Te_{30}$	347					α
5	2172	$Si_{35}As_{20}Te_{45}$	b					
5	2173	$Si_{35}As_{30}Te_{35}$	450					σ, α
5	2174	$Si_{35}As_{40}Te_{25}$	b					α, s
5	2175	$Si_{45}As_{30}Te_{25}$	b					
5	2176	$Si_{25}As_{30}Te_{45}$	349					α
5	2177	$Si_{25}As_{40}Te_{35}$	347					α
5	2178	$Si_{25}As_{50}Te_{25}$	368					α
5	2179	$Si_{15}As_{40}Te_{45}$	a					
4	2180	$Si_{50}As_{10}Se_{40}$	Ingots 2180 – 2193 were discarded without examination; extreme hydrolysis reactions released H_2Se vapor					
4	2181	$Si_{50}As_{25}Se_{25}$						
4	2182	$Si_{40}As_{10}Se_{50}$						
4	2183	$Si_{40}As_{20}Se_{40}$						
4	2184	$Si_{40}As_{35}Se_{25}$						
4	2185	$Si_{40}As_{45}Se_{15}$						

Category	Number	Composition	Form and Properties Measured					
			Bulk			Sputtered Film		
			T_g, °C	T_x, °C	other properties	T_g, °C	T_x, °C	other properties
4	2186	$Si_{30}As_{30}Se_{40}$						
4	2187	$Si_{30}As_{45}Se_{25}$						
4	2188	$Si_{20}As_{30}Se_{50}$						
4	2189	$Si_{20}As_{40}Se_{40}$						
4	2190	$Si_{20}As_{55}Se_{25}$						
4	2191	$Si_{20}As_{65}Se_{15}$						
4	2192	$Si_{10}As_{50}Se_{40}$						
4	2193	$Si_{10}As_{65}Se_{25}$						
5	2194	$Si_{15}As_{55}Te_{30}$	296					
5	2195	$Si_{15}As_{50}Te_{35}$	272					
5	2196	$Si_{20}As_{45}Te_{35}$	305					
5	2197	$Si_{30}As_{35}Te_{35}$	390					
5	2198	$Si_{35}As_{25}Te_{40}$	438					
5	2199	$Si_{40}As_{25}Te_{35}$	368					
5	2200	$Si_{45}As_{10}Te_{45}$	402					
5	2201	$Si_{50}As_{15}Te_{35}$	402					
1, 6b	2202	$Ge_{33.33}Se_{66.67}$	422			408		σ, α, s

Category	Number	Composition	Form and Properties Measured: Bulk T_g, °C	Bulk T_x, °C	Bulk other properties	Sputtered Film T_g, °C	Sputtered Film T_x, °C	Sputtered Film other properties
1, 6b	2203	$Ge_{33.33}Se_{60}Te_{6.67}$	388					σ, α, s
1, 6b	2204	$Ge_{33.33}Se_{53.33}Te_{13.33}$	354		σ, s			
1, 6b	2205	$Ge_{33.33}Se_{50}Te_{16.67}$	340					
1, 6b	2206	$Ge_{33.33}Se_{46.67}Te_{20}$	326		k			σ, α, s
1, 6b	2207	$Ge_{33.33}Se_{40}Te_{26.67}$	312					
1, 6b	2208	$Ge_{33.33}Se_{33.33}Te_{33.33}$	292		α, k			σ, α, s
1, 6b	2209	$Ge_{33.33}Se_{26.67}Te_{40}$	282					σ, s
1, 6b	2210	$Ge_{33.33}Se_{20}Te_{46.67}$	263					σ, α, s
1, 6b	2211	$Ge_{33.33}Se_{16.67}Te_{50}$	254					
1, 6b	2212	$Ge_{33.33}Se_{13.33}Te_{53.33}$	217					
1, 5b	2213	$Ge_{33.33}Se_{6.67}Te_{60}$	b			242		σ, α, s
1	2214	$Si_{13.33}Ge_{20}Te_{66.67}$	b					
1	2215	$Si_{10}Ge_{23.33}Te_{66.67}$	b					
1	2216	$Si_{6.6}Ge_{26.7}Te_{66.7}$	b					
1	2217	$Si_{3.3}Ge_{30}Te_{66.7}$	b					
1	2218	$Ge_{20}As_{16}Se_{40}Te_{24}$	b					
1	2219	$Ge_{23.3}As_{12}Se_{46.7}Te_{18}$	b					

Category	Number	Composition	Form and Properties Measured					
			Bulk			Sputtered Film		
			T_g, °C	T_x, °C	other properties	T_g, °C	T_x, °C	other properties
1	2220	$Ge_{26.7}As_8Se_{53.3}Te_{12}$	b					
1	2221	$Ge_{30}As_4Se_{60}Te_6$	b					
2	2222	$Ga_{28}Ge_{10}Te_{62}$	b					
2	2223	$Ga_{24}Ge_{13.3}Te_{62.7}$	b					
2	2224	$Ga_{20}Ge_{16.7}Te_{63.3}$	b					
2	2225	$Ga_{16}Ge_{20}Te_{64}$	b					
2	2226	$Ga_{12}Ge_{23.3}Te_{64.7}$	b					
6a	2227	$Ge_{15}Se_{42.5}Te_{42.5}$	105	157				
6a	2228	$Ge_{20}Se_{40}Te_{40}$	bulk sample appeared glassy but contained Te crystallites				100	σ, α, s
6a	2229	$Ge_{25}Se_{37.5}Te_{37.5}$	236					
6a	2230	$Ge_{30}Se_{35}Te_{35}$	270					
6c	2231	$Ge_{40}Se_{30}Te_{30}$	296					σ, α, s
8a	2232	$Zn_{80}Ga_{10}Ge_{10}$	b					
8a	2233	$Zn_{70}Ga_{15}Ge_{15}$	b					
8a	2234	$Zn_{70}Ga_{10}Ge_{20}$	b					
8a	2235	$Zn_{70}Ga_{20}Ge_{10}$	b					
8a	2236	$Zn_{30}Ga_{60}Ge_{10}$	b					

Category	Number	Composition	Form and Properties Measured					
			Bulk			Sputtered Film		
			T_g, °C	T_x, °C	other properties	T_g, °C	T_x, °C	other properties
8a	2237	$Zn_{20}Ga_{60}Ge_{20}$	b					
8a	2238	$Zn_{30}Ga_{50}Ge_{20}$	b					
8a	2239	$Zn_{35}Ga_{50}Ge_{15}$	b					
8a	2240	$Zn_{20}Ga_{50}Ge_{30}$	b					
8a	2241	$Zn_{40}Ga_{40}Ge_{20}$	b					
8a	2242	$Zn_{30}Ga_{40}Ge_{30}$	b					
8b	2243	$Zn_5Ge_{15}Se_{80}$	144					
8b	2244	$Cu_5Ge_{15}Se_{80}$	a					
8b	2245	$Ga_5Ge_{15}Se_{80}$	a					
8b	2246	$Zn_{10}Ge_{15}Se_{75}$	a					
8b	2247	$Cu_{10}Ge_{15}Se_{75}$	b					
8b	2248	$Ga_{10}Ge_{15}Se_{75}$	a					
8b	2249	$Zn_{15}Ge_{15}Se_{70}$	a					
8b	2250	$Cu_{15}Ge_{15}Se_{70}$	b					
8b	2251	$Ga_{15}Ge_{15}Se_{70}$	b					
8b	2252	$Cu_{25}As_{25}Se_{50}$	b					
8b	2253	$Cu_{25}As_{25}S_{25}Se_{25}$	b					

Category	Number	Composition	Form and Properties Measured					
			Bulk			Sputtered Film		
			T_g, °C	T_x, °C	other properties	T_g, °C	T_x, °C	other properties
1	2254	$Si_{33.3}Te_{66.6}$	b					
1	3000	$Ge_{33.33}S_{6.67}Te_{60}$	b					
1	3001	$Ge_{33.33}S_{3.33}Te_{63.3}$	b					
1	3002	$Ge_{33.33}S_{0.67}Te_{66}$	b					
1	3003	$Ge_{33.33}S_{13.33}Te_{53.33}$	b					
1	3004	$Ge_{33.33}O_{5.13}Te_{61.54}$	b					
1	3005	$Ge_{33.33}O_{2.38}Te_{64.29}$	b					
1	3006	$Ge_{33.33}O_{1.15}Te_{65.5}$	b			258		α, s
1	3007	$Ge_{33.33}O_{0.23}Te_{66.44}$	b			145	235	σ, α
4	3008	$In_{16.67}Sb_{16.67}Te_{66.66}$	b					
4	3009	$In_{18.75}Sb_{18.75}Te_{62.5}$	b					
4	3010	$In_{20}Sb_{20}Te_{60}$	b					
4	3011	$In_{16.67}Sb_{16.67}Se_{66.66}$	b					
4	3012	$In_{18.75}Sb_{18.75}Se_{62.5}$	b					
4	3013	$In_{20}Sb_{20}Se_{60}$	b					
4	3014	$Ga_{16.67}As_{16.67}Te_{66.66}$	b					
4	3015	$Ga_{18.75}As_{18.75}Te_{62.5}$	b					

Category	Number	Composition	Form and Properties Measured: Bulk T_g, °C	Bulk T_x, °C	Bulk other properties	Sputtered Film T_g, °C	Sputtered Film T_x, °C	Sputtered Film other properties
4	3016	$Ga_{20}As_{20}Te_{60}$	b					
4	3017	$Ga_{16.67}As_{16.67}Se_{66.66}$	b					
4	3018	$Ga_{18.25}As_{18.75}Se_{62.5}$	b					
4	3019	$Ga_{20}As_{20}Se_{60}$	b					
9	3020	$Si_{25}Ge_{10}As_{30}Te_{35}$	404					σ, α
9	3021	$Si_{40}Ge_{5}As_{10}Te_{45}$	392,396	458				
9	3022	$Si_{35}Ge_{5}As_{20}Te_{40}$	378,420					
9	3023	$Si_{20}Ge_{15}As_{30}Te_{35}$	372					
9	3024	$Si_{20}Ge_{20}As_{20}Te_{40}$	376					
9	3025	$Si_{25}Ge_{20}As_{10}Te_{45}$	352	428				
9	3026	$Si_{10}Ge_{30}As_{20}Te_{40}$	359					
9	3027	$Si_{30}Ge_{10}As_{20}Te_{40}$	396					
9	3028	$Si_{30}Ge_{5}As_{30}Te_{35}$	390					
8b	3029	$Cu_{1}Ge_{33}Se_{19.8}Te_{46.2}$	b					
8b	3030	$Cu_{5}Ge_{31.67}Se_{19}Te_{44.33}$	b					
8b	3031	$Cu_{1}Ge_{33}Se_{33}Te_{33}$	340					s
8b	3032	$Cu_{5}Ge_{31.66}Se_{31.67}Te_{31.67}$	b					

Category	Number	Composition	Form and Properties Measured: Bulk T_g, °C	Bulk T_x, °C	Bulk other properties	Sputtered Film T_g, °C	Sputtered Film T_x, °C	Sputtered Film other properties
7a	3033	$Ge_{36.6}Te_{63.3}$	b				220	σ, α, s
9	3034	$Si_{20}Ge_{10}As_{40}Te_{30}$	326					
9	3035	$Si_{15}Ge_{20}As_{30}Te_{35}$	358		σ			α
9	3036	$Si_{12.5}Ge_{25}As_{25}Te_{37.5}$	339					
9	3037	$Si_{12.5}Ge_{12.5}As_{50}Te_{25}$	339					
9	3038	$Si_5Ge_{25}As_{40}Te_{30}$	352					
9	3039	$Si_5Ge_{30}As_{30}Te_{35}$	366	408				
9	3040	$Si_{10}Ge_{25}As_{30}Te_{35}$	318	420				
9	3041	$Si_{17.5}Ge_{17.5}As_{30}Te_{35}$	340					
5	3042	$Cd_{25}Ge_{25}As_{50}$	400	454				
9	3043	$Si_{35}Ge_{10}As_{10}Te_{45}$	380	480				
9	3044	$Si_{32.5}Ge_{12.5}As_{10}Te_{45}$	355	425				
9	3045	$Si_{30}Ge_{15}As_{10}Te_{45}$	365	385				
9	3046	$Si_{25}Ge_{15}As_{20}Te_{40}$	375	480				
9	3047	$Si_{20}Ge_{25}As_{10}Te_{45}$	356	400				
9	3048	$Si_{15}Ge_{30}As_{10}Te_{45}$	380	400				
5	3049	$Si_{25}As_{50}Te_{25}$	a					

Category	Number	Composition	Form and Properties Measured: Bulk T_g, °C	Bulk T_x, °C	Bulk other properties	Sputtered Film T_g, °C	Sputtered Film T_x, °C	Sputtered Film other properties
9	3050	$Si_{25}Ge_5As_{40}Te_{30}$	394	400				
9	3051	$Si_{20}Ge_5As_{50}Te_{25}$	365	370				
9	3052	$Si_{15}Ge_{15}As_{40}Te_{30}$	328	368				
9	3053	$Ge_{30}As_{40}Se_{15}Te_{15}$	362	>500				
9	3054	$Ge_{35}As_{30}Se_{17.5}Te_{17.5}$	346	>450				
9	3055	$Ge_{40}As_{20}Se_{20}Te_{20}$	352	424				
9	3056	$Ge_{40}As_{20}Se_{10}Te_{30}$	b					
9	3057	$Ge_{30}As_{40}Se_{10}Te_{20}$	347	>500				
9	3058	$Ge_{33.3}As_{33.3}Se_{16.6}Te_{16.6}$	342	380				
9	3059	$Ge_{33.3}As_{33.3}Se_{11.1}Te_{22.2}$	346	>500				
9	3060	$Ge_{22.2}As_{33.3}Se_{11.1}Te_{33.3}$	a					
9	3061	$Ge_{22.2}As_{33.3}Se_{22.2}Te_{22.2}$	a					
5	3062	$Ge_{16.7}As_{33.3}Se_{25}Te_{25}$	376	>500				
5	3063	$Ge_{16.7}As_{33.3}Se_{16.7}Te_{33.3}$	a					
9	3064	$Ge_{33.3}As_{33.3}Se_{16.7}Te_{16.7}$	342	380				σ, s
9	3065	$Ge_{33.3}As_{33.3}S_{16.7}Se_{16.7}$	423	>500				
5	3066	$Si_{27.78}Ge_{11.11}As_{33.33}Te_{27.78}$	b					

Category	Number	Composition	Form and Properties Measured: Bulk T_g, °C	Bulk T_x, °C	Bulk other properties	Sputtered Film T_g, °C	Sputtered Film T_x, °C	Sputtered Film other properties
5	3067	$Si_{22.73}Ge_{9.09}As_{27.27}Te_{40.91}$	350	> 500				
5	3068	$Si_{26.32}Ge_{10.53}As_{31.58}Te_{31.58}$	388	425				
9, 10	3069	$Ge_{33.33}As_{33.33}Se_{33.33}$	404	> 500		407		σ, α, s
9	3070	$Ge_{33.33}As_{33.33}Se_{29.97}Te_{3.36}$	391	> 420				
9	3071	$Ge_{33.33}As_{33.33}Se_{26.64}Te_{6.69}$	394,460	> 500				
9	3072	$Ge_{33.33}As_{33.33}Se_{23.31}Te_{10.02}$	380	> 500				
9	3073	$Ge_{33.33}As_{33.33}Se_{19.98}Te_{13.35}$	376	> 435				
9	3074	$Ge_{33.33}As_{33.33}Se_{16.65}Te_{16.68}$	364	> 410				α
9	3075	$Ge_{33.33}As_{33.33}Se_{13.32}Te_{20.01}$	352	370				
9	3076	$Ge_{33.33}As_{33.33}Se_{9.99}Te_{23.34}$	340	428				
9	3077	$Ge_{33.33}As_{33.33}Se_{3.33}Te_{30}$	338	420				
9,10	3078	$Ge_{33.33}As_{33.33}Te_{33.33}$	332	~ 383		333	393	α, σ, s
9	3079	$Si_{35}Ge_{7.5}As_{15}Te_{42.5}$	354	> 500				
9	3080	$Ge_{33.33}As_{33.33}Se_{6.67}Te_{26.67}$	337	430				
5	3081	$Ge_{50}As_{20}Se_{15}Te_{15}$	b					
5	3082	$Ge_{30}As_{20}Se_{25}Te_{25}$	319	434				
5	3083	$Ge_{45}As_{10}Se_{22.5}Te_{22.5}$	b					

Category	Number	Composition	Form and Properties Measured: Bulk T_g, °C	Bulk T_x, °C	Bulk other properties	Sputtered Film T_g, °C	Sputtered Film T_x, °C	Sputtered Film other properties
5	3084	$Ge_{45}As_{20}Se_{17.5}Te_{17.5}$	362	427				
5	3085	$Ge_{35}As_{20}Se_{22.5}Te_{22.5}$	342	430				
9	3086	$Ge_{40}As_{20}Te_{40}$	b			324	357	σ,α,s
9, 6c	3087	$Ge_{50}Se_{25}Te_{25}$	b			275	275	σ,α,s
10	3088	$Si_{33.33}As_{33.33}Te_{33.33}$	a					
4	3089	$Zn_{50}Te_{50}$	b					
4	3090	$Ga_{33.33}As_{33.33}Se_{33.33}$	b					
4	3091	$Ga_{33.33}As_{33.33}Te_{33.33}$	b					
4	3092	$In_{33.33}As_{33.33}Se_{33.33}$	b					
4	3093	$In_{33.33}As_{33.33}Te_{33.33}$	b					
11	3094	$Ga_{33.33}Ge_{33.33}Se_{33.33}$	b			350	405	σ,α,x
11	3095	$In_{33.33}Ge_{33.33}Se_{33.33}$	b			295	336	σ,α,x
11	3096	$Ga_{33.33}Ge_{33.33}Te_{33.33}$	b				410	σ,α
11	3097	$In_{33.33}Ge_{33.33}Te_{33.33}$	b				410	σ,α
10	3098	$Sn_{33.33}As_{33.33}S_{33.33}$	b			162	218	σ,σ,x
10	3099	$Pb_{33.33}As_{33.33}Se_{33.33}$	b					α,σ
4	3100	$Zn_{33.33}As_{33.33}Se_{33.33}$	b					

Category	Number	Composition	Form and Properties Measured: Bulk T_g, °C	Bulk T_x, °C	Bulk other properties	Sputtered Film T_g, °C	Sputtered Film T_x, °C	Sputtered Film other properties
4	3101	$Zn_{33.33}As_{33.33}S_{33.33}$	b					
10	3102	$Sn_{33.33}As_{33.33}Te_{33.33}$	b					α,x
10	3103	$Pb_{33.33}As_{33.33}Te_{33.33}$	b					α,x
4	3104	$Zn_{33.33}As_{33.33}Te_{33.33}$	b					
9	3105	$Ge_{30}As_{40}Te_{30}$	b			335	412	σ,α
4	3106	$Zn_{10}Ge_{20}Se_{70}$	b					
10	3107	$Si_{33.33}Sb_{33.33}Te_{33.33}$	b					
10	3108	$Ge_{33.33}Sb_{33.33}Te_{33.33}$	b			249	263	σ,α,s,x
10	3109	$Ge_{33.33}Sb_{33.33}Se_{33.33}$	b			301	358	σ,α,s,x
10	3110	$Pb_{33.33}As_{33.33}S_{33.33}$	b					α,x
11	3111	$Ga_{33.33}Sn_{33.33}Se_{33.33}$	b					
11	3112	$Ga_{33.33}Sn_{33.33}S_{33.33}$	b					
11	3113	$Ga_{33.33}Sn_{33.33}Te_{33.33}$	b					
11	3114	$In_{33.33}Sn_{33.33}Se_{33.33}$	b					
11	3115	$In_{33.33}Sn_{33.33}S_{33.33}$	b					
11	3116	$In_{33.33}Sn_{33.33}Te_{33.33}$	b			83	175	σ,α,x
3, 6a	3117	$Ge_{10}Se_{45}Te_{45}$	110,280	180				

Category	Number	Composition	Form and Properties Measured: Bulk T_g, °C	Bulk T_x, °C	Bulk other properties	Sputtered Film T_g, °C	Sputtered Film T_x, °C	Sputtered Film other properties
6a	3118	$Ge_{22}Se_{39}Te_{39}$	208	230				
6a	3119	$Ge_{18}Se_{41}Te_{41}$	320(Tg_2)	334				
6a	3120	$Ge_{16}Se_{42}Te_{42}$	284(Tg_2)	165				
6a	3121	$Ge_{27}Se_{36.5}Te_{36.5}$	260	350				
6a	3122	$Ge_{32}Se_{34}Te_{34}$	282					
7b	3123	$Ge_{30}Se_{70}$	364					
7b	3124	$Ge_{20}Se_{80}$	168					
7b	3125	$Ge_{10}Se_{90}$	95					
7b	3126	$Ge_{35}Se_{65}$	423					
7c	3127	$Se_{50}Te_{50}$	b			57		α, s
6a	3128	$Ge_5Se_{65}Te_{30}$	82	220				
6a	3129	$Ge_{10}Se_{65}Te_{25}$	105					
6a	3130	$Ge_{15}Se_{65}Te_{20}$	145					
6a	3131	$Ge_{20}Se_{65}Te_{15}$	190					
6a	3132	$Ge_{25}Se_{65}Te_{10}$	252					
6a	3133	$Ge_{30}Se_{65}Te_5$	375					
6a	3134	$Ge_{20}Se_{70}Te_{10}$	175					

Category	Number	Composition	Form and Properties Measured: Bulk T_g, °C	Bulk T_x, °C	Bulk other properties	Sputtered Film T_g, °C	Sputtered Film T_x, °C	Sputtered Film other properties
6a	3135	$Ge_{15}Se_{75}Te_{10}$	135					
6a	3136	$Ge_{10}Se_{80}Te_{10}$	102					
6a	3137	$Ge_{5}Se_{85}Te_{10}$	78					
7b	3138	$Ge_{40}Se_{60}$	302	430				σ, α
7b	3139	$Ge_{32}Se_{68}$	a					
7b	3140	$Ge_{37}Se_{63}$	398	475				
5	3141	$Si_{12}Ge_{10}As_{30}Te_{48}$	a					
6a	3142	$Ge_{5}Se_{50}Te_{45}$	78	160				
6a	3143	$Ge_{10}Se_{55}Te_{35}$	106	236				
6a	3144	$Ge_{10}Se_{10}Te_{80}$	b					
6a	3145	$Ge_{15}Se_{10}Te_{75}$	140	210				
6a	3146	$Ge_{20}Se_{5}Te_{75}$	168	260				
6a	3147	$Ge_{20}Se_{20}Te_{60}$	169	260				
6a	3148	$Ge_{25}Se_{10}Te_{65}$	201					
6a	3149	$Ge_{25}Se_{20}Te_{55}$	210	338				
6a	3150	$Ge_{25}Se_{30}Te_{45}$	208	350				
6a	3151	$Ge_{10}Se_{20}Te_{70}$	b					

Category	Number	Composition	Bulk			Sputtered Film		
			T_g, °C	T_x, °C	other properties	T_g, °C	T_x, °C	other properties
6c	3152	$Ge_{90}Se_5Te_5$	b					
6c	3153	$Ge_{80}Se_{10}Te_{10}$	b					σ, α
6c	3154	$Ge_{70}Se_{15}Te_{15}$	b					
6c	3155	$Ge_{60}Se_{20}Te_{20}$	b					σ, α, s
6c	3156	$Ge_{55}Se_{22.5}Te_{22.5}$	b					
6c	3157	$Ge_{45}Se_{27.5}Te_{27.5}$	b					
6a	3158	$Ge_5Se_{47.5}Te_{47.5}$	86	172				
3	3159	$Te_{81}S_2Ge_{15}Sb_2$	130	183	σ,α,k	123	175	σ,α,s
5	3160	$As_{34.5}Te_{27.9}Ge_{15.6}S_{22}$	a		σ,α,k			σ,α
6a	3161	Se	45	106				α
7c	0083	$Se_{92}Te_8$	54					
1, 7a	1003	$Ge_{33.3}Te_{66.6}$	b			225	256	σ,α,s
3	1004	$As_{20}Te_{80}$	b			90	130	
6a	1029	Te	b		s			σ,α,s
7c	1044	$Se_{96}Te_4$	47					
7c	1045	$Se_{88}Te_{12}$	56					
7c	1046	$Se_{84}Te_{16}$	59					

Category	Number	Composition	Form and Properties Measured: Bulk T_g, °C	Bulk T_x, °C	Bulk other properties	Sputtered Film T_g, °C	Sputtered Film T_x, °C	Sputtered Film other properties
7a	1075	$Ge_{10}Te_{90}$	b			114	152	σ,α,s
7a	1076	$Ge_{20}Te_{80}$	a			147	222	
7a	1078	$Ge_{25}Te_{75}$	a			185	203	σ,α,s
1	1088	$As_{40}Se_{60}$	195	305	k,x			α,s,x
7a	1089	$Ge_{17}Te_{83}$	a		k,s	147	213	σ,α,s
7a	1130	$Ge_{45}Te_{55}$	b					
7a	1135	$Ge_{15}Te_{85}$	a					
7a	1136	$Ge_{67}Te_{33}$	b					σ,α
7a	1137	$Ge_{50}Te_{50}$	b				160-232	σ,α,s
7c	1152	$Se_{40}Te_{60}$	78	86				
7c	1153	$Se_{30}Te_{70}$	45	68				
7c	1154	$Se_{20}Te_{80}$	b					
7c	1155	$Se_{10}Te_{90}$	b					
7a	1159	$Ge_{22}Te_{78}$	162			170	240	
7a	1196	Ge_5Te_{95}	b					σ,α,s
7c	1226	$Se_{75}Te_{25}$	a				65	α,s
7c	1227	$Se_{60}Te_{40}$	75					
6a	1254	$Ge_{15}Se_5Te_{80}$	138					

Category	Number	Composition	Form and Properties Measured: Bulk T_g, °C	Bulk T_x, °C	Bulk other properties	Sputtered Film T_g, °C	Sputtered Film T_x, °C	Sputtered Film other properties
6c	1270	$Ge_{36}Se_{32}Te_{32}$	295					
6c	1271	$Ge_{38}Se_{31}Te_{31}$	302					
7a	1274	$Ge_{30}Te_{70}$	b			213	243	σ,α,s
7a	1276	$Ge_{40}Te_{60}$	b				201	σ,α,s
7c	1304	$Se_{90}Te_{10}$	55					
7a	1306	$Ge_{60}Te_{40}$	b				267	σ,α,s
7b	1310	$Ge_{50}Se_{50}$	b			322	322	σ,α,s
3	1316	$As_{50}Te_{50}$	154	234				σ,α,s
7a	1326	$Ge_{70}Te_{30}$	b				352	σ,α,s
7a	1327	$Ge_{80}Te_{20}$	b					σ,α,s
7a	1328	$Ge_{90}Te_{10}$	b					σ,α,s
6b	1339	$Ge_{33.3}Se_{36.7}Te_{30}$	a					σ,s
9	1364	As	b			343	360	σ,α,s
7b	1387	$Ge_{25}Se_{75}$	a					σ,s
7b	1388	$Ge_{60}Se_{40}$	b					σ,α,s
6c	1389	$Ge_{50}Se_{35}Te_{15}$	b					σ,α,s

Category	Number	Composition	Form and Properties Measured					
			Bulk			Sputtered Film		
			T_g, °C	T_x, °C	other properties	T_g, °C	T_x, °C	other properties
7b	1391	$Ge_{90}Se_{10}$	b					σ, α, s
6a	1396	$Ge_{15}Se_{60}Te_{25}$	131					σ, s
7b	1397	$Ge_{80}Se_{20}$	b					σ, α
6a	1412	$Ge_{25}Se_{50}Te_{25}$	238	279				α

cation and deposition time. For example, the measurement of a T_g value requires roughly a 20 μm thick film which in turn requires 20 hours of deposition time. Thus the number of alloys which can be investigated even to this minimal extent is severely limited.

The following text identifies the eleven categories of investigations by number, and summarizes to some extent the nature of the information obtained. The table itself merely lists the compositions, and identifies the properties, if any, which were measured. Inasmuch as the primary focus of this study was high temperature behavior, however, we have also tabulated T_g and T_x for all specimens on which these quantities were measured, in order to indicate the degree of thermal stability attained.

Category 1. Chalcogen-Saturated Pseudo-Binary Systems containing only V_2-VI_3 and IV VI_2 Components.

Because tellurium was a universal component in almost all amorphous threshold and memory switching alloys reported through the middle of 1970, we focused our early emphasis in this program on the analysis of multi-component telluride glasses. The concept of "chalcogen saturation" turned out to be very useful in subdividing multi-component alloys systems, and we initially studied only alloys which appeared to meet this criterion. When Group IV or Group V components are added to a Group VI chalcogen component, application of the 8-N rule for each component and assumption of complete chemical ordering lead to certain stoichiometric

ratios which permit $8-N_A$ B neighbors around each A atom and $8-N_B$ A neighbors around each B atom, where N_A and N_B are the number of valence electrons of A & B atoms. These ratios are easily derived to be IV VI_2 and V_2 VI_3 where IV, etc., represent the Group IV, etc. components. We thus studied pseudobinary systems of the sort As_2Te_3 - IV VI_2 and As_2Te_3 - V_2 VI_3, surveying the basic physical properties including T_g, electrical conductivity and optical absorption edge, in order to perceive the connection between composition, structure and properties for alloys whose structure could, to a first approximation, be represented as a random mixture of two chemically ordered components. We broadened this Category 1 to include other alloys of the IV VI_2 or V_2 VI_3 type, or a mixture of the two, in which As_2 Te_3 was not necessarily a component.

The results of our investigations of Category 1 chalcogen-saturated alloys have been reported in the First Semi-Annual Technical Report[54] under this contract and have been published, in part, elsewhere. With regard to thermal stability, the principal result of these studies was that no intermediate T_g maxima were observed in any of these chalcogen-saturated pseudobinary systems, and that $T_g(x)$, for those systems which did not phase separate, was a monotonic function of composition. Several of these systems showed gross liquid immiscibility, and could only be prepared as homogeneous amorphous phases by rf sputtering. Examples include GeS_2 - As_2Te_3 (2080-2084) and As_2S_3 - As_2Te_3 (2055-2064).

Category 2. Chalcogen-Saturated Pseudo-Binary, Systems Containing a III VI Component.

Category 2 includes a series of pseudo-binary chalcogen saturated alloys based on components of the sort III_2 VI_3 in combination with As_2 Te_3 or $GeTe_2$. This group of alloys is separated from Category 1 because short range order in glassy chalcogenide alloys containing a Group III constituent has not previously, to our knowledge, been considered in any detail. Our assumption that the III_2 VI_3 stoichiometry corresponds to chalcogen saturation in these systems must therefore be examined in some detail but, at the same time, recognized as an unsubstantiated hypothesis.

Some indication of the short range order in III_2 VI_3 glasses comes from the short range order in the corresponding crystalline structures. For example Ga_2Se_3 has a defect chalcopyrite structure with 1/3 of the Ga sites unoccupied.[24] Thus each Ga has four Se nearest neighbors and each Se has an average, $4 \times 2/3 = 2\ 2/3$ Ga neighbors. Stated differently, two out of every three Se atoms are bonded to three Ga atoms while one out of every three Se atoms is bonded to only two Ga atoms. Another way of visualizing such a topological relationship is to consider Ga_2Se_3 layers analogous to As_2Se_3 layers, as in the orpiment structure. Now, however, in order to complete the valence shell of each Ga atom, one Se lone pair per Ga atom (i.e. 2/3 of the Se atoms) forms an inter-layer

coordinate bond. By symmetry, all the bonds about each Ga atom become tetrahedrally disposed and equal in length, (cf. the resonance concept in chemical bonding) so that it is no longer possible to distinguish the coordinate bonds (two Se lone pair electrons valence electrons per bond) from the covalent bonds (one Se and one Ga valence electron per bond). We assume that all such covalently bonded crystalline materials retain their covalent short range order when prepared as amorphous solids.

Let us now consider the case of amorphous binary Ga-Se alloys in the excess chalcogen Se-rich portion of the system. We assume that the Ga covalency requirements are satisfied by the formation of four bonds: three covalent bonds each containing one Ga and one Se valence electron, and one coordinate bond containing only Se lone pair electrons. This situation has some features in common with the topology of a Group IV atom in an excess chalcogen matrix, which also occupies a tetrahedral site. Figure 2.1 serves to make the distinction clear. Ga provides orbitals which are shared by 5 Se electrons, creating a site where five separate segments of chalcogen chain are joined together. Of course the Ga atom itself is only 4-connected, but its contribution to the average connectedness of the structure is greater than that of Ge, consistent with the 8-N=C rule. Indeed, by this rule, Ga_2Se_3 has C=3.2 versus C=2.4 for, say, As_2Se_3.

If Ga_2Se_3 has C=3.2 and As_2Se_3 has C=2.4, how can they both be chalcogen saturated? Reference to Figure 2.1 shows that each Ga atom eliminates 1.5 Se-Se bonds by creating a branching point where 3 chain segments come together.

Figure 2.1

Schematic representation of the coordination of Gallium (a) and Germanium (b) in a Se-rich amorphous matrix. Cross-linked chain segments are indicated by circled numbers (1)-(5) for Ga, (1)-(4) for Ge.

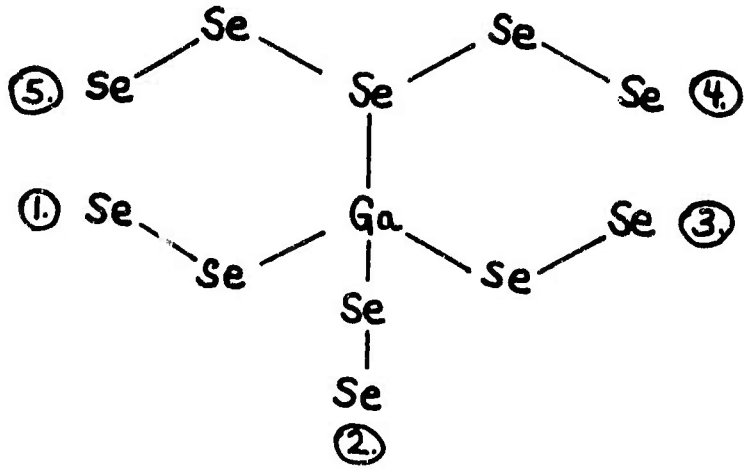
Se
Se
Se
Se
Se
Se
Se
Ga
Se
Se
Se
Se
Se
Se
Se
Se
Se
1.
2.
3.
4.
5.

(a)

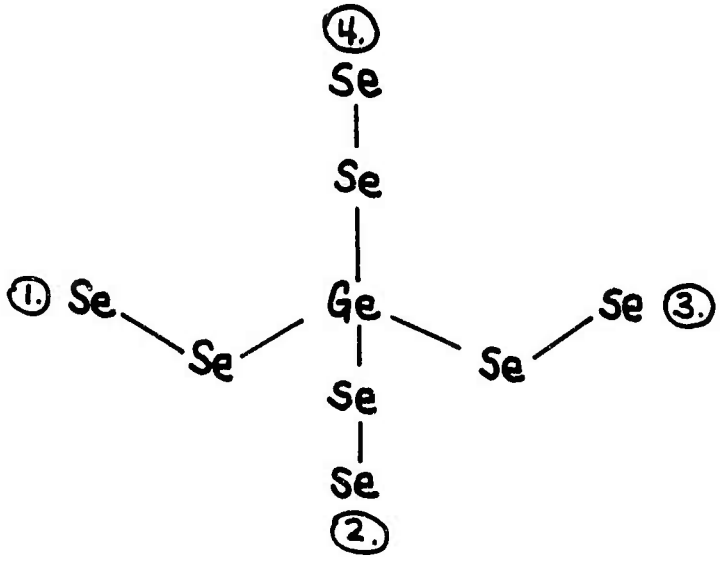
Se
Se
Se
Se
Se
Se
Se
Ge
Se
Se
Se
Se
Se
1.
2.
3.
4.

(b)

Figure 2.1

The chain segments attached to the three-connected Se atom which forms the coordinate bond to Ga (segments 4 and 5 in Fig. 2.1) do not deplete the concentration of Se-Se bonds. Thus at Ga_2Se_3 or $Ga_{40}Se_{60}$, we have .6 x 2 singly occupied Se orbitals and .4 x 3 singly occupied Ga orbitals, establishing an equality of singly occupied Se and Ga orbitals and leading to chalcogen saturation (no chalcogen-chalcogen bonds) for the case of Ga_2Se_3.

Ga_2Se_3 and Ga_2S_3 tend to have such high melting points that mixtures containing them could not be melted at all. Most of the other category 2 alloys were not obtained as glasses, and no films were sputtered. The In_2S_3-As_2Te_3 alloys (2045-2049) were obtained as glasses, but only T_g values were measured. These alloy studies were abandoned in favor of studies where glass formation tendencies were greater or where the structural state of the alloy was better established. A further problem with mixed systems containing III_2 VI_3 chalcogen saturated components in combination with V_2 VI_3 components is the strong compound-forming tendency between the Group III and Group V components (GaAs, etc). This problem is crucial in formulating stable multi-component A.S. materials, and we shall return to discuss this issue in connection with studies of alloys in Categories 4 and 5.

Category 3. Binary, Ternary and Quaternary Excess Chalcogen Alloys.

Category 3 includes a variety of one, two, three and four component alloys which have excess chalcogen (i.e. chalcogen-chalcogen covalent bonds are present).

These excess chalcogen alloys include the common electrical memory switching alloys based on the GeTe-Te eutectic and a variety of experiments on them, including photoconductivity[55] and rf sputter deposition experiments[55] on alloy 3160, $Ge_{15}Sb_2S_2Te_{81}$, have been reported in the course of these investigations. Subtle features of the thermal transformations of this alloy, especially the morphology of the Te crystallites and the role of Sb in supressing GeTe crystallization, have been described in the Second Semi-Annual Technical Report and in two publications.

Phase separation appears to be a common feature of excess chalcogen multi-component alloys (even in certain binary systems, such as Se-Bi_2Se_3),[56] and a detailed study of this phenomenon has been reported for Category 6a Ge-Se-Te alloys.[32] The immiscibility observed along the As_2S_3 - As_2Te_3 chalcogen saturated join has been extended within the chalcogen saturated portion of the As-S-Te system, and many of the Category 3 alloys (2120-2132) were synthesized to pursue that problem. As described in the Introduction, such immiscibility has been termed "secondary" phase separation since it does not arise from a tendency to form a certain set of covalent bonds. Rather it apparently arises from the additional tendency to arrange fixed concentrations of bond types in space so as to minimize strain energy. When we discovered the "primary" phase separation phenomenon in the excess chalcogen Ge-Se-Te alloys described in the Fourth Semi-Annual Technical Report, we abandoned the detailed investigation of the As-S-Te Category 3 alloys.

Category 4. Ternary or Quaternary Chalcogenide Alloys, (Mostly Chalcogen Deficient) with Stable Binary Compound Forming Tendency.

Category 4 alloys have in common the presence of 2 components with significantly different electronegativities (e.g. Zn and Te, Ga and As etc.) Thus these two tend to form a binary compound phase with a much higher melting point and bonding strength than any other pair of components present. The effects of this imbalance in the pairwise interaction of the elemental components include:

1. A difficulty in creating a homogeneous alloy liquid, due to the high melting point of the stable binary compound;

2. A tendency for complete fractionation to occur during cooling, resulting in uncombined or weakly combined elemental components; and

3. A difficulty in fabricating sputtering cathodes due to the refractory nature of the highly stable binary compound.

As a consequence of these various problems, we rarely attempted to prepare amorphous phases of alloys in Category 4. Of course, the highly stable binary crystalline compounds themselves can be prepared as stable amorphous compounds, but this stability is not imparted to multicomponent alloys based on these compounds. When a third component is added, the glass stability is limited by the stability of this weakly-bonded component, which is not enhanced by any ionic stabilization from the binary compound-forming components.

A good example of this Category 4 phenomenon appears to be the Si-As-Se alloys, which are considerably harder to form and less stable then their Si-As-Te counterparts which, at first glance, are less strongly bonded. The resolution of this paradox lies in the larger electronegativity difference between Si and Se than between Si and Te. Thus, strong Si-Se bonds are formed in Si-As-Se liquids, and the As atoms are left to fend for themselves, forming a high vapor pressure phase which condenses upon cooling. This very important principle is well recognized as the requirement for forming ternary crystalline compounds, where the presence of stable binary compounds is viewed as an impediment.[30] The extension to ternary glassy compounds is self evident.

Category 5. Ternary and Quaternary Chalcogen Deficient (or Absent) Alloys Without Stable Binary Compound Forming Tendency.

This category of alloys provides the best examples of high thermal stability coupled with easy glass formation which we have encountered in A.S. systems. The excess chalcogen and the chalcogen-saturated alloys can be very easy glass-formers in many cases. However, the highest values of T_g in these systems are always associated with the largest band-gap chalcogen saturated compositions of the sort GeS_2 or SiO_2, which are essentially insulators and are partially opaque in the mid IR wavelengths (9-14nm) of interest for many optical applications. Some of the chalcogen-deficient alloys, on the other hand, can combine higher conductivity and thus better mid IR transparency (e.g. the reststrahl absorption comes at $\sim 25\,\mu$) with values of T_g well above 400°C.

We focused our exploratory studies of these alloys on two ternary systems which appeared promising: Si-As-Te and Cd-Ge-As. While it is interesting to note that the published compositions of many electrical threshold switching alloys fall into this broad chalcogen deficient classification, we reported in the Second Semi-Annual Technical Report that the highest T_g Si-As-Te alloys did not appear promising for threshold switching. This may be related to their relatively high resistivities. It is possible that their disappointing performance as threshold switches is an artifact of our evaluation procedure, which was designed to test lower resistivity films in thicknesses of ca. 2μm. The higher resistivity Si-Te-As alloys may demand much thinner films, which in turn demand a more sophisticated probe than the simple carbon pin we used.

Alternatively, as one proceeds far enough into the chalcogen-deficient regime to obtain the highest T_g's ($\bar{N} \approx 5$ for Si-As-Te, $\bar{N} \approx 4$ for Cd-As-Ge) the role of lone pair chalcogen electrons is essentially eliminated, if each atom has the average coordination number $C=8-\bar{N}$, of 3 or 4. Ovshinsky[57] has suggested that lone pair electrons may be an essential feature of reversible stable threshold switching alloys, because these electrons can be placed in excited states without affecting the lower lying covalently bonded valence electrons. Thus the glass can retain its structural coherence during massive electronic excitation of the lone pair valence band electrons. Presumably $\bar{N}$ must be somewhat greater than 5 to permit a sufficient concentration of lone pair chalcogen electrons to

be liberated at high fields, producing the reversible threshold switching phenomenon without concomitant structural changes. Alloy 3160, with $\bar{N} = 5.34$ is an example of a composition which has been frequently studied in the reversible threshold switching mode.

Category 6. Ternary Ge-Se-Te Alloys.

We chose this system, as described in the Introduction of the Fourth Semi-Annual Technical Report,[32] in order to analyze in considerable detail the interplay of structure (via composition) and properties (thermal, electrical and optical) in a single ternary chalcogenide system. Included in this system are the first examples of glassy chalcogenide alloys exhibiting an n-type Seebeck coefficient, including many alloys which are p-type before annealing and become n-type after annealing.[48] In addition we have shown that a band level analysis which attempts to interpret the compositional dependence of d.c. conductivity, thermoelectric power and optical absorption in a structurally simple alloy system ($GeSe_2$-$GeTe_2$) can be remarkably successful.[49] Furthermore, by investigating sputtered films, we have been able to introduce, control, and interpret an additional materials parameter, namely the defects introduced during the rf sputter deposition process.

6a. Excess Chalcogen Alloys

In the excess chalcogen portion of the Ge-Se-Te ternary system (i.e., the area bounded by $GeSe_2$, $GeTe_2$, Se, and Te, but excluding the binary join itself), there is a strong tendency for a GeSe-rich liquid phase to segregate from a Te-rich liquid phase, due to the energetic favoring of Ge-Se and Te-Te bonds relative to more random mixtures

involving other bond types (e.g. Ge-Ge, Se-Se, Te-Se and Ge-Te). This ordering phenomenon leads to phase separation only when weaker bonds can thus be excluded. Phase separation is not observed along the $GeSe_2$-Se or $GeSe_2$-$GeTe_2$ joins, where the lowest energy bond types (Ge-Se and Se-Se or Ge-Se and Ge-Te) can coexist in a random distribution without topological impediments. The region of phase separation is elongated along the $GeSe_2$-Te join and disappears as either excess Se or excess $GeTe_2$ is added.[32]

6b. Chalcogen Saturated $GeSe_2$-$GeTe_2$ Alloys

We selected this system for detailed investigation in the fall of 1970 as a logical sequel to our survey studies of the chalcogen saturated pseudo-binary alloy systems described in Categories 1 and 2 above. The first results of these studies were reported at the 1971 International Conference at Ann Arbor[58] and have been further extended and analyzed in preprints which are listed in Appendix 2.[48,49]

The results of investigations of alloys in Categories 6a, b and c have confirmed that optical gap and electrical activation energy maxima occur along the $Ge(Te,Se_2)$ join as intersected by pseudo-binary joins of the sort $Ge-(Te_xSe_{1-x})$, e.g. Ge-Te, Ge-Se and Ge_{100}-$Se_{50}Te_{50}$. Rockstad and Flasck[28] have interpreted these results as a confirmation of chemical ordering tendencies with respect to the exclusive formation of Ge-chalcogen bonds for well annealed amorphous phases in the $GeTe_2$-$GeSe_2$ system. This key feature, while it is the basis of the "chalcogen-saturation" definition,[58]

was unproven prior to the acquisition of these ternary system optical and transport results. Proof that chalcogen-saturation in this system coincides with the exclusion of chalcogen-chalcogen and germanium-germanium bonds greatly simplifies the analysis of the compositional dependence of the band edge energies and Fermi level position and the concomitant electrical and optical properties.

6c. Chalcogen Deficient Ge-Se-Te Alloys

These alloys nominally belong to Category 5, having relatively high glass transition temperatures and no highly stable binary crystalline pnase. However, the chalcogen deficient Ge-Se-Te alloys are not good glass formers, requiring deposition by rf sputtering to obtain any amorphous material at all. Furthermore, the structure of these alloys and the structure-property relationships appear to be anomalous with respect to other alloys having $\bar{N} \approx 5$. GeSe, for example, has a relatively low value of T_g ($322^{o}C$) with respect to its band gap (for annealed material, E_{04} = 1.70 eV) as compared to other $\bar{N} = 5$ glasses such as As ($T_g = 343^{o}C$; $E_{04} = 1.39$ eV). Many of the chalcogen-deficient Ge-Se-Te alloys, including all Ge-Te alloys between $GeTe_2$ and Ge, have no experimentally observable value of T_g. Rather, upon heating, they crystallize directly from the glassy state before reaching T_g, reducing the number of chalcogen-deficient ternary alloys whose T_g's are known.

We have argued on the basis of enthalpy of formation data that amorphous GeTe contains an ordered network of 3-fold Ge and 3-fold Te, by analogy to the amorphous As structure,[60] but this model appears less

tenable than the conventional 4-fold Ge, 2-fold chalcogen model in the case of GeSe. Indeed, aside from the enthalpy of formation measurements there are few data which are best satisfied by the 3-fold model for GeTe. From a structure-property standpoint the question is fundamental, because the identification of the valence band states depends on whether the chalcogen atoms are 2-coordinated, thus retaining their lone pair non-bonding p-type electrons, or 3-coordinated, presumably forming coordinate bonds to Ge atoms with these lone pair electrons. These are, of course, the same structure-property questions which came up in the analysis of the high T_g alloys in Category 5, and well exemplify the questions which remain unanswered even for two-component chalcogenide systems (e.g., the GeTe composition).

Category 7. Binary Joins Bounding Ge-Se-Te System.

7a. Ge-Te System

We initially focused our attention in the Ge-Te system on the excess chalcogen "memory" alloys in the vicinity of $Ge_{15}Te_{85}$ and to the chalcogen saturated composition $GeTe_2$.[9,58] However, by the fall of 1971 we recognized that a thorough study of at least one entire amorphous chalcogenide binary system would be essential to address the general questions which arose, for example, in interpreting the band levels for amorphous $GeTe_2$.[49] The decision to extend our interest in Ge-Te alloys beyond the region of conventional glass formation (roughly embracing $Ge_{10}Te_{90}$ to $Ge_{25}Te_{75}$) or even beyond the range of observability of the glass transition

phenomenon for sputtered films (Ge > 33%) was a significant shift away from our initial goal of identifying and synthesizing new high temperature glassy chalcogenide alloys. However, when we attempted to extend the empirical rules for glass formation in the various systems surveyed by ourselves and others, the limitation of these studies to the easy glass forming compositions or to specific compounds (Ge, As_2S_3, etc.) emerged as their major drawback. By varying, for example, the number of valence electrons, N, across the entire range of covalent network formation from N=6 (chalcogen chains) to N=4 (diamond-like random networks), quite irrespective of glass forming tendency or thermal stability, it became possible to encompass in a single system many specific alloys which had been previously studied only in isolation, e.g., $Ge_{85}Te_{85}$, $GeTe_2$, GeTe and Ge. Thus, a careful investigation of the optical, transport and thermal properties of the amorphous phases in this prototypical binary chalcogenide system became necessary to achieve further progress in understanding the structure-property relationships in the more complicated, albeit better glass-forming, multicomponent A.S. systems.

The results of our investigations of the Ge-Te system were first published in the proceedings of the 1972 Warsaw International Semiconductor Conference.[59] These studies have recently been extended to include the Ge-rich alloys as reported in Section 2.3.2 of this Final Report, and two articles are in preparation describing these alloys.[47,61]

7b. Ge-Se System

This system, and the Se-Te system described below, were studied as adjuncts to our examination of the Ge-Se-Te ternary system. The $GeSe_2$ composition is especially to be noted in this system, as it corresponds to maxima of T_g, E_{04} and E_0 as a function of composition, indicating a high degree of chemical ordering and concomitant cross-linking at this composition. If Ge remains in 4-fold coordination and Se remains in 2-fold coordination as Ge is added to $GeSe_2$, then connectedness increases with additional Ge as weaker Ge-Ge bonds are formed. This is analogous to the behavior of GeO_2 [62] or GeS_2 [63] as Ge is added, and the attendant decrease in T_g is to be expected. While we have studied the electrical and optical properties of unannealed and annealed sputtered films ranging between $GeSe_2$ and Ge in composition we did not attempt to anneal most of these films above T_g to incude the phase separation which has been reported, [64] for example, at $Ge_{40}Se_{60}$. Thus we cannot report on the generality of this phenomenon in the chalcogen-deficient portion of the Ge-Se system. Indeed, the ordering tendency observed at GeTe in the Ge-Te system [60] contrasts with the phase separating tendency observed at GeO in the Ge-O system. [62] However, our preliminary thermal analysis of rf sputtered GeS films indicates a broad exotherm just at T_g reminiscent at the phase separation exotherm observed for evaporated GeO films.

7c. The Se-Te System

This system is of modest interest due to its inherent complexity, arising from the presence of Se_8 and $(Se\text{-}Te_8)$ copolymer rings mixed with chains in Se-rich glasses. Also, Se-Te alloys have relatively little interest for high temperature applications, as the T_g maximum is roughly 75°C at ~ $Se_{60}Te_{40}$. Another question of interest in this system is the degree of chemical ordering which would be predicted because of the significant electronegativity difference between Se and Te.[65] TeSe should thus be an ordered glass, if the Pauling criteria adequately reflect the relative Se-Se, Te-Te and Se-Te bond strengths, as calculated on p. 47 of reference 32. Evidence of ordering in crystalline SeTe has been obtained,[66] but we are unaware of any information regarding the amorphous phase. Our E_{04} and ΔE_o data for sputtered Se-Te alloys plotted vs. composition indicate no discontinuity of slope or curvature at SeTe, casting some doubt on the extent of chemical ordering at TeSe.

Category 8. Ternary and Quaternary Chalcogenide Alloys Containing Only Low Atomic Number Components, Z < 34: The Search For a Radiation Hardened Tellurium Analogue.

This Category of alloys represents an unprofitable excursion from our main investigation of glassy chalcogenide alloys, motivated by a short-lived desire to investigate potential high temperature threshold and memory alloys which contained no Te. This investigation began in the spring of 1971, when we had not yet adequately appreciated the impact of the 8-N rule with respect to covalent binding. Thus Category 8a contains

alloys with $N << 4$, which were thus highly metallic and showed no tendency to form semiconducting glasses. These ingots were placed in storage and not examined further.

Category 8b comprises alloys with $N > 4$, some of which did form glasses. In place of components such as Te, Sb and In we substituted components such as Cu, Zn and Ga, recognizing that alloys composed only of Ge, As, Se and lighter Group IV, V and VI components had very large band gaps and were essentially insulators. In effect, we were inadvertently varying $\bar{N}$, albeit in a relatively unsystematic fashion.

This investigation opened up, without answering, the question of the coordination of Group I, II, and III components in chalcogenide glasses. We now postulate, based on the observations of other investigations for the $Cd\,As_2\,Ge$[27] and As_2Se_3-Cu[26] systems, that each of these elemental constituents is tetrahedrally coordinated if covalent bonding occurs and if $\bar{N} > 4$. Of the four tetrahedral bonds, N_c are shared electron covalent bonds, where N_c is the cation valency, and the balance arise from coordinate bonds with chalcogen lone-pair electrons. This postulate requires substantial confirming evidence to establish its limitations and areas of applicability. These studies were abandoned after calculations indicated that the temperature rise accompanying short intense x-ray pulses of thin telluride films were insufficient to degrade A.S. memory devices under these conditions.

Category 9. $\bar{N}$ = 5 Chalcogen Deficient Ternary and Quaternary Alloys.

After we discovered that the T_g maxima in the Si-Te-As system lay along the line with $\bar{N}$ = 5 connecting As to SiTe , we explored the behavior of T_g in numerous other ternary and quaternary alloys having $\bar{N}$ = 5. These alloys were mostly based on the SiTe-As join with the addition of the component GeTe, although many other systems were investigated as well, including GeSe-As and GeSe-GeTe-As. All the alloys we investigated in this category have high values of T_g, ranging between 320°C - 450°C. We consider that these alloys constitute a very useful family of materials, and postulate that they may derive their enhanced thermal stability relative to slightly higher and lower values on $\bar{N}$ by the assumption of 3-fold coordination of each elemental component. This interesting hypothesis remains untested, and is discussed later in this Report in Section 2.3 where recent results of some of these investigations are presented.

Category 10. Equimolar Ternary Alloys with $\bar{N}$ = 5.

These alloys contain Group IV, V and VI compounds in equal concentrations. This category is distinguished from Category 9 because the optical and electrical properties of most of the equimolar $\bar{N}$ = 5 alloys were extensively surveyed, whereas many of the Category 9 alloys were merely synthesized and evaluated by scanning calorimetry. Furthermore, the investigations of the Category 10 alloys primarily involved sputtered film samples, while the Category 9 alloy studies primarily involved bulk glass samples. The results of some of the Category 10 alloy studies are combined with data for Category 9 and 11 sputtered films and reported in Section 2.3 of the Report.

Category 11. Equimolar Ternary Alloys With $\bar{N} = 4.33$.

These alloys contain Group III, IV and VI components in equal concentrations, and were prepared to compare and contrast the roles of Group III and Group V components in alloys of the sort $(\text{III or V})_1\text{IV}_1\text{VI}_1$.

2.3 Recent Progress in the Structure-Property Relationships for Glassy Alloy Systems

2.3.1 Introduction

This section reports some recently completed studies of binary and ternary alloys systems bearing on the question of structure-property relationships in A.S. alloys. These are the less tractable chalcogen-deficient systems, including many poor glass formers which can only be studied as sputtered amorphous films, and for which there still exist few structural guideposts. Conversely, these alloy studies break some interesting new ground, with the synthesis and careful examination of many new and relatively simple amorphous alloys which have never been previously examined.

Historically these studies represent our final excursion under this Contract into the largely uncharted waters of the physics and chemistry of amorphous semiconductor alloys. Our earlier studies focused first on the stoichiometric chalcogen-saturated alloys of the sort $GeSe_2$, As_2Te_3, etc., and upon pseudo-binary systems based on them. We then emphasized the study of the broad family of ternary and quaternary alloys which have $\bar{N} = 5$. These alloys combine glass formation with relatively high values of T_g with respect to optical gap energy, E_{O4}. In this report we show that most of these $\bar{N} = 5$ alloys fall into an orderly linear grouping of T_g as a function of E_{O4}, including the prototypical case of amorphous arsenic.

The remaining territory to be mapped out among covalently bonded

chalcogenide glasses is thus the region between $\bar{N} = 5$ and $\bar{N} = 4$, covering alloys of the sort GeTe - Ge ($4 \leq \bar{N} \leq 5$) and GaGeTe ($\bar{N} = 4.33$). As described in Section 2.2, the coordination of the chalcogen component in this range of $\bar{N}$ is not well established, and, as $\bar{N}$ approaches 4 in the II-IV and IV-VI systems, models for the chalcogen coordination include both 2-fold and 3-fold possibilities. These alloys are unfamiliar and largely unexplored and yet they appear to hold the key to understanding the properties of the entire range of amorphous chalcogenide phases containing either large amounts of a Group IV component (e.g. GeTe to Ge) or moderate amounts of Group I, II, or III components (e.g. Cu, Zn or Ga).

In the following discussion we take the unproven view that the IV-VI systems contain the Group VI component only in 2-coordinated environments, while the III-VI and IV-V-VI systems contain the Group VI component in 3-fold coordination. The GeTe-Ge discussion, which assumes that Te is in 2-fold coordination, is thus in conflict with our own earlier interpretation of the GeTe amorphous structure as an ordered analogue to the 3-fold arsenic structure.[60] We make no apology for this discrepancy of interpretation; the facts, as they have been accumulated to date, do not clearly indicate a preference for one model or the other. Further studies of this point, which are in progress, will be required.

2.3.2 Ge-rich side of Ge-Te System

In the 3rd Semiannual Report, electrical and optical data were given

for the Te-rich half of the Ge-Te binary showing that there were extrema in these properties at $GeTe_2$.[67] An explanation of these extrema was given in terms of bond strength and the structure of $GeTe_2$, with Ge and Te atoms in four and two-fold coordination, respectively. The Ge-rich half of the binary also shows strong variations of the conductivity activation energy ΔE_o and σ with composition. Figures 2.2, 2.3 and 2.4 show the variations of the optical gap, ΔE_o, and σ with composition, all evaluated at 25°C. Here ΔE_o is taken as $-\partial \ln\sigma/\partial(1/kT)$. In the case of $Ge_{80}Te_{20}$ to Ge, as indicated by the weak temperature dependence of the thermopower, ΔE_o cannot be interpreted as a true mobility gap, but only an operationally defined tanget to $\ln\sigma$. The Seebeck coefficient S vs 1/T is shown in Fig. 2.5 for the annealed Ge_xTe_{1-x} alloys. Features of these figures are:

1. σ increases as up to 10% of Te is added to Ge, i.e., from $x = 1.0$ to 0.9.
2. For annealed alloys there is a sharp increase in ΔE_o between $x = 0.8$ and $x = 0.7$.
3. The optical gap varies relatively smoothly between GeTe and Ge, although there is a shallow minimum at about $x = 0.7$.
4. The slope of the thermopower S vs. 1/T plot is significant for $x = 0.7$, but is small for $x = 0.8$ and for the low temperature portion of the curve for Ge.

Figure 2.2

Optical gaps E_{O4} and E_o at 25°C versus composition for amorphous Ge_xTe_{1-x} virgin and annealed sputtered alloy films.

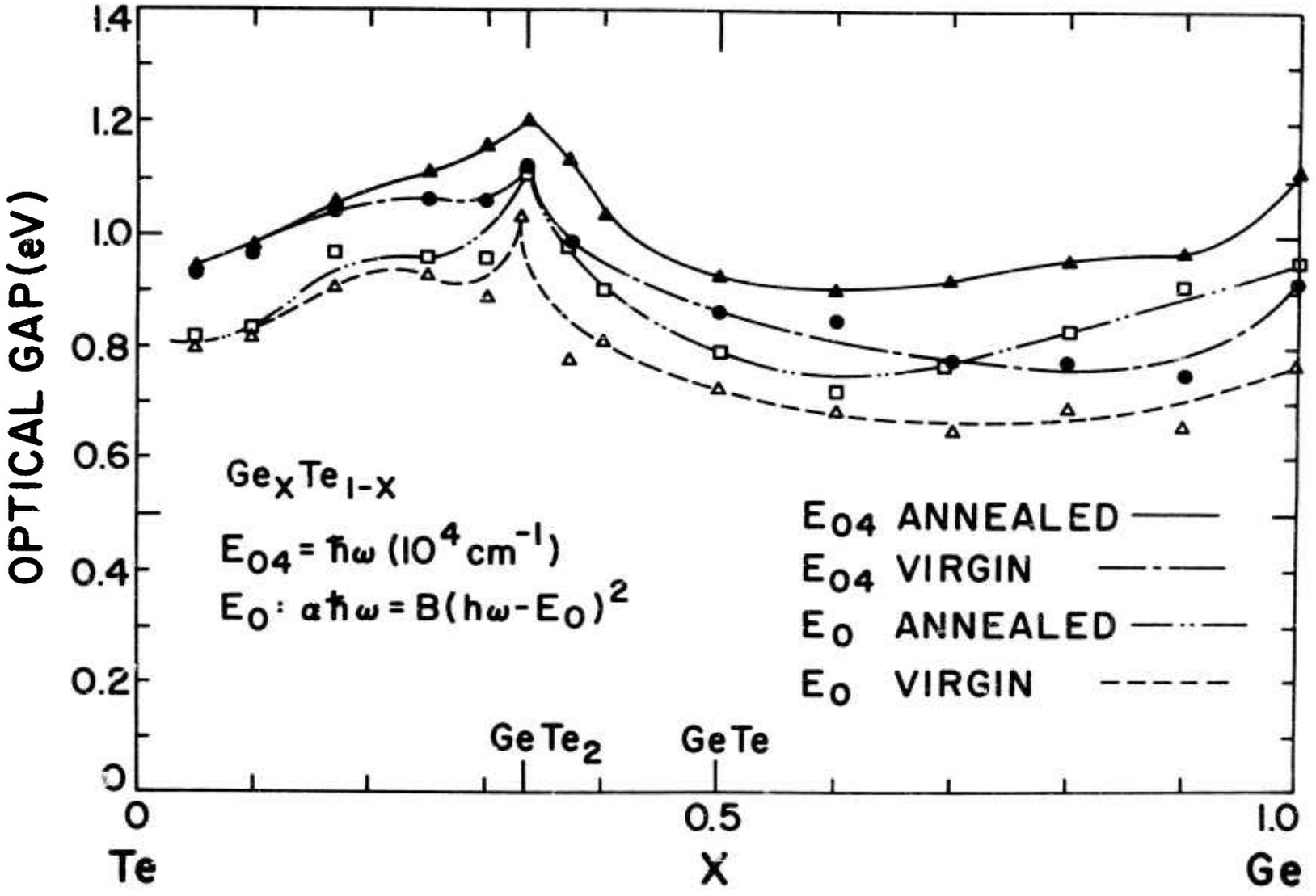
OPTICAL GAP(eV)
1.4
1.2
1.0
0.8
0.6
0.4
0.2
0
Ge_xTe_{1-x}
$E_{04} = \hbar\omega\ (10^4 cm^{-1})$
$E_0 : \alpha\hbar\omega = B(h\omega - E_0)^2$
E_{04} ANNEALED
E_{04} VIRGIN
E_0 ANNEALED
E_0 VIRGIN
$GeTe_2$
GeTe
0
Te
0.5
X
1.0
Ge

Figure 2.2

Figure 2.3

Conductivity activation energy ΔE_o versus composition for amorphous Ge_xTe_{1-x} virgin and annealed sputtered alloy films. By definition, $\Delta E_o = -\partial(\ln\sigma)/\partial(1/kt)$ evaluated at 25°C.

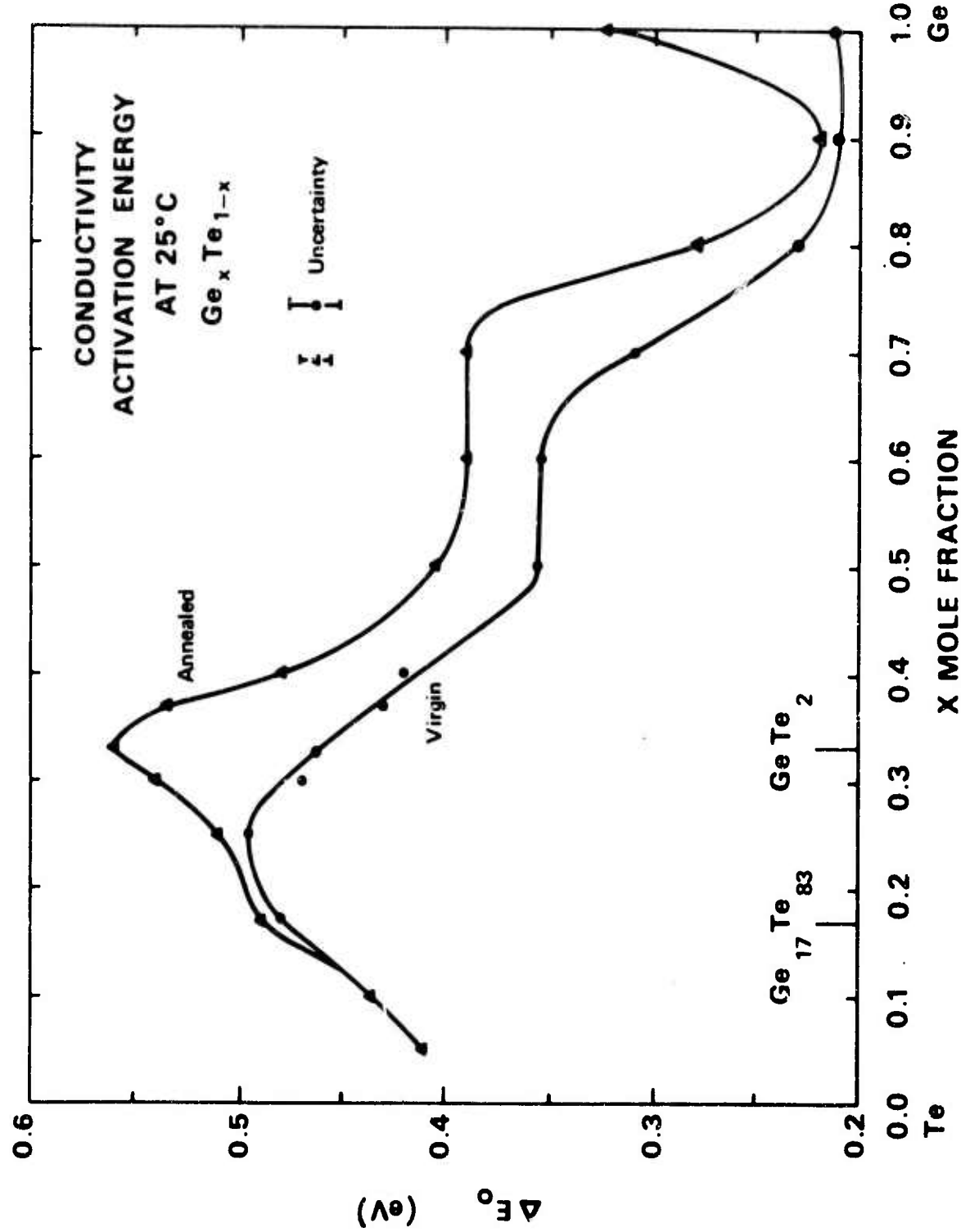
CONDUCTIVITY
ACTIVATION ENERGY
AT 25°C
$Ge_x Te_{1-x}$
Uncertainty
Annealed
Virgin
$Ge_{17} Te_{83}$
$Ge Te_2$
ΔE_o (eV)
0.6
0.5
0.4
0.3
0.2
0.0 Te
0.1
0.2
0.3
0.4
0.5
0.6
0.7
0.8
0.9
1.0 Ge
X MOLE FRACTION

Figure 2.3

Figure 2.4

Electrical conductivity at 25°C versus composition for amorphous Ge_xTe_{1-x} virgin and annealed sputtered alloy films.

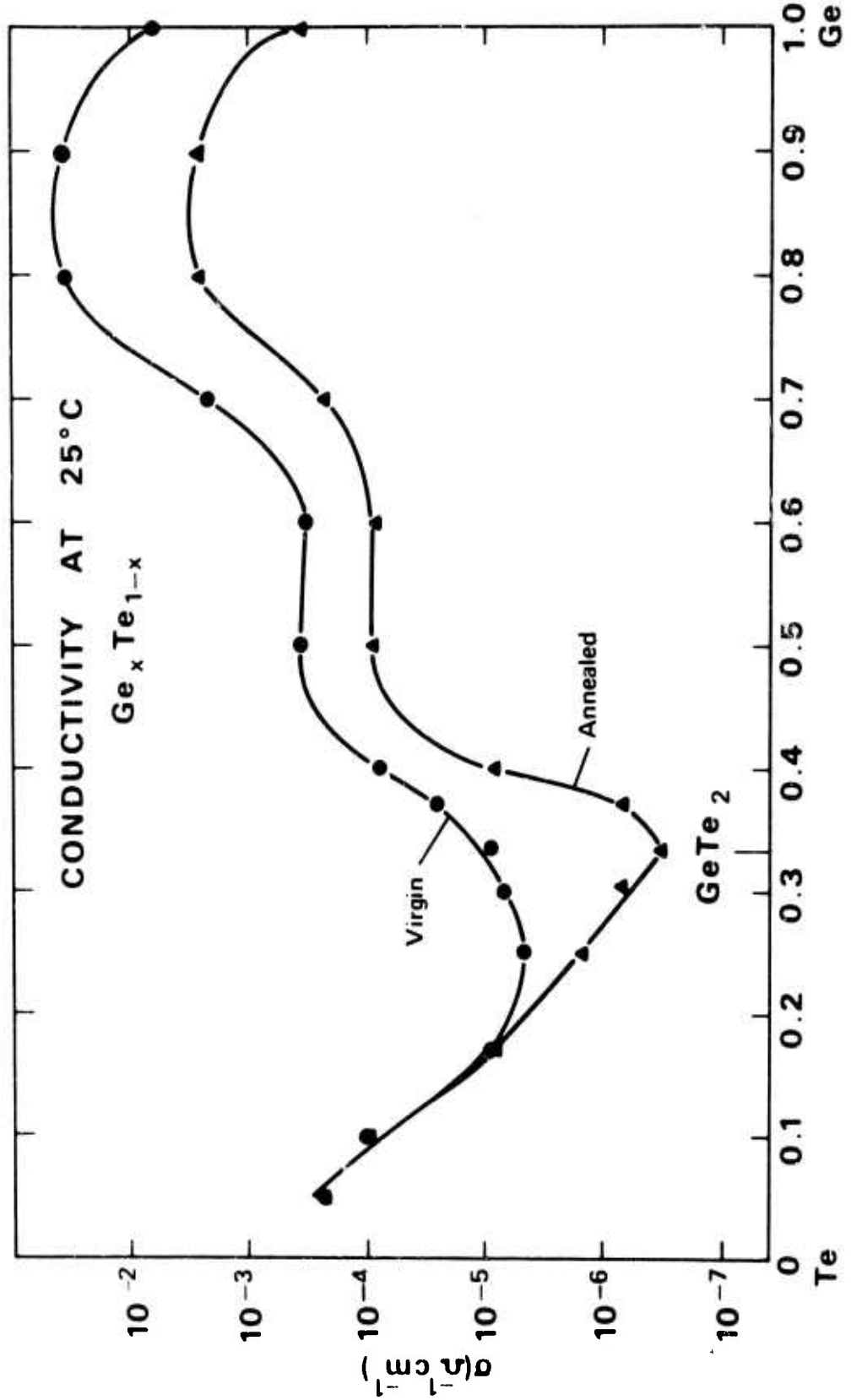
CONDUCTIVITY AT 25°C
$Ge_x Te_{1-x}$
Virgin
Annealed
$GeTe_2$
$\sigma(\Omega^{-1} cm^{-1})$
10^{-2}
10^{-3}
10^{-4}
10^{-5}
10^{-6}
10^{-7}
0
0.1
0.2
0.3
0.4
0.5
0.6
0.7
0.8
0.9
1.0
Te
Ge
X MOLE FRACTION

Figure 2.4

Figure 2.5

Thermopower S(mV/deg) versus $10^3/T$ for amorphous Ge_xTe_{1-x} annealed sputtered alloy films.

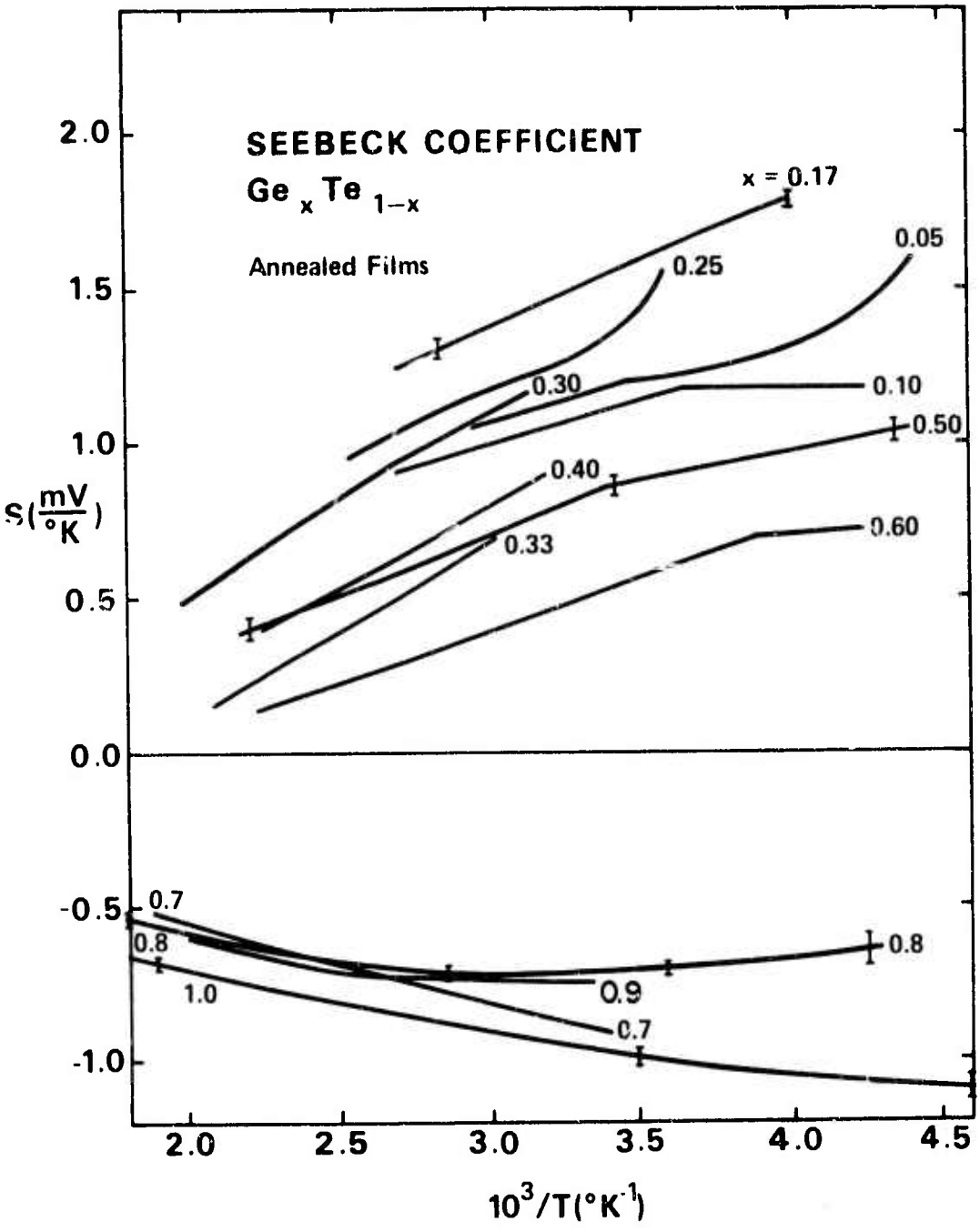
SEEBECK COEFFICIENT
Ge x Te 1−x
Annealed Films
x = 0.17
0.25
0.05
0.30
0.10
0.50
0.40
0.33
0.60
0.7
0.8
0.8
1.0
0.9
0.7
2.0
1.5
1.0
0.5
0.0
-0.5
-1.0
S(mV/°K)
2.0
2.5
3.0
3.5
4.0
4.5
10³/T(°K⁻¹)

Figure 2.5

An interpretation of these data is as follows: Transport at room temperature and below for Ge is due predominantly to hopping among localized states in the vicinity of the Fermi level. Additions of up to 20% Te to Ge increase the density of localized states by adding lone pair localized states. Hence, predominant transport for up to 20% Te is also due to hopping at the Fermi level, and σ (25°C) increases with increasing Te content over that of pure Ge.

At 30% Te, the lone pair states from the Te atoms no longer go into the solid as localized states; rather, they form part of the valence band. Further, it is important to note that materials with 30 to 100% Te apparently have much lower densities of localized states at the Fermi level than does amorphous Ge. Hence, carrier transport in these latter materials takes place predominantly in either the valence or conduction band rather than by hopping at the Fermi level. The Fermi level for these latter materials is located in the vicinity of midgap.

Pure amorphous Te has a lone pair band which is higher in energy than the bonding band; yet there is partial overlap of these bands. As Ge is added, the lone pair band continues to exist but its overlap with the bonding bands progressively increases as the composition changes from Te to $Ge_{70}Te_{30}$. At $Ge_{70}Te_{30}$, the two bands have merged and are indistinguishable. The merging of these bands, from Te to $Ge_{70}Te_{30}$, can be seen in the photoemission results of G. B. Fisher.[68] Because of this progressively increasing overlap with increasing Ge-

content, the variation of the optical gap with composition is relatively smooth except for the peak at $GeTe_2$. As predicted by Kastner,[42] a transformation from lone pair localized states to lone pair bonding states (albeit, with hybridization between the lone pair and bonding states) takes place between Ge and $Ge_{70}Te_{30}$. Nevertheless, the optical gap varies smoothly in this region because when the lone pair states merge into a band, they merge with the bonding band rather than forming a new band centered between the bonding and anti-bonding bands. Furthermore, the change of properties with composition may be a gradual transformation rather than the sharp transition suggested by Kastner. We interpret the lower conductivity at $x = 0.7$ relative to that at $x = 0.8$ to mean: 1) the former material has a much lower density of localized states in the gap, and 2) the magnitude of the thermally activated band conduction at $x = 0.7$ at $25^{o}C$, is less than that of hopping conduction at $x = 0.8$.

2.3.3 Thermal, Optical and Transport Properties of Selected Sputtered Amorphous Alloy Films.

2.3.3.1 Introduction

In Appendix II to this report can be found a summary of the relationship between T_g and E_{O4} for a variety of A.S. alloys grouped as a function of $\bar{N}$ or C. $C \leq 3$ in this summary, because most of the amorphous chalcogenide alloys crystallize below T_g for $C > 3$. We predict in that report that T_g for a fixed value of E_{O4} should increase as C increases from 3 to 4, but

this has not been proved. Furthermore there appears to exist a counter-example: T_g in the Si-As-Te system tends to peak at $\bar{N} = 5$ as the Si/Te ratio is varied for a wide range of fixed As content.[55] While E_{O4} has not been measured for most of the Si-As-Te alloys, our preliminary results[55] indicate that it is a relatively insensitive function of composition in the $\bar{N} = 5$ portion of the system and thus variations in E_{O4} seem unlikely to account for the shallow T_g maximum at $\bar{N} = 5$.

In this section we summarize some thermal, optical and transport data for a wide variety of systems including many with $\bar{N} = 5$. We also report new data on the variation of T_g with $\bar{N}$ in two systems, Cd-Ge-As and Ge-As-Se-Te, which have extensive glass forming regions embracing $C = 4$ and $C = 3$ compositions respectively. These studies were undertaken to indicate the presence or absence of T_g maxima at the $C = 4$, $\bar{N} = 4$ and $C = 3$, $N = 5$ compositions. Finally we present our preliminary T_g, ΔE_o and E_{O4} data for the $\bar{N}$ 4.33, $C = 3.66$ ternary alloys of the sort GaGeSe, etc., and compare these results with the $\bar{N} = 5$ class of alloys.

2.3.3.2 Optical, Electrical and Thermoelectric Properties.

Fig. 2.6 shows the compositional variations of the optical gap E_{O4}, the electrical activation energy ΔE_o, and the conductivity at 25°C, as arsenic is added to $(GeTe)_{0.5}$, $(GeSe)_{0.5}$, and Te, respectively. Figure 2.7 shows C and the thermopower S for the same alloys. ΔE_o is taken as $-\partial \ln\sigma/\partial(1/kT)$ at 25°C and C is the preexponential in $\sigma = C \exp(-\Delta E_o/kT)$, also evaluated at 25°C. It is necessary to specify that ΔE_o and C are

Figure 2.6

The optical gap (E_{O4}), the conductivity activation energy (ΔE_o), and the conductivity (σ) vs. composition in the $(GeTe)_{0.5}$-As, $(GeSe)_{0.5}$-As, and Te-As binaries at room temperature unannealed states (virgin, v) and the annealed states (a). E_{O4} is the photon energy at which the absorption coefficient is $10^4 cm^{-1}$. $\Delta E_o \equiv -\partial \ln\sigma / \partial(1/kT)$.

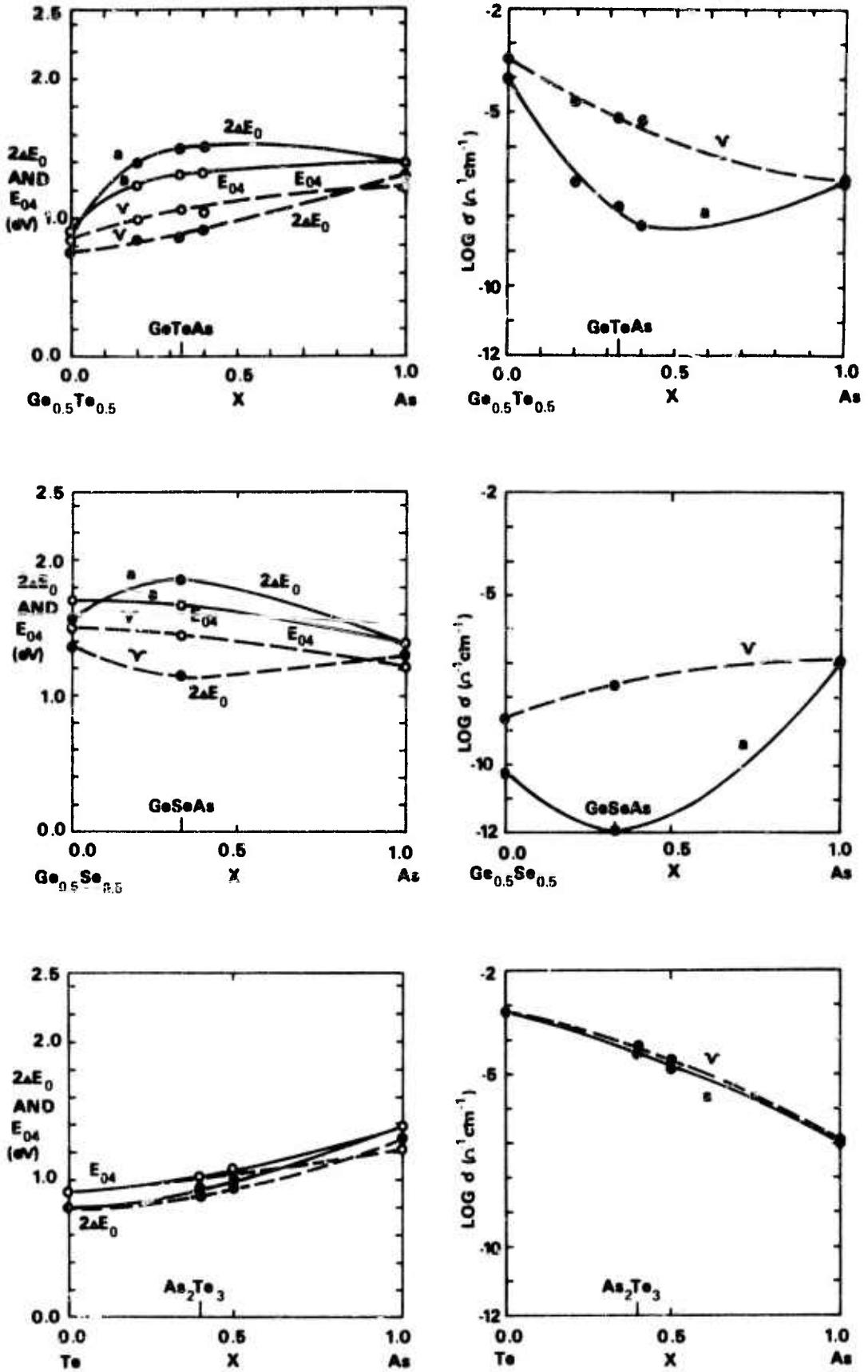
2.5
2.0
1.0
0.0
$2\Delta E_0$ AND E_{04} (eV)
$2\Delta E_0$
E_{04}
E_{04}
$2\Delta E_0$
a
b
V
V
GeTeAs
0.0
0.5
1.0
$Ge_{0.5}Te_{0.5}$
X
As
-2
-5
-10
-12
LOG σ ($\Omega^{-1}cm^{-1}$)
V
a
GeTeAs
$Ge_{0.5}Te_{0.5}$
$2\Delta E_0$
E_{04}
GeSeAs
$Ge_{0.5}Se_{0.5}$
As_2Te_3
Te

Figure 2.6

evaluated at 25°C since $\ln\sigma$ vs 1/T curves for these alloy films are generally not precisely linear, even though the conductivity is thermally activated. In all these figures solid lines represent annealed (a) alloys and dashed lines represent unannealed (virgin, v) alloys. The variations of E_{O4}, ΔE_o, and σ are relatively straightforward and require little comment. One noteworthy feature of Fig. 2.6, however, is that, except at the endpoints of the pseudobinaries $2\ \Delta E_o$ increases more upon annealing than does E_{O4}. That is, the ratio $\Delta E_o/E_{O4}$ is larger for annealed materials than for unannealed materials. We discussed this same effect earlier for sputtered amorphous $GeTe_2$-$GeSe_2$ alloys and interpreted it to mean that the Fermi level is relatively closer to the valence band in unannealed than in annealed materials. The same interpretation probably applies to the new materials described here.

Another interesting feature of Fig. 2.6 is that there are large minima in conductivity at GeTeAs and GeSeAs with respect to the endpoints for the annealed materials. These minima correspond to observed maxima in ΔE_o. These minima are nonexistent for the unannealed materials. Apparently, in sputtered alloys deposited on substrates near room temperature (or below, presumably), the properties of alloys generally are fair averages of the properties of the endpoint materials. Annealing of such alloys changes the detailed structure sufficiently to bring out interesting alloying effects such as the minima in $\sigma(25^{\circ})$. Temperature-dependent conductivity curves are shown in Fig. 2.8 for the $(Ge_{0.5}Se_{0.5})_{1-x}As_x$ alloy system.

Turning to the thermopower plots of Fig. 2.7 we see that pure amorphous arsenic is n-type in both the unannealed and annealed states. Further we note two general trends: As arsenic is added to GeTe, GeSe, or Te the materials tend to become more n-type whether in the unannealed or annealed states. Second, annealing tends to make the materials more n-type. The only exception to this rule are the materials containing about 50% or more tellurium, i.e., x = 0 in the $(Ge_{0.5}Te_{0.5})_{1-x}As_x$ system and x = 0 to 0.5 in the $Te_{1-x}As_x$ system. In these latter materials, either annealing causes no change because of the low T_g, or else annealing increases the separation of the Fermi level and the valence band, but not sufficiently to cause the material to become n-type. For the materials with less than about 50% Te, annealing also causes the Fermi level - valence band separation to increase. This increase is sufficient to make the material n-type if they were originally p-type (e.g., GeTeAs) or it makes them more strongly n-type if they were originally weakly n-type (e.g., GeSeAs). The materials showing a thermopower between about -0.5 and 0.5 mV/^{o}K probably have mixed valence and conduction band transport.

In the As-Te binary it might be considered surprising that there are no extrema in E_{O4} or other properties at the stoichiometric composition, As_2Te_3, as there are in the Ge-Te binary. However, this lack of extrema is no doubt due to the small ionicity of the As-Te bond, as indicated by the small electronegativity difference for As and Te on Pauling's[65] electronegativity scale.

Figure 2.7

Left hand column: the conductivity pre-exponential C for the $(GeTe)_{0.5}$-As, $(GeSe)_{0.5}$-As, and the Te-As binaries. C is an extrapolation to infinite temperature of the tangent at room temperature to $\ln\sigma$ vs. $1/T$.

Right hand column: The thermopower for specific compositions within the same binaries.

In both columns, broken lines represent the unannealed (virgin) materials and the solid lines represent the annealed materials.

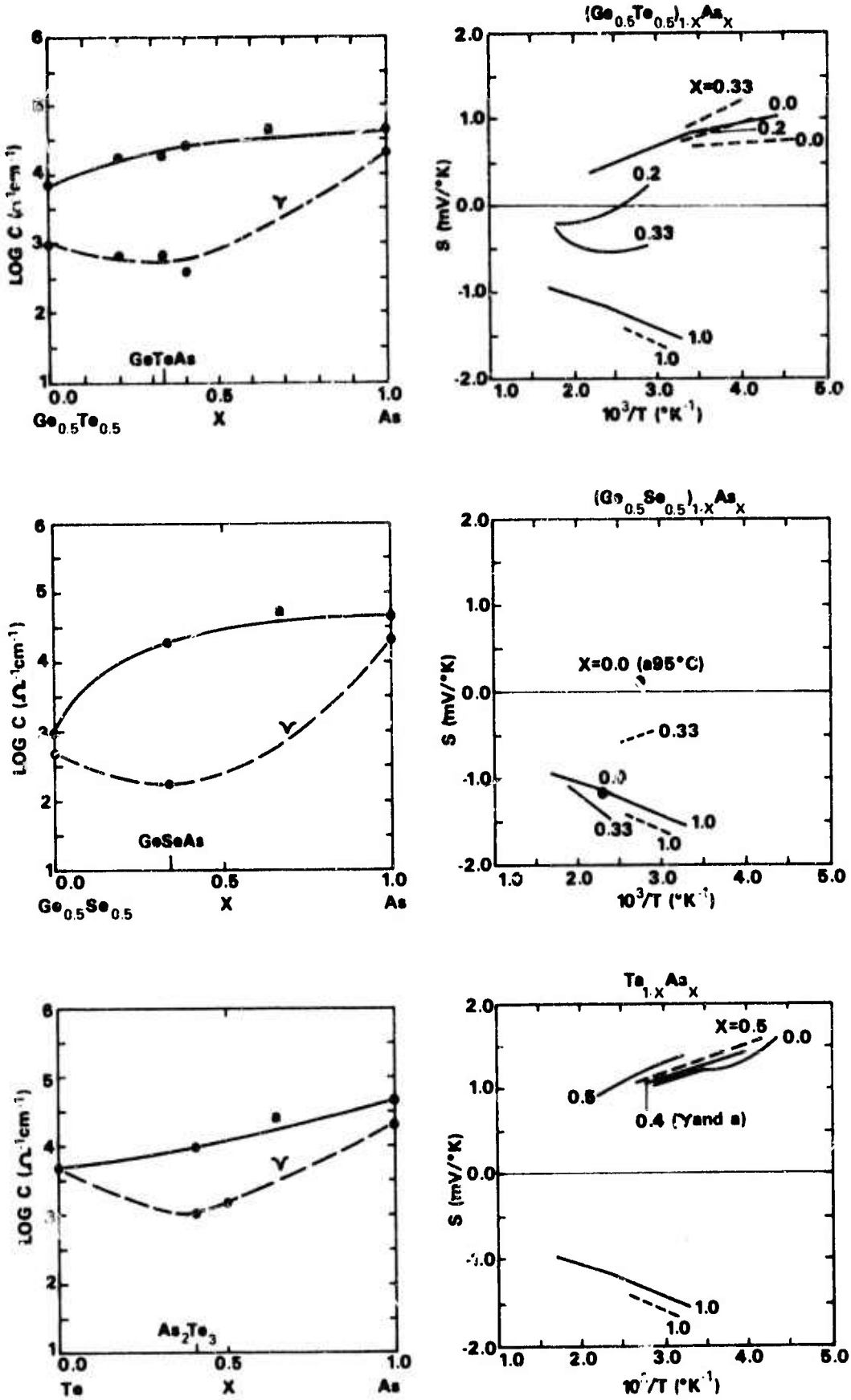
(Ge0.5Te0.5)1-XAsX
LOG C (Ω-1cm-1)
GeTeAs
Ge0.5Te0.5
X
As
S (mV/°K)
X=0.33
0.0
0.2
0.0
0.2
0.33
1.0
1.0
10³/T (°K-1)
(Ge0.5Se0.5)1-XAsX
GeSeAs
Ge0.5Se0.5
X=0.0 (a95°C)
0.33
0.0
0.33
1.0
1.0
Te1-XAsX
As2Te3
Te
X=0.5
0.0
0.5
0.4 (Yand a)
1.0
1.0

Figure 2.7

Figure 2.8

The temperature dependence of the conductivity for unannealed and annealed amorphous GeSe, GeSeAs, and arsenic.

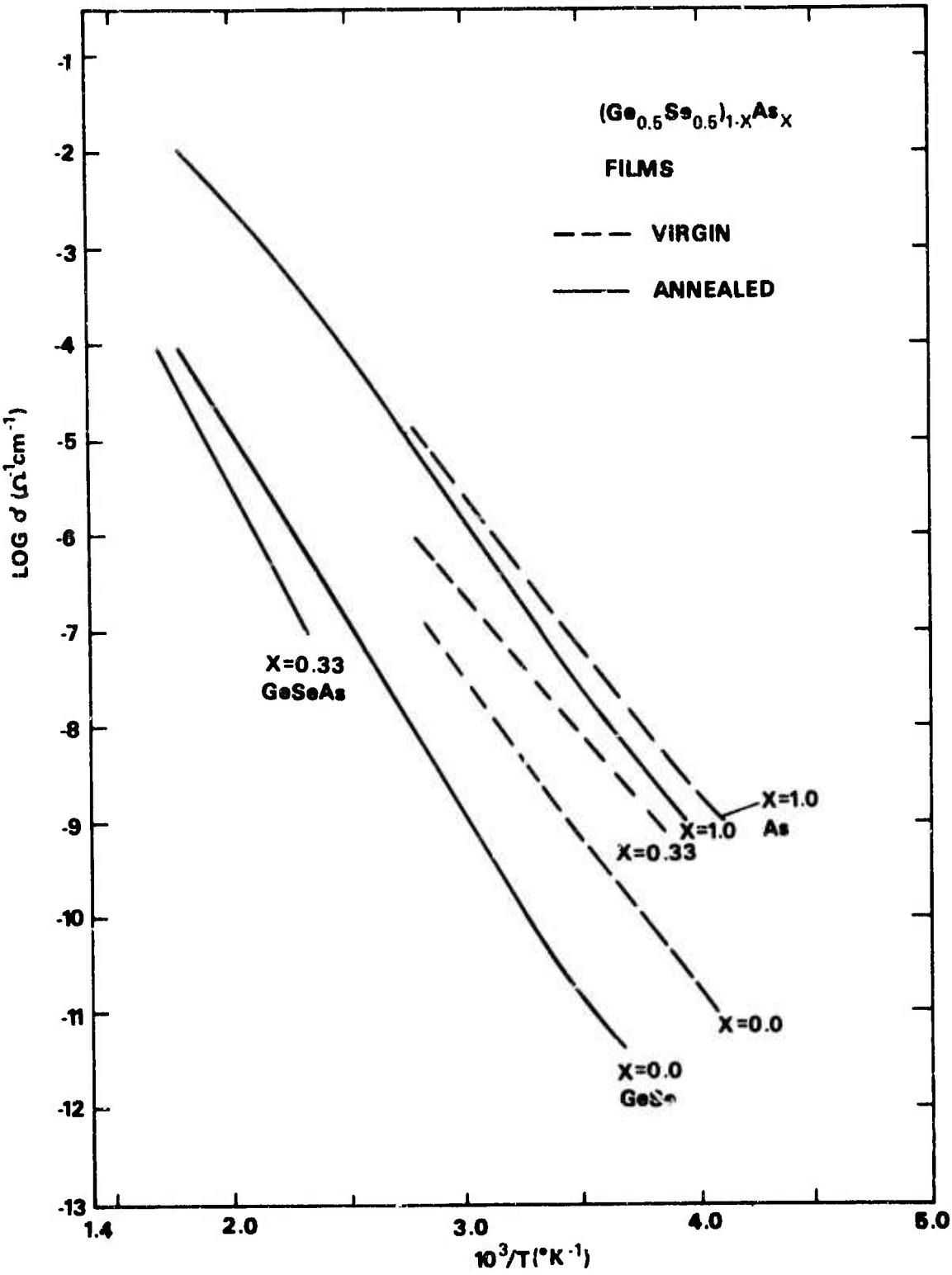
$(Ge_{0.5}Se_{0.5})_{1-X}As_X$
FILMS
VIRGIN
ANNEALED
LOG σ (Ω⁻¹cm⁻¹)
-1
-2
-3
-4
-5
-6
-7
-8
-9
-10
-11
-12
-13
X=0.33
GeSeAs
X=1.0
As
X=1.0
X=0.33
X=0.0
X=0.0
GeSe
1.4
2.0
3.0
4.0
5.0
10³/T(°K⁻¹)

Figure 2.8

Fig. 2.9 and 2.10 show the above-discussed properties as Te is replaced by Se for the $GeTe_2$-$GeSe_2$, GeTe-GeSe, and GeTeAs-GeSeAs pseudobinaries. The $GeTe_2$-$GeSe_2$ pseudobinary was treated in detail in earlier technical reports and on accompanying peprints,[48,49] but is included for comparison with the other alloy systems. For all these systems the optical bandgap and electrical activation energy increase with increasing Se:Te ratio, as expected, and the conductivity decreases.

The most salient feature of the optical and electrical data is that the annealing effect on ΔE_o and log σ is <u>much</u> greater in the system containing arsenic than it is in the other two systems. This can be related back to our discussion of Figs. 2.6 and 2.7 where we noted that ΔE_o and log σ for unannealed films of GeTeAs and GeSeAs lay on nearly straight lines between the endpoints of the GeTe-As and GeSe-As systems. In contrast, annealed GeTeAs and GeSeAs had unusually large values of ΔE_o (and small values of log σ with respect to the endpoints), yet such extrema were not seen in E_{O4}. From Fig. 2.6 we deduce that $\Delta E_o/E_{O4}$ is largest for annealed GeTeAs and GeSeAs, suggesting that the Fermi level is closer to the center of the gap between the valence and conduction bands for these particular materials than for the other materials.

The other salient feature of Figs. 2.9 and 2.10 is the general trend for a stronger n-type tendency as the Se:Te ratio increases; this is true for both the unannealed and annealed materials. Also, as similarly noted in Figs. 2.6 and 2.7, annealing increases the tendency toward n-type behavior

Figure 2.9

The optical gap (E_{O4}), the conductivity activation energy (ΔE_o), ard the conductivity (σ) vs. composition in the ($GeTe_2$)-($GeSe_2$), GeTe-GeSe, and GeTeAs-GeSeAs binaries at room temperature for the unannealed (v, broken lines) and the annealed (a, solid lines) states. E_{O4} is the photon energy at which the absorption coefficient is $10^4 cm^{-1}$. $\Delta E_o = -\partial \ln\sigma/\partial(1/kT)$.

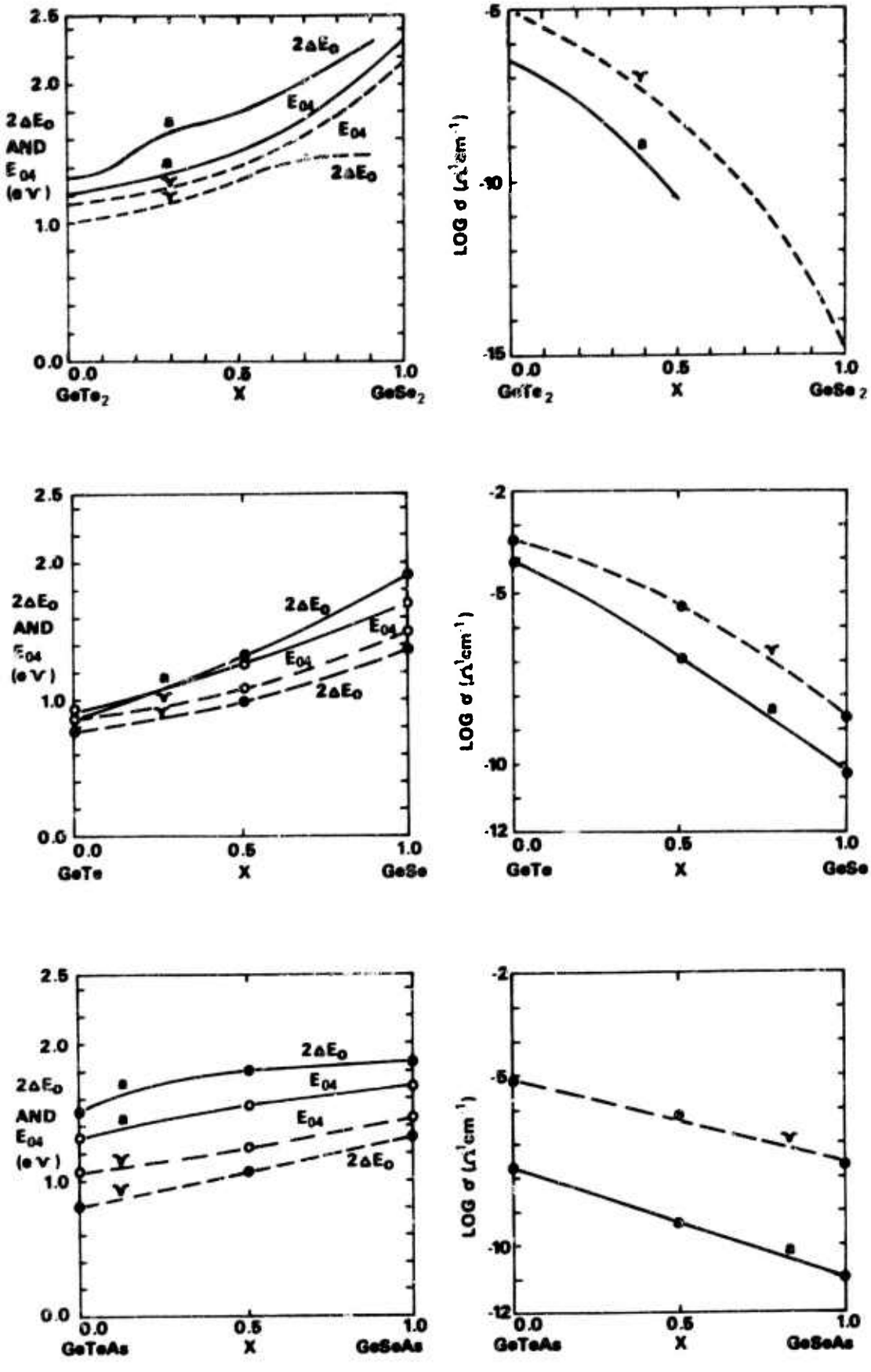
2.5
2.0
1.0
0.0
2ΔE0 AND E04 (eV)
2ΔE0
E04
E04
2ΔE0
a
a
γ
γ
0.0
0.5
1.0
GeTe2
X
GeSe2
-5
-10
-15
LOG σ (Ω-1cm-1)
γ
a
GeTe2
X
GeSe2
GeTe
GeSe
GeTeAs
GeSeAs

Figure 2.9

Figure 2.10

Left hand column: the conductivity pre-exponential C for the $(GeTe_2)$-$(GeSe_2)$, GeTe-GeSe, and GeTeAs-GeSeAs binaries. C is an extrapolation to infinite temperature of the tangent at room temperature to $\ln\sigma$ vs. $1/T$.

Right hand column: The thermopower for specific compositions within the same binaries.

In both columns, broken lines represent the unannealed (virgin) materials and solid lines represent the annealed materials.

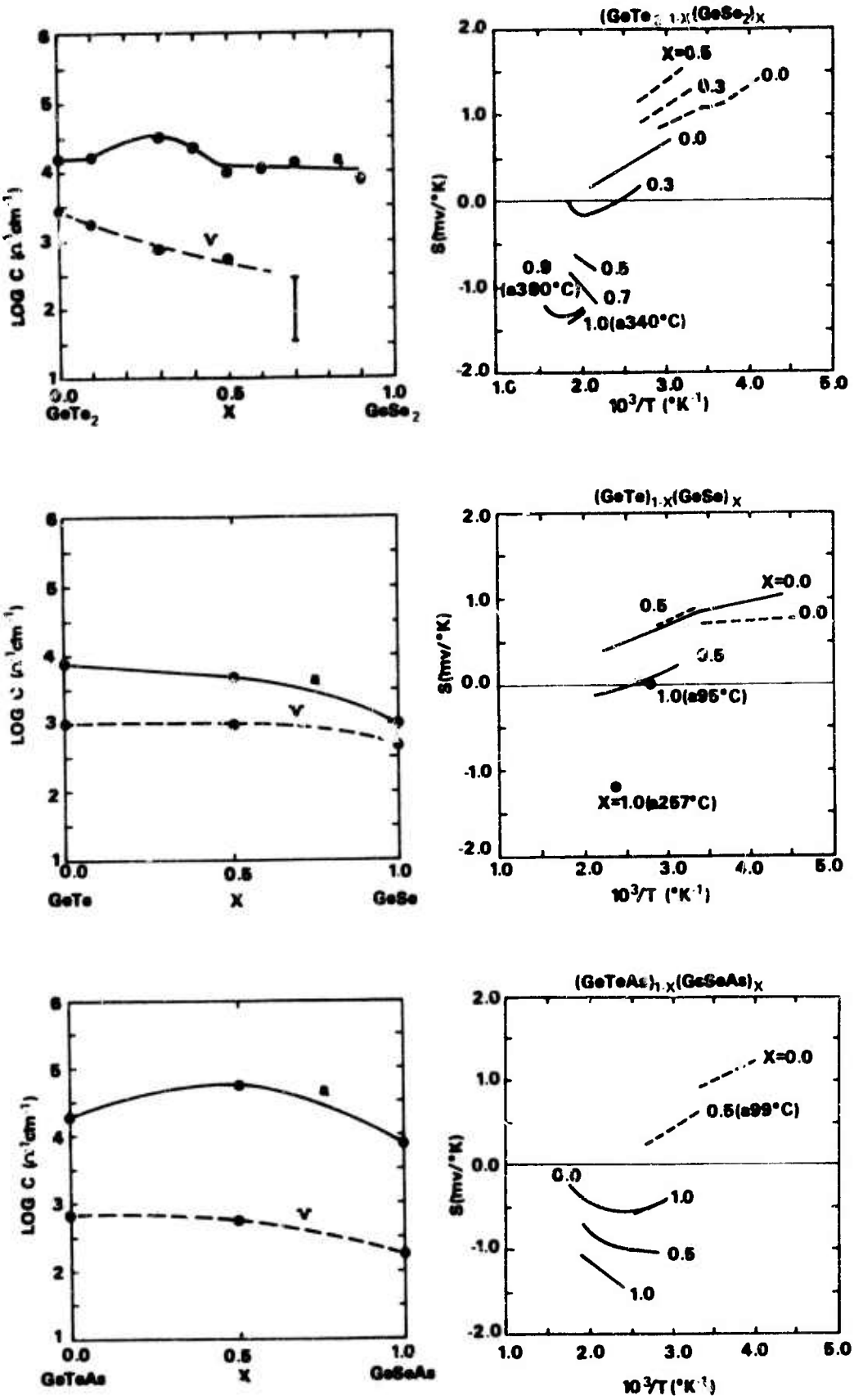
LOG C (Ω⁻¹cm⁻¹)
a
V
0.0
0.5
1.0
GeTe₂
X
GeSe₂
(GeTe)1-X(GeSe2)X
X=0.5
0.3
0.0
0.0
0.3
0.9
0.5
(a390°C)
0.7
1.0(a340°C)
S(mv/°K)
10³/T (°K⁻¹)
LOG C (Ω⁻¹cm⁻¹)
a
V
GeTe
X
GeSe
(GeTe)1-X(GeSe)X
X=0.0
0.5
0.0
0.5
1.0(a95°C)
X=1.0(a257°C)
S(mv/°K)
10³/T (°K⁻¹)
LOG C (Ω⁻¹cm⁻¹)
a
V
GeTeAs
X
GeSeAs
(GeTeAs)1-X(GeSeAs)X
X=0.0
0.5(a99°C)
0.0
1.0
0.5
1.0
S(mv/°K)
10³/T (°K⁻¹)

Figure 2.10

by reducing the positive thermopowers, increasing the magnitude of the negative thermopowers, or by changing positive thermopowers to negative.

In summary we can note several characteristics:

1. Germanium telluride and tellurium have positive thermopowers.
2. Adding arsenic and/or replacing tellurium with selenium causes a tendency toward negative thermopowers.
3. a) Annealing of films deposited on room temperature substrates causes a tendency toward negative thermopowers, provided that the total tellurium content of the alloys is less than about 50%.

   b) In all cases, aside from bringing about increases in the band gaps, annealing moves the Fermi level further from the valence band than it was before annealing.

   The only exceptions are pure arsenic and those materials which are annealed as-deposited because of low T_g's.

2.3.3.3 Thermal Properties

The variation of T_g and T_x with $\bar{N}$ along a portion of the pseudo-binary join $Ge_{80}As_{20}$-$As_{20}Se_{40}Te_{40}$ in the Ge-As-Se-Te quarternary system is displayed in Fig. 2.11. This system has an extensive volume in which glasses can be prepared by quenching of the liquid phase, and the data in Fig. 2.11 were obtained on bulk glass samples. While the T_g and T_x data could be further extended to $As_{20}Se_{40}Te_{40}$ ($\bar{N} = 5.8$), $Ge_{50}As_{20}Se_{15}Te_{15}$ ($\bar{N} = 4.8$) and lower $\bar{N}$ alloys could not be quenched to form bulk glasses.

Figure 2.11

Variation of T_g and T_x with composition and $\bar{N}$, where $\bar{N}$ is the average number of outer electrons per atom, in a portion of the pseudo-binary system $As_{20}Se_{40}Te_{40}$ - $As_{20}Te_{80}$. Only bulk glass samples were used.

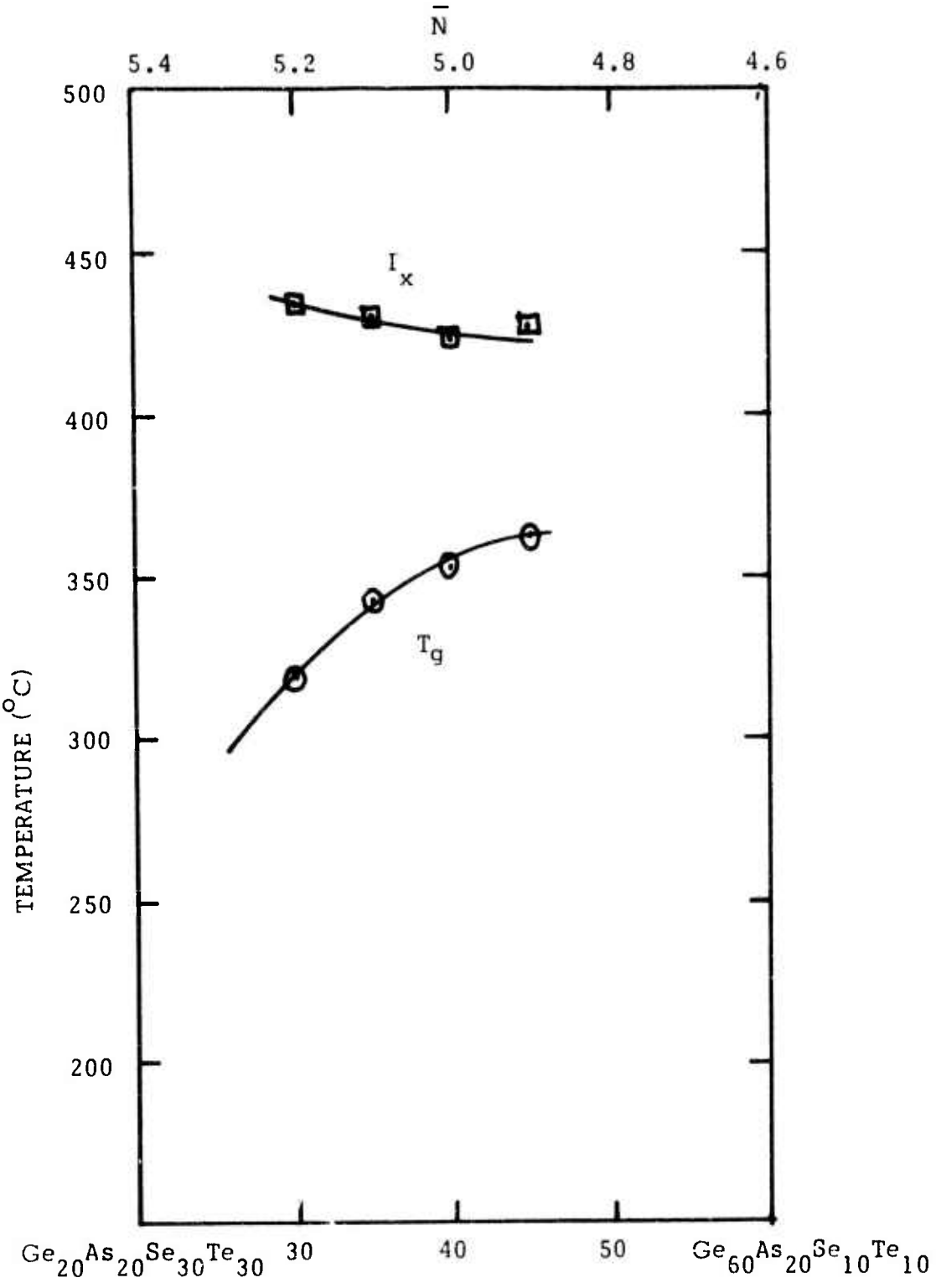
$\bar{N}$
5.4
5.2
5.0
4.8
4.6
500
450
400
350
300
250
200
I_x
T_g
TEMPERATURE (°C)
$Ge_{20}As_{20}Se_{30}Te_{30}$
30
40
50
$Ge_{60}As_{20}Se_{10}Te_{10}$
ATOMIC PERCENT Ge

Figure 2.11

We note in Figure 2.11 that T_g increases monotonically with decreasing $\bar{N}$, and thus that no T_g maximum occurs at $\bar{N} = 5$. The extension of this trend beyond $\bar{N} = 4.9$ would require sputtered film samples. Furthermore, we note that the interval between T_g and T_x decreases with decreasing $\bar{N}$, indicating a decreasing kinetic stability of the amorphous phase above T_g. Such trends have been observed in the Ge-Te and Ge-Se systems,[28] and generally lead to the condition $T_x < T_g$ when $\bar{N}$ has decreased to some particular value $\bar{N}^*$ ($\bar{N}^* = 5.33$ in the Ge-Te system, $\bar{N}^* = 5$ in the Ge-Se system). These results are in agreement with the conjectures in reference 69 regarding the dependence of T_g upon $C = 8 - \bar{N}$ but are inconsistent with our observations of T_g vs $\bar{N}$ in the Si-As-Te system, where T_g peaked at $\bar{N} = 5$.[55]

The same question arises in a different context in the Cd-Ge-As ternary system, which is unusual because easy glass formation occurs for $\bar{N} \approx 4$ whereas easy glass formation normally occurs only for $\bar{N} = 5 - 6$. In Figure 2.12 we plot T_g and T_x versus $\bar{N}$ along a portion of the pseudobinary system Cd_2Ge-As. The T_g and T_x data could not be further extended towards Cd_2Ge without sputtered samples because the alloy $As_{50}Cd_{33.3}Ge_{16.6}$ ($\bar{N} = 3.833$) and all lower $\bar{N}$ alloys could not be prepared as bulk glasses. Extension of the data towards pure As was not attempted, although the T_g of sputtered amorphous As glass is 343°C.

We were surprised by the result that a glass with $\bar{N} < 4$ could be prepared in this system, and, furthermore, that this glass had the highest

Figure 2.12

Variation of T_g and T_x with composition and $\bar{N}$, where $\bar{N}$ is the average number of outer electrons per atom, in a portion of the pseudo-binary system Cd_2Ge-As. Only bulk glass samples were used.

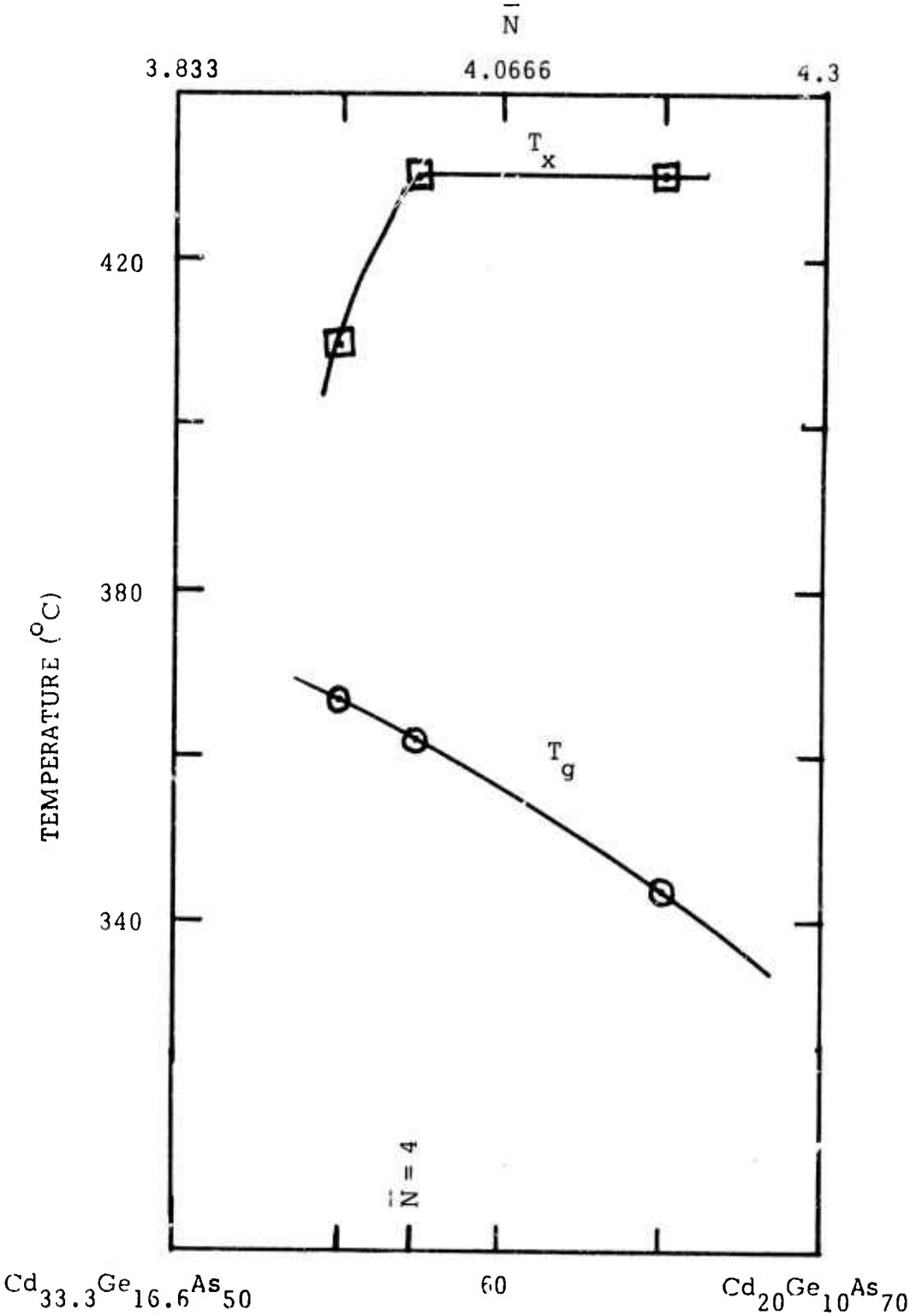
$\bar{N}$
3.833
4.0666
4.3
T_x
420
380
340
T_g
TEMPERATURE (°C)
$\bar{N} = 4$
$Cd_{33.3}Ge_{16.6}As_{50}$
60
$Cd_{20}Ge_{10}As_{70}$
ATOMIC PERCENT As

Figure 2.12

value of T_g measured along the As-Cd_2Ge join. While no electrical or optical properties of this glass were measured, it can be concluded from its high value of T_g that covalently bonded glasses can be prepared with $\bar{N} < 4$. Cd_2Ge does not form a stable crystalline compound[70] and yet its stoichiometry is suggestive of a possible ordering tendency which may only manifest itself in the amorphous phase. More work is needed to evaluate this unusual behavior.

We now turn to a comparison of some $\bar{N} = 5$ IV V VI equimolar sputtered amorphous alloys with the $\bar{N} = 4.33$ equimolar III IV VI analoges with the Group V element by the Group III element from the same row of the Periodic Table. The data for T_g, T_x and E_{O4} for these eight alloys are listed in Table 2.2. The T_g and E_{O4} data for the alloys with $\bar{N} = 5$ have been reported in reference 69 and fall along the line $T_g(^oK) = 350 + 195\ E_{O4}(eV)$ which includes amorphous arsenic. We therefore speculate that these alloys share in common with As a 3-connected network where every atom has three-fold coordination.

The $\bar{N} = 4.33$ alloys containing a Group III component have values of E_{O4} comparable to those of the Group V analogues. This result suggests that the increase in bonds per atom from C = 3 to C = 3.66 just balances the increase in the heat of atomization involved in the substitution and thus that the average bond strength is unchanged by these substitutions. Of course we would then predict that T_g should be higher for the $\bar{N} = 4.33$ alloys than for their $\bar{N} = 5$ analogues. The T_g results

TABLE 2.2 Comparison of E_{O4}, T_g and T_x for $\bar{N} = 5$ and $\bar{N} = 4.33$ Equimolar Ternary Alloys. T_a is the temperature of annealing prior to measurement of E_{O4}.

Composition		E_{O4}, eV	T_a, °C	T_g, °C	T_x, °C
$\bar{N} = 5$					
3069	AsGeSe	1.674	301	404	>500
3078	AsGeTe	1.318	302	333	383
3109	SbGeSe	1.142	271	301	358
3108	SbGeTe	0.880	217	249	263
$\bar{N} = 4.33$					
3094	GaGeSe	1.604	304	(350)	(405)
3096	GaGeTe	1.230	299		410
3095	InGeSe	1.292	300	(295)	(336)
3097	InGeTe	1.176	297		410

in Table 2.2 for the $\bar{N} = 4.33$ alloys are missing or bracketed. For the two $\bar{N} = 4.33$ telluride alloys, no T_g was observed and T_x was, indeed, significantly higher than for the two $\bar{N} = 5$ telluride glasses. or the two $\bar{N} = 4.33$ selenide alloys, T_g was only observed upon rescanning the appropriate temperature intervals; the initial scans revealed exothermic effects which are normally associated with the removal of defects by annealing. However, the substantial exotherm associated with defect annealing <u>never</u> occurs above T_g, so we must conclude that phase separation accompanied the defect removal in this instance. Therefore, the T_g and T_x values which we subsequently measured pertain to one of the separated amorphous phases and not to the homogeneous $\bar{N} = 4.33$ glass. These T_g and T_x values are thus bracketed, and should not properly be compared to those obtained on the analogous $\bar{N} = 5$ selenide glasses which displayed the normal thermal effects in the vicinity of T_g.

3. LIST OF CONTRIBUTORS

Numerous scientists and technicians have contributed to this research program over its three year history, and their contributions have been acknowledged in the Semi-Annual Technical Reports as they have occurred. This final report continues this procedure by identifying the contributions to the work reported herein.

Scientists

J. P. deNeufville

E. A. Fagen

H. K. Rockstad

Technicians

R. Flasck

R. Goss

R. S. Nowicki

D. J. Sarrach

R. Seguin

J. E. Tyler

Consultants

S. C. Moss, University of Houston

M. P. Shaw, Wayne State University

4. REFERENCES

1. S. R. Ovshinsky, Phys. Rev. Letters 21 (1968) 1450.

2. R. G. Neale and J. A. Aseltine, IEEE Trans. Electron Devices ED-20 195 (1973); M. H. Cohen, R. G. Neale and A. Paskin, J. Non-Crystalline Solids 8-10 (1972) 885.

3. J. Feinleib, J. P. deNeufville, S. C. Moss and S. R. Ovshinsky, Appl. Phys. Letters 18 (1971) 254; J. Feinleib, S. Iwasa, S. C. Moss, J. P. deNeufville and S. R. Ovshinsky, J. Non-Crystalline Solids 8-10 (1972) 909.

4. A. Ray Hilton, C. E. Jones and M. Brau, Infrared Physics 6 (1966) 183.

5. E. A. Fagen, Materials Res. Bull. 7 (1972) 279.

6. E. A. Fagen, R. S. Nowicki and R. Seguin, submitted to J. Appl. Phys. (August, 1973).

7. W. D. Buckley and S. Holmberg, (to be submitted).

8. M. P. Shaw et al., Appl. Phys. Letters 22 (1973) 114.

9. S. C. Moss and J. P. deNeufville, J. Non-Crystalline Solids 8-10 (1972) 45; Materials Res. Bull. 7 (1972) 423.

10. J. P. deNeufville, S. C. Moss and S. R. Ovshinsky, submitted to J. Non-Crystalline Solids (August 1973).

11. N. F. Mott, Advan. Phys. 16 (1967) 49.

12. Energy Conversion Devices, Proposal SP 125 to A.R.P.A. (October 20, 1969).

13. J. P. deNeufville, J. Non-Crystalline Solids 8-10 (1972) 85; H. K. Rockstad and J. P. deNeufville, Proceedings 11th International Conference on the Physics of Semiconductors (Polish Scientific Publishers, Warsaw, 1972) 542.

14. S. C. Moss and J. F. Graczyk, Phys. Rev. Letters 23 (1969) 1167.

15. D. E. Polk, J. Non-Crystalline Solids 5 (1971) 365; D. Turnbull and D. E. Polk, J. Non-Crystalline Solids 8-10 (1972) 19.

16. H. Keller and J. Stuke, Phys. Status, Solidi 8 (1965) 831.

17. G. Lucovsky and R. M. Martin, J. Non-Crystalline Solids 8-10 (1972) 185.

18. G. Lucovsky, J. P. deNeufville, F. L. Galeener, (submitted to Physical Review, 1973).

19. A. Krebs and R. Steffen, Z. Anorg. Allg. Chem. 327 (1964) 224.

20. N. J. Shevchik and W. Paul, J. Non-Crystalline Solids 8-10 (1972) 381.

21. J. Schottmiller, M. Tabak, G. Lucovsky and A. Ward, J. Non-Crystalline Solids 4 (1970) 80.

22. D. L. Evans and S. V. King, Nature 212 (1966) 1353. R. Mozzi and B. E. Warren, J. Appl. Cryst. 2, 164 (1969).

23. E. Mooser and W. B. Pearson, Progress in Semiconductors 5 (1960) 105.

34. R. W. G. Wyckoff, Crystal Structures (Interscience, New York, 1965).

25. N. J. Schevchik and W. Paul, (submitted to J. Non-Crystalline Solids); see also N. J. Shevchik, Ph.D. Thesis, Harvard University (1972).

26. K. S. Liang and A. I. Bienenstock, Bull. Amer. Phys. Soc. 18 (1973) 421.

27. L. A. Cervinka et al., J. Non-Crystalline Solids 4 (1970) 258.

28. H. K. Rockstad, R. Flasck and J. P. deNeufville, Bull Amer. Phys. Soc. 18 (1973) 454.

29. C. Lucovsky, Phys. Rev. B6 (1972) 1480.

30. Yu.V. Shmartsev et al., Refractory Semiconductor Materials (Consultants Bureau, New York, 1969).

31. J. P. deNeufville, S. C. Moss and S. R. Ovshinsky (submitted to J. Non-Crystalline Solids, August 1973).

32. Fourth Semi-Annual Technical Report, Contract DAHC15-70-C-0187, Advanced Research Projects Agency, Washington, D. C. (1973).

33. D. Turnbull and M. H. Cohen in Modern Aspects of the Vitreous State 1 (Butterworths, New York, 1960)

34. G. Busch et al., Phys. Letters 33A (1970) 64.

35. J. T. Edmond, Brit. J. Appl. Phys. 17 (1966) 979.

36. N. F. Mott and E. A. Davis, Electronic Process in Non-Crystalline Materials (Claredon Press, Oxford, 1971).

37. R. E. Drews, R. L. Emerald, M. L. Slade and R. Zallen, Solid State Comm. 10 (1972) 293.

38. R. J. F. Dalrymple and W. E. Spear, J. Phys. Chem. Solids 33 (1972) 1071.

39. M. H. Cohen, H. Fritzsche and S. R. Ovshinsky, Phys. Rev. Letters 22 (1969) 1065.

40. M. H. Cohen, J. Non-Crystalline Solids 4 (1970) 391.

41. H. Fritzsche, J. Non-Crystalline Solids 6 (1971) 49.

42. M. Kastner, Phys. Rev. Letters 28 (1972) 355.

43. T. M. Donovan et al., Phys. Rev. B2 (1970) 397.

44. J. Stuke, J. Non-Crystalline Solids 4 (1970) 1.

45. G. A. N. Connell and W. Paul, J. Non-Crystalline Solids 8-10 (1972) 215.

46. M.-L. Theye, Materials Res. Bull. 6 (1971) 103.

47. H. K. Rockstad and R. Flasck, (to be submitted to Phys. Rev. 1973).

48. H. K. Rockstad and R. Flasck, (to be submitted to Phys. Rev. 1973).

49. H. K. Rockstad (submitted to Phys. Rev. 1973).

50. H. K. Rockstad, J. Non-Crystalline Solids 8-10 (1972) 621.

51. E. A. Fagen and H. Fritzsche, J. Non-Crystalline Solids 4 (1970) 480.

52. T. C. Arnoldussen et al, J. Appl. Phys. 43 (1972) 1798.

53. H. K. Rockstad, Solid State Comm. 9 (1971) 2233.

54. First Semi-Annual Technical Report, Contract DAHC15-70-C-0187, Advanced Research Projects Agency, Washington, D.C. (1970).

55. Second Semi-Annual Technical Report, Contract DAHC15-70-C-0187, Advanced Research Projects Agency, Washington, D.C. (1971).

56. M. B. Myers and J. S. Berkes, J. Non-Crystalline Solids 8-10 (1972) 804.

57. S. R. Ovshinsky and K. Sapru, Fifth Intl. Conf. on Amorphous and Liquid Semiconductors, Garmisch-Partenkirchen, September 1973.

58. J. P. deNeufville, J. Non-Crystalline Solids 8-10 (1972) 85.

59. H. K. Rockstad and J. P. deNeufville, Proceedings 11th International Conference on the Physics of Semiconductors (Polish Scientific Publishers, Warsaw, 1972) 542.

60. J. P. deNeufville and D. Sarrach, Bull. Amer. Phys. Soc. 18 (1973) 421.

61. J. P. deNeufville (in preparation).

62. J. P. deNeufville and D. Turnbull, Discussions of the Faraday Society No.50 (1970) 182.

63. Y. Kawamoto and S. Tsuchihashi, J. Amer. Ceram. Soc. 54 (1971) 131.

64. A. Feltz et al., J. Non-Crystalline Solids 8-10 (1972) 64.

65. L. Pauling, The Nature of the Chemical Bond (Cornell University Press, Ithaca, 1970).

66. P. Boolchand and P. Surany, Phys. Rev. B-7 (1973) 57.

67. Third Semi-Annual Technical Report, Contract DAHC15-70-C-0187, Advanced Research Projects Agency, Washington, D.C. (1972).

68. G. Fisher and W. B. Spicer, J. Non-Crystalline Solids 8-10 (1972) 978.

69. J. P. deNeufville and H. K. Rockstad, Fifth Intl. Conf. on Amorphous and Liquid Semiconductors, Garmisch-Partenkirchen, Spetember 1973.

70. M. Hansen, Constitution of Binary Alloys (McGraw-Hill, New York, 1958).

APPENDIX I

1970

1. "Temperature and Pressure Dependence of the Optical and Electrical Gap in Chalcogenide Glasses"*, Proceedings 10th International Conference on the Physics of Semiconductors (USAEC Division of Technical Information, Oak Ridge), (1970), p.672, E. A. Fagen, S. H. Holmberg, R. W. Seguin, . C. Thompson and H. Fritzsche.

1971

2. "Comments on the ac Conductivity of Amorphous Chalcogenides"*, Solid State Communications 9, 2233 (1971), H. K. Rockstad.

1972

3. "A Model for Photoconductivity in Amorphous Chalcogenide Alloys", Journal of Non-Crystalline Solids 8-10, 933 (1972), T. C. Arnoldussen, R. H. Bube, E. A. Fagen*, and S. H. Holmberg.

4. "Analysis of Photoconductivity in Amorphous Chalcogenides", Journal of Applied Physics 43, 1798 (1972), T. C. Arnoldussen, R. H. Bube, E. A. Fagen*, and S. H. Holmberg.

5. "Neutron and X-ray Diffraction Radial Distribution Studies of Amorphous $Ge_{0.17}Te_{0.83}$", Journal of Non-Crystalline Solids 7, 417 (1972), F. Betts, A. Bienenstock, D. T. Keating, and J. P. deNeufville*.

6. "Structure and Electrical Characteristics of Epitaxial Palladium Silicide Contacts on Single Crystal Silicon and Diffused P-N Diodes", Solid State Electronics 15, 1131 (1972), W. D. Buckley and S. C. Moss*.

7. "Chemical Aspects of Glass Formation in Telluride Systems"*, Journal of Non-Crystalline Solids 8-10, 85 (1972), J. P. deNeufville.

8. "Atomic Transport in Liquid Chalcogenide Alloys"*, Journal of Non-Crystalline Solids 8-10, 702 (1972), E. J. Evans.

9. "Thermally Stimulated Argon Release from Amorphous Alloy Films"*, Materials Research Bulletin 7, 279 (1972), E. A. Fagen.

10. "Amorphous-Crystal Boundaries: An Artifact in Electron Diffraction"*, Journal of Non-Crystalline Solids 11, 247 (1972), S. C. Moss and P. Flynn.

11. "Thermal Crystallization of Selected Thin Films of Te-Based Memory Glasses"*, Materials Research Bulletin 7, 432 (1972), S. C. Moss and J. P. deNeufville.

12. "Thermal Crystallization of Selected Te-Based Sputtered Thin Films"*, Journal of Non-Crystalline Solids 8-10, 45 (1972), S. C. Moss and

J. P. deNeufville.

13. "Seebeck Coefficient in Amorphous Chalcogenide Films"*, Journal of Non-Crystalline Solids 8-10, 326 (1972), H. K. Rockstad, R. Flasck, and S. Iwasa.

14. "Optical, Electrical, and Thermoelectric Properties of Ge_xTe_{1-x} Alloy Films"*, Proceedings of the 11th International Conference on the Physics of Semiconductors, (Polish Scientific Publishers, Warsaw, 1972), p. 542, H. K. Rockstad and J. P. deNeufville.

1973

15. "Threshold Switching in Amorphous Semiconductor Memory Devices"*, (to be submitted), W. D. Buckley and S. H. Holmberg.

16. "Ordering Tendencies in Ge-Te Liquids and Glasses"*, (in preparation), J. P. deNeufville.

17. "Photostructural Transformations in Amorphous As_2Se_3 and As_2S_3 Films"*, submitted to Journal of Non-Crystalline Solids, August 1973), J. P. deNeufville, S. C. Moss, and S. R. Ovshinsky.

18. "Effects of DC Substrate Bias on the Properties of RF Sputtered Amorphous $GeTe_2$ Films"*, Journal of Applied Physics (submitted for publication, August, 1973).

19. "The Thermal Conductivity of Some Chalcogenide Glasses"*, Journal of Non-Crystalline Solids, (in press), R. Flasck, H. K. Rockstad.

20. "Impurity Effects on the Structure of Amorphous Silicon and Germanium Prepared in Various Ways"*, Philosophical Magazine 27, 441 (1973), S. C. Moss, P. Flynn, and L. O. Bauer.

21. "Band Level Diagram for Amorphous $(GeTe_2)_{1-x}(GeSe_2)_x$ Alloy Films"*, Physical Review (submitted for publication).

22. "The Role of Connectedness in the Relationship Between Optical Gap and the Glass Transition Temperature for Amorphous Semiconductors"*, Fifth International Conference on Amorphous and Liquid Semiconductors, Garmisch-Partenkirchen, September, 1973, J. P. deNeufville and H. K. Rockstad.

23. "Transport and Optical Properties of Amorphous $(GeTe_2)_{1-x}(GeSe_2)_x$ Alloy Films"*, (to be submitted), H. K. Rockstad, and R. Flasck.

24. "Transport and Optical Properties of Amorphous Ge_xTe_{1-x} Alloy Films"*, (in preparation), H. K. Rockstad, and R. Flasck.

25. "Electrical, Thermoelectric, and Optical Properties of Germanium - Tellurium - Selenium Ternary Amorphous Films"*, (in preparation), H. K. Rockstad, and R. Flasck.

26. "Electrical Stability of Bulk 'S-Shaped' Negative Differential Conductivity Media", IEEE Trans. Electron Devices ED-20, 593 (1973), H. K. Rockstad* and M. P. Shaw.

27. "Preswitching and Postswitching Phenomena in Amorphous Semiconducting Films", Applied Physics Letters 22, 114 (1973), M. P. Shaw, S. C. Moss*, S. A. Kostylev and L. H. Slack.

* Supported under Contract DAHC15-70-C-0187

APPENDIX II

Preprints accompanying this report:

1. "Effects of D.C. Substrate Bias on the Properties of RF Sputtered Amorphous Germanium Ditelluride Films," submitted to J. Applied Physics. E. A. Fagen, R. S. Nowicki and R. W. Seguin.
2. "The Role of Connectedness in the Relationship between the Optical Gap and the Glass Transition Temperature for Amorphous Semiconductors," Fifth International Conference on Amorphous and Liquid Semiconductors, Garmisch-Partenkirchen, September, 1973.
3. "The Thermal Conductivity of Some Chalcogenide Glasses," J. Non-Crystalline Solids, in press. R. Flasck and H. K. Rockstad.
4. "Transport and Optical Properties of Amorphous $(GeTe_2)_{1-x}(GeSe_2)_x$ Alloy Films," to be submitted. H. K. Rockstad and R. Flasck.
5. "Band Level Diagram for Amorphous $(GeTe_2)_{1-x}(GeSe_2)_x$ Alloy Films," in preparation. H. K. Rockstad.

Submitted for publication to the Journal of Applied Physics

EFFECTS OF DC SUBSTRATE BIAS ON THE PROPERTIES OF RF SPUTTERED AMORPHOUS GERMANIUM DITELLURIDE FILMS

E. A. Fagen, R. S. Nowicki, and R. W. Seguin

Energy Conversion Devices, Inc., Troy, Michigan

ABSTRACT

We have studied the changes in chemical composition, capture and release of argon, electrical conductivity, and morphology of crystallization which result from changes in DC bias applied to the substrate during the RF sputtering of amorphous thin films of nominally stoichiometric $GeTe_2$. We find (1) a strong increase of Te deficiency with negative bias, (2) a strong increase in incorporated argon content with negative bias, (3) a strong correlation between Te deficiency and argon content, (4) no dependence of argon content on film thickness, (5) violent release of argon under certain circumstances, (6) scant correlation between argon content and electrical properties, (7) slightly stronger correlation between compositional variation and electrical properties, (8) a residuum of unexplained variation in electrical properties, and (9) morphological variations consistent with departures from stoichiometry. We conclude that the rare gas content of nonreactively sputtered chalcogenide alloys is largely inactive except insofar as it determines the kinetics of its own release at elevated temperatures, but that control of substrate potential during deposition is nevertheless essential for the attainment of quantitatively reproducible transport properties.

I. INTRODUCTION

It is now generally recognized that the reduction of amorphous semiconductor technology to an exact science demands complete and careful control of every aspect of sample preparation and history, and that failure to exercise such control accounts for most if not all of the disparities between published observations on nominally identical materials. While these problems are in general less acute with chalcogenide alloy glasses than with elemental amorphous semiconductors, it is nevertheless true that even the former class of materials demands more rigorous characterization than it has hitherto received if quantitative reproducibility of properties from specimen to specimen and laboratory to laboratory is to be achieved. The present study forms a portion of a continuing exploration of the effects of deposition parameters on the properties of non-reactively sputtered thin films of chalcogenide alloys, in order that the choice of these parameters may be put on a rational basis and reduced to routine. Previous portions of this research program, largely unpublished,[1] have examined the effects of substrate temperature, sputtering rate, and sputtering pressure on the properties of technically useful alloys near the eutectic composition of the Ge-Te binary system. In the present investigation we have focused on the effects of DC bias applied to the substrate during deposition. In essence, this important parameter controls both the kinetic energy and charge state of atoms bombarding the substrate. Thus it can profoundly influence the short-range

ordering, conformation, morphology, or impurity content of deposited films, and through these their optical, magnetic and transport properties, as has been abundantly demonstrated in the case of elemental metals.[2-13] In the case of alloys and compounds it can in addition affect the composition, with still further consequences for their measured properties.[10,14]

As work on the chalcogenide alloys progressed, it soon became apparent that the principal effects of bias variation (at least within the range defined by other, fixed, parameters of deposition[4,15,16]) were to vary the degree of departure from the nominal composition and the amount of argon gas incorporated in the film in roughly comparable amounts. This proved so interesting in itself that it thenceforth seemed more sensible to regard composition and argon content rather than DC bias as the primary independent variables, and the electrical and morphological properties as derived or dependent quantities. This point of view has been adopted in much of the description which follows. In particular, we have addressed the problem of the correlation (if any) between the argon content and other properties of our films, in response to the lingering suspicion that uncontrolled variations in argon content are the cause of many otherwise inexplicable discrepancies.[17] In this connection we have made extensive use of a new diagnostic technique, thermally induced argon release, which yields information not merely about the total argon content but also about the detailed mechanisms of its desorption.

Apart from this, we have not attempted any description of our observations in terms of the atomic mechanisms which underlie them. We believe that this phenomenological approach presently offers the best hope of embracing the wide variety of behavior exhibited by amorphous semiconductors, and bringing their characterization to the standards of completeness and accuracy set by crystalline semiconductors.

II. SAMPLE PREPARATION AND CHARACTERIZATION

The amorphous alloy $GeTe_2$ was chosen as the subject of this investigation because of the extensive study which has already been devoted to its electrical, optical, thermal and structural properties, and their variation with composition in the neighborhood of stoichiometry.[18,19] The fact that many of these properties exhibit a local maximum or minimum at the stoichiometric composition seemed to provide assurance that small departures from stoichiometry would be immediately visible. In retrospect, it might have been more useful to choose a region of the binary system in which these properties vary rapidly but monotonically, so that the sign as well as the magnitude of the compositional shift might be discerned on sight.

A sputtering target 8.9 cm. in diameter was hot-pressed under inert gas cover from vacuum-melted constituents of "five 9's" purity.

This was mounted in a Mathis SP-310 RF diode sputtering assembly atop a conventional oil-pumped vacuum system with liquid-nitrogen cooled chevron baffle. Background pressure before throttling was of order 2×10^{-6} torr. Power was supplied by a Mathis Mark III RF generator and matching network operating at 13.56 MHz. All other deposition parameters were fixed at values empirically determined through previous experience to yield stable and reproducible films of high quality, without regard for compositional accuracy or argon content. The target-substrate spacing was 3.5 cm. Substrate temperature was limited to a maximum of $45^{\circ}C$ under all conditions of operation. Normal sputtering pressure was 6 millitorr of UHP argon. The matching network was tuned to an indicated 700 V rms of RF, giving an average power of 30 W, or a power density of approximately 0.5 W/cm^2 at the target face. The average DC component of the applied RF was 750 V, varying slightly with substrate bias. The resultant deposition rate varied from 21 to 32 nm/min., with larger values corresponding generally to more positive substrate bias. Throughout the entire sequence of runs no parameter was changed excepting the bias voltage and the duration of the run. In every instance the target was first stabilized or "seasoned" by sputtering against a closed shutter for 30 minutes. After deposition the bell jar was backfilled with UHP argon and the substrates were quickly

removed to a desiccator to be stored until needed.

In order to ensure that the active surface of the growing film was truly equipotential, it was found necessary to coat the substrates (Corning 7059 glass) with approximately 100 nm. of previously sputtered molybdenum. In the case of specimens intended for mass spectrometry this coating was continuous. In the case of specimens intended for electrical conductivity measurements this coating was divided into two coplanar interdigitated electrodes by a serpentine gap 0.31 mm. wide and 31 cm. long. Subsequent optical microscopy of the crystallized films (to be described more fully below) established that there was no significant potential variation across the width of this gap. In either case, DC bias from a heavily bypassed power supply was applied directly to the molybdenum with spring clips which served also to hold the substrates in position. The range of applied bias was restricted to $\pm$ 10% of the average DC component of the applied RF, in order not to perturb the plasma too greatly. Bias more negative than -75 V led to substantial reemission from the substrates, and drastically reduced the deposition rate. Positive bias larger than +75 V could be tolerated if precautions were taken to prevent shorting of the substrate-anode insulation.

Table I gives the physical characteristics of all samples in the principal series of runs in this study. Note that a zero entered in the

second column signifies a grounded, not a floating, substrate. Additional runs, not tabulated, were made under substantially identical conditions in order to provide samples for other diagnostic techniques. Film thicknesses were measured with a Sloan Dektak and confirmed with a Watson interference microscope. The fifth column gives the germanium content as determined by electron microprobe analysis, normalized such that tellurium constitutes the balance. Inasmuch as bulk glassy $GeTe_2$ cannot be prepared by quenching from the melt,[20] it was necessary to standardize the microprobe data with respect to the composition GeTe. This led in turn to certain problems of interpolation which forbid assigning absolute accuracy higher than 1% to compositions determined in this fashion. Repeated readings on the same specimen, however, yielded determinations differing by only 0.2%, suggesting that the relative or internal accuracy of the data is much higher. Finally the sixth column gives the total argon content of the sample, here expressed as atoms per atom of glass, in percent. This was determined by heating the sample to exhaustion in a residual gas analyser and integrating the resultant argon ion current, in a manner to be described more fully below. Rather large limits of uncertainty ($\pm$20%) must be ascribed to this column too, owing to uncertainty in some constants of the computation. Here again, however, the internal consistency and reproducibility of the data appear to be substantially higher, as may be judged by comparison of the results

for nominally identical specimens.

In Figs. 1(a) and 1(b) the composition and total argon content of our samples are displayed explicitly as functions of bias voltage. Note first that there exists a plateau extending from 0 to +50 V in which the composition is sensibly independent of bias. Unfortunately the composition within this plateau does not coincide with stoichiometry, contrary to what one might expect from consideration of local ordering tendencies[18]. In view of the somewhat arbitrary normalization procedure described above, we are unable to state whether this discrepancy is an artifact of data reduction or real, and if real, how it originates. In any event the composition clearly departs in the direction of tellurium deficiency at negative bias, and germanium deficiency at high positive bias. We tentatively interpret the former effect as the preferential resputtering of tellurium, owing perhaps to its smaller atomization energy. We are unable to propose a comparable mechanism for germanium deficiency. The total argon content, on the other hand, exhibits a shallow minimum in the neighborhood of +25 V. Following Winters and Kay,[4] we attribute the rise of argon content with negative bias to the implantation of energetic Ar^+ ions accelerated through the bias potential, and the substantially bias-independent portion of the curve to the embedding of energetic neutrals which have escaped thermalization within the plasma. Note that the chosen range of DC bias produces approximately a sixfold variation in argon content.

The qualitative resemblance between Fig. 1(a) and Fig. 1(b) suggests plotting argon content directly against composition. The result is shown in Fig. 2, and it can be seen that there is indeed a high degree of correlation. It is tempting but improper to conclude from this correlation that there exists a microscopic connection between the mechanism of argon incorporation and the mechanism of tellurium resputtering, e.g., perhaps argon atoms take up residence predominantly in tellurium ion vacancies. The discussion of this appealing conjecture cannot be undertaken, however, until more is known about the character of molecular complexes in amorphous chalcogenide films.

III. EXPERIMENTAL RESULTS

1. Thermally Induced Argon Release

The determinations of total argon content discussed in the previous section are merely a byproduct of a much more elaborate and informative diagnostic technique, the technique of thermally induced argon release or argon effusion analysis.[21] We applied this technique to all samples listed in Table 1. The specimen is placed in a continuously pumped high vacuum oven and heated at a uniform slow rate. Argon is progressively liberated from it, and is detected with a residual gas analyser tuned to 40 amu. The resultant plots of argon partial pressure vs. oven temperature are rich in structure, and can be correlated with various stages in the thermal

decomposition of the film. Moreover, the area under the partial pressure curve up to any temperature is proportional to the argon released up to that temperature; the constant of proportionality can be evaluated by leaking argon into the vacuum system at a known rate. Thus the total argon content can be determined by heating the sample to exhaustion and integrating the entire curve, and the fraction of that total associated with any chosen temperature interval or thermodynamic phase can be determined by partial integration.

Before presenting the results of these tests, however, it is important to clarify certain technical points which bear on their interpretation. Note first that the manner in which the sample is contained profoundly affects the shape of the argon release curve. In prior work[21] the sample was mechanically scraped from its substrate and loaded into a Knudsen cell. If the cell orifice is sufficiently small, quasi-equilibrium is maintained between condensed and vapor phases as heating proceeds. This yields a curve well suited to comparison with equilibrium phase diagrams and with measurements on other closed systems, e.g., to scanning calorimetry on specimens sealed in capsules. On the other hand, because substantial quantities of argon can be retained in crystalline phases, argon release tends to be delayed until these crystals melt, and drops to exhaustion only as the last liquid evaporates. In the present study it was found to be both simpler and more

instructive to omit the Knudsen cell, merely placing the intact substrates in an externally heated quartz tube furnace of large diameter. (Of course it must be established through ancillary experiments that the substrates themselves contribute no argon release.) In this open method there is no quasi-equilibrium. Every molecule freed from the surface of the film is promptly pumped away. Thus the argon retained in each phase is progressively exhausted as that phase sublimes. This has the effect of enhancing the structure of the release curve at low temperatures in multiphasic materials, and renders interpretation much less difficult. Total argon content determinations by the two methods are in satisfactory agreement, despite the very different shapes of the release curves.

Regardless of whether the closed or open method is chosen, it must be recognized that the technique is essentially a dynamic one, like scanning calorimetry, and unavoidably mixes together the effects of temperature and rate-of-change of temperature. In general, the smallest heating rate which yields adequate signal from the residual gas analyser is to be preferred. With an Associated Electrical Industries (U.K.) model MS-10 mass spectrometer, a residual argon background pressure of order 10^{-10} torr, a pumping speed of order 100 liters/sec, and specimen masses of order 10 mg, we have obtained a range in excess of four decades at heating rates of 5 to 10 deg/min. The accuracy of temperature measurement in our apparatus at these heating rates was

confirmed by calibration at the melting point of lead.

Figure 3 shows in detail the argon release curves for a sequence of seven specimens sputtered at different values of DC bias, but otherwise similar, i.e., the first seven rows of Table 1. For reasons which will become apparent shortly, comparison between these curves is strictly valid only when all specimens have precisely the same mass and surface-to-volume ratio. Inasmuch as we used always the same area of film throughout this sequence of runs, and the thicknesses are not precisely equal, we attempted to adjust the heating rate in each case so that the product of rate and specimen mass (on which the partial pressure depends) had a substantially constant value. The remaining slight differences have been left unnormalized, and are of no consequence on the scale of presentation in Fig. 3.

Basically, each curve contains four major regimes, as shown in the insert portion of Fig. 4. Roughly speaking, each regime consists of a rising portion followed by a rather more abrupt decline, and may be associated with a dominant mechanism of argon release. Thus regime I represents the thermal diffusion of argon on an atomic scale through the homogeneous glass, and presumably reflects the loss of free volume as the glass attains its equilibrium state; i.e., annealing. This regime terminates somewhat below the glass transition temperature, 220°C, determined independently by scanning calorimetry.[18] A few degrees

above this, phase separation occurs as Te and GeTe crystallites begin to nucleate almost simultaneously from the liquid. This is accompanied by a narrow and often noisy burst of argon release denoted as regime II. We believe that in this regime the crystallites serve as nuclei for macroscopic argon bubbles; and indeed such bubbling has often been seen optically under a hot stage microscope at these temperatures. Other possible explanations for this peak include rejection of argon into the remaining liquid by the crystalline phases, perhaps combined with an abrupt increase in diffusion coefficient at the glass transition temperature. We find these alternative mechanisms of argon release less plausible, however, because the former fails to explain why the peak grows at large negative bias, while the latter fails to explain the valley between regimes I and II at positive bias. Regime III is identified with the evaporation of crystalline Te, as suggested by the first appearance of silvery deposits on the walls of the tube furnace. There appear to be two or more unresolved peaks within this broad regime, for whose occurrence we can presently offer no explanation. This regime ends at the eutectic temperature, 385^{o}C, or a little below. Above this temperature only GeTe crystallites remain. They too evaporate, liberating their argon content and giving rise to Regime IV. The exponential slope of this regime, one of the more stable features of the entire family of curves, corresponds to an

activation energy of about 1.8 eV, in good accord with the measured heat of vaporization of GeTe.[22] It must be acknowledged, however, that an activation energy of order 2 eV is characteristic of many other argon sorption processes as well,[23] so that this observation is by no means decisive. Finally, at about 475°C, the thermal decomposition of the sample is complete, and the argon partial pressure drops precipitously to the background level. Subsequent X-ray diffraction of the specimen shows only residual traces of crystalline Ge clinging to the substrate. It may be remarked that at no time in the entire sequence of events do the crystalline phases melt, in contrast to the situation when a Knudsen cell is employed.

Clearly, the most interesting aspect of this family of curves is the manner in which their proportions change with DC bias. This is shown explicitly in Fig. 4, where the total argon content [i.e., Fig. 1(b)] is decomposed into partial contributions from each regime. For zero and positive bias, regime IV (=GeTe evaporation) contributes an almost constant 38% of the total, and regime III (=Te evaporation) an almost constant 60% of the total, with the small remainder divided between regimes I and II. As the bias becomes increasingly negative the contribution from regime IV remains approximately constant; that from regime III first grows, then shrinks; and that from regime II

(= bubbling) grows enormously, being nearly 300 times as large at -75 V as at 0 V. At no time does the contribution from regime I (= diffusion) exceed 1% of the total argon content or 0.01 atom-percent in absolute magnitude.

Several conclusions of practical importance may immediately be drawn from these results. Although these inferences rest primarily on our experiences with amorphous germanium ditelluride films, they would seem to apply to other chalcogenide alloy glasses as well. First, it is evidently impossible to anneal out the majority of incorporated argon from a thick sputtered film in any reasonable length of time at temperatures below crystallization. The mechanism of release by diffusion is far too slow.[15] In order to minimize argon content it is necessary to prevent its incorporation in the first place, through appropriate choice of deposition parameters. As a corollary, it seems extremely unlikely that any form of conductivity annealing can be caused by argon desorption, inasmuch as more than 99% of the argon still remains in the specimen at the annealing temperature. We shall return to this point in our later discussion of electrical conductivity. Finally, it should be noted that the mechanism of release by bubble nucleation can be a non-trivial source of mechanical disruption of the film. A mole of argon at STP occupies roughly a thousand times the volume of a mole of $GeTe_2$. Thus an argon content of, say,

1 atom-percent, suddenly aggregated into bubbles occupying, say, 3% of the volume of the solid, exerts a pressure of several hundred atmospheres. This is a conceivable mode of failure in thin film devices whose operation depends on an amorphous-to-crystalline phase transition, and in which the argon content of the film is sufficiently high that bubble nucleation constitutes the dominant mode of release. We have on occasion observed catastrophic mechanical failure of certain experimental thin film devices for which this seems the most probable explanation.

Another question of interest is whether the argon content is uniformly distributed throughout the volume of the film. We investigated this by varying only the duration of the sputtering run, with all other deposition parameters fixed. This produced the sequence of runs tabulated in the last five rows of Table 1. It can be seen that over a range of nearly 60:1 in thickness the total argon content does not vary outside the experimental uncertainty. Thus it appears that the process of argon incorporation quickly reaches and thereafter maintains a steady state during deposition, in agreement with the observations of Hoffmeister and Zeugel,[15] but contrary to those of Schwartz and Jones.[16] The argon release curves pertaining to this sequence of runs are shown in Fig. 5, and contain additional information of interest. Note that some features of the curves are stationary, whereas others progress toward higher temperatures as the thickness increases.

For example, the little blip at about 245°C, which is all that remains of the bubbling regime at zero bias, is locked to the onset of crystallization, which is surface nucleated and therefore independent of thickness. Only in the thinnest specimen does this regime occur at lower temperature, owing perhaps to additional nucleation at the film substrate interface. Regimes III and IV, on the other hand, are due to evaporation, and therefore proceed more slowly when the surface-to-volume ratio of the specimen is small. This in turn varies inversely with thickness because in the present sequence we adjusted the area of the specimen so as to maintain roughly constant mass. Hence these regimes are progressively displaced to the right as thickness increases. At first glance the uppermost curve, on the thickest specimen, appears to be anomalous. We think that in this instance the film cracked or fragmented from thermal stress at about 350°C - a not unusual occurrence in thick films - causing an abrupt increase in surface-to-volume ratio and thus evaporation rate. There is even a hint of the development of this peak in the previous (8 μm.) curve. All in all, this sequence of runs provides welcome support for the interpretation we have made of the previous sequence. It is particularly gratifying, in terms of confidence in the technique of thermally induced argon release, that the computed argon content appears to be independent of the mass of the specimen and the shape of the release curve.

2. Electrical Conductivity

Electrical conductivity measurements were also made on one specimen from each of the seven sets of bias-sputtered substrates whose argon release curves are shown in Fig. 3, plus additional specimens at the extremes of bias. A dry nitrogen ambient was used to retard surface contamination, and heating rates were restricted to ca. 3 deg/min. A representative result is shown in Fig. 6, taken from run SI-363. The conductivity of the as-deposited film (labelled "virgin" in Fig. 6) is thermally activated to first approximation, with only slight upward curvature. The prefactor obtained by extrapolation to infinite temperature lies between 10^3 and 10^4 $(\text{ohm-cm})^{-1}$. On approaching the glass transition temperature the conductivity anneals downward to a new thermally activated portion, with substantially the same prefactor. This annealed branch of the curve can now be reversibly traversed at all lower temperatures. (Recall that this large change occurs while more than 99% of the total argon content remains in the sample.) At slightly higher temperatures, however, crystallization ensues, causing the conductivity to rise abruptly about four decades. The crystallized branch of the curve can now be reversibly traversed. Note that there exists a narrow but nevertheless genuine temperature interval between the glass transition and the onset of crystallization for stoichiometric $GeTe_2$.[18] A slight degree of germanium enrichment causes this interval to vanish entirely; i.e., crystallization supervenes before annealing is complete. This leads to some ambiguity in the meaning of "annealed" with respect to our most negatively biased specimens; in such cases we take it to mean the state of lowest conductivity attainable by heat treatment.

Inasmuch as the effects of DC bias on the conductivity are not very great, we have found it more useful to characterize these curves numerically than to present them graphically. We do this in terms of five numbers, operationally defined as shown in Fig. 6: the conductivity and its apparent activation energy at room temperature in the virgin state, the same quantities in the annealed state, and the temperature of the onset of crystallization. (We make no assertion regarding the relation between these activation energies and the band structure or mechanism of transport.) These five numbers are tabulated vs. DC bias in Table 2.

Inspection of Table 2 reveals some disturbing irregularities. On the basis of the coarse-grained survey of the Ge-Te system by Rockstad and deNeufville[19] we had expected a minimum of conductivity and a maximum of activation energy at some composition near stoichiometric $GeTe_2$. We find instead that no one sample possesses both properties. Particularly distressing is the failure of the electrical parameters of the two nominally identical zero bias specimens to coincide within reasonable limits of experimental error. Thus, although the distributions of conductivities and activation energies over bias have very roughly the expected parabolic shape, when viewed closely they exhibit discrepancies larger than we consider permissible.

We therefore attempted to correlate the electrical measurements with either measured composition or argon content, in the hope that they might be well-ordered with respect to one or another of these secondary variables. The results are shown in Figs. 7 and 8 respectively. While our sample

populations are far too small to permit drawing conclusions of a statistical nature, it nevertheless seems possible to offer the following remarks on the overall appearance of the distributions. We find little or no evidence for correlation between electrical conductivity and argon content. At zero and low positive bias the conductivity varies and the argon content does not. At negative bias the argon content varies and the conductivity does not. Only for the most negative bias, -75 V, do either the conductivity or activation energy depart significantly from the mean. The situation is scarcely better with respect to composition, as shown in Fig. 7; and in light of the strong similarity in trend between composition and argon content, one could hardly expect it to be. Nevertheless we are able to convince ourselves that the correlation is marginally stronger in this case, at least to the extent that the sets of points corresponding to negative bias form monotone sequences; i.e., for relatively large departures from stoichiometry the composition appears to control the electrical properties. The plausibility of this inference is strengthened somewhat by comparison with the results of Rockstad and deNeufville.[19] shown in Fig. 7 as open points. The magnitude of shift upon annealing, and the general trend of electrical parameters with composition, agree well enough with our results. The discrepancies in absolute magnitude of these parameters, however, are again larger than we consider permissible, and will be the subject of further discussion.

3. Morphology of Crystallization

As described in the preceding section, each of the film specimens listed in Table 2 was slowly crystallized in a dry nitrogen atmosphere during the course of electrical measurements. These crystallized specimens were then examined optically at low magnification for further clues to the effects of bias variation. The results nicely exemplify the delicate balance between competitive nucleation and growth mechanisms in this portion of the Ge-Te system, and provide qualititative support for the compositional trends depicted in Fig. 1(a). Arguments from morphology of crystallization in thin film form are of course perilous, owing to the variety of external factors which can influence crystal growth. However, by careful attention to such matters as substrate cleanliness and exclusion of water vapor, we have produced a series of micrographs in which external factors, if not wholly without effect, are at least consistent from one member of the bias sputtering series to the next. In any event it may be argued that results obtained on thin films are more truly representative of phenomena to be encountered in device applications than those obtained from bulk glasses.

Inasmuch as crystalline $GeTe_2$ does not exist, the crystallization of amorphous $GeTe_2$ (and indeed all amorphous Ge-Te alloys containing 0 to 50% Ge) proceeds via phase separation into GeTe and Te.[20] In the neighborhood of stoichiometry it appears that the nucleation probabilities of

these two phases are both small and approximately equal.[24] Crystallization begins at approximately 230°C with the heterogeneous nucleation of planar spherulites of relatively low density (10^3 to 10^6 cm^{-2}) at surface defect sites. X-ray diffraction reveals that these spherulites contain both Te and GeTe crystallites in aliquot proportion, intermingled on a very fine (ca. 100 Å) scale. Hence the spherulites may expand radially into the surrounding glassy matrix, attaining very large diameters, without affecting the average composition of that matrix. Crystallization ends when the spherulite boundaries touch everywhere, resulting in a cellular structure. The partial and complete stages of this process are illustrated in Figs. 9(d) and 9(e) respectively, taken from the zero bias specimen. Substantially identical morphology was exhibited by the +25 and +50 V bias specimens (not illustrated), in accord with the microprobe estimates of their composition.

On either side of stoichiometry, both the nucleation rates and the mechanism of crystallization depart from the canonical behavior of $GeTe_2$. On the germanium-rich side, the Te nucleation rate becomes vanishingly small, whereas the GeTe nucleation rate rises abruptly with increasing Ge content. Hence crystallization begins with the formation of numerous small GeTe spherulites, whose subsequent growth enriches the surrounding matrix in Te. When enrichment proceeds to the point that the Te nucleation rate becomes appreciable, Te then crystallizes from the matrix. The final result is a dense reticulated network whose scale depends on the degree of departure from stoichiometry. This progression is shown in reverse in

Fig. 9(a)-(c). In Fig. 9(c), taken on the -25 V specimen, the cellular structure is already markedly diminished in size, even though the composition differs by less than 2% from that of the zero bias specimen. In Fig. 9(b), taken on the -50 V specimen, only traces of cell structure remain. These are barely visible in the original photo, and may not survive halftone reproduction. At -75 V, as shown in Fig. 9(a), the copious nucleation of GeTe has erased all vestiges of cell structure, and the surface presents a uniform pebbly appearance composed of sub-micron crystallites and argon bubbles too small to resolve clearly.

Conversely, on the tellurium-rich side of stoichiometry, the Te nucleation rate rapidly becomes large at temperatures where the GeTe nucleation rate is still vanishingly small. Hence Te crystallizes first, in dendritic rather than spherulitic habit, until the matrix is sufficiently depleted of Te for GeTe crystallization to begin. This sequence of events is well established at the eutectic composition $Ge_{15}Te_{85}$.[25] In the present study, however, it appears that even the most extreme positive bias did not cause sufficient departure from stoichiometry for this morphology to manifest itself. Thus Fig. 9(f), taken on the +75 V specimen, substantially resembles Fig. 9(e), the zero bias specimen, except that the spherulites are still larger, and somewhat more rumpled at their boundaries. Note that the measured degree of tellurium enrichment in this case is only of order 0.5%.

Finally, it may be remarked that no crystallized specimen showed any

essential differences between those portions of the film overlying the molybdenum equipotential coating, and those portions overlying the glass substrate but within ca. 0.2 mm. of the molybdenum. This demonstrates that nucleation occurs on the upper or exposed surface of the film, and gives assurance that the material contained between the coplanar molybdenum electrodes (0.31 mm. apart) was representative of the bias applied to the electrodes themselves. At points more remote from the molybdenum coating, however, especially at the borders of negatively biased samples, the micrographs revealed a strong gradient back toward the morphology (and hence presumably the composition) characteristic of unbiased or "floating" depositions. Clearly the sheet resistivity of the growing film is an important factor in choosing the method of bias application.

In any event, the central result of this portion of the study is that the morphological variations produced by biasing are entirely consistent with those previously established through the deliberate change of composition of unbiased specimens. We therefore conclude that the observed variations are controlled by composition alone, and are quite independent of the fortuitous argon content. Indeed, as will be recalled from prior discussions, there is reason to believe that the influence runs the other way, and that the most copious nucleation provokes the most rapid release of argon during the crystallization regime.

IV. SUMMARY AND DISCUSSION

By and large, we feel that the results reported above present a satisfactorily cohesive picture. The variation of composition and incorporated argon content with DC substrate bias conform reasonably well to prior experience, and appear to be explicable in terms of simple electrostatic arguments. It may seem surprising that argon ion implantation apparently occurs at smaller values of negative bias than in elemental metals, and that a small positive bias is necessary to produce minimum argon content. We believe that this can be explained in terms of the generally looser structure and greater configurational freedom of amorphous chalcogenide alloys, which offer a more accommodating environment than epitaxially grown metal films. We find scant support for the conjecture that incorporated argon directly influences the electrical conductivity in either the virgin or annealed state of the glass, or the rates of nucleation and growth of crystalline phases. It appears on the contrary that the argon content is largely inactive except insofar as it determines the kinetics of its own release at elevated temperatures. This release may attain near-explosive rapidity under certain circumstances, with important consequences for the mechanical integrity of the film and the technology of device manufacture. Finally, it appears that variations in the morphology of crystallized films may be entirely explained in terms of departures from stoichiometry produced by biasing, without invoking other mechanisms.

The primary exceptions to the overall success of the study are the electrical measurements. We find a residuum of unexplained variation in both the conductivity and its apparent activation energy. This scatter is especially disappointing in the case of zero bias specimens, where every effort has been made to ensure complete similarity of deposition parameters and thermal history. Barring undiscovered sources of systematic error in our measurements, we can only conclude that not all determinants of the conductivity of $GeTe_2$ have been identified and brought under control. Of these determinants we suspect chiefly reactive contaminants, i.e., residual oxygen, water vapor and hydrocarbons present in the sputtering atmosphere. In an effort to answer this question we have embarked on a program of mass spectrometry and optical spectroscopy of the plasma, and have tentatively identified the 6563Å emission line of hydrogen. Should such contaminants prove to be the source of conductivity variations, this would signify a hitherto unsuspected sensitivity to impurity content in chalcogenide alloys. It is of course possible that the effects of impurities are magnified in the immediate neighborhood of a stoichiometric composition, where strong local ordering tendencies are present. In any event, it appears that the present study furnishes yet another proof that transport properties are enormously more sensitive as indicators of trace constituents than are static physical properties.

Finally, the failure of bias regulation to produce complete regularity of transport properties in no way lessens our conviction that its employment

is essential. The attainment of quantitatively reproducible conductivity may be problematic when the substrate potential is controlled, but it is certainly hopeless when the potential is not controlled. The wide range of floating substrate potentials (ca. -100 to +20 V) observed during the deposition of other chalcogenide alloys in our laboratory is sufficient evidence that this important parameter cannot be ignored.

ACKNOWLEDGEMENTS

We are indebted to J. P. deNeufville for guidance in every aspect of this study, and especially for assistance in the interpretation of crystallization morphology, and for a critical reading of the manuscript. L. Allard and F. Bleicher of the Scanning Electron Microscopy Laboratory, University of Michigan, are to be thanked for performing the electron microprobe analysis and its computer reduction. This work was supported by the Advanced Research Projects Agency under Contract DAHC15-70-C-0187.

REFERENCES

1. But see the Second Semi-Annual Technical Report to ARPA Contract DAHC15-70-C-0187, Energy Conversion Devices, Inc., June, 1972, ed. by J. P. deNeufville, pp. 92-108.
2. L. I. Maissel and P. M. Schaible, J. Appl. Phys. 36, 237 (1965).
3. F. M. d'Heurle, Trans. Met. Soc. AIME 236, 321 (1966).
4. H. F. Winters and E. Kay, J. Appl. Phys. 38, 3928 (1967).
5. J. L. Vossen and J. J. O'Neill, Jr., RCA Rev. 29, 566 (1968).
6. E. Stern and T. B. Light, Appl. Phys. Letters 13, 381 (1968).
7. F. M. D'Heurle, Met. Trans. 1, 725 (1970).
8. J. L. Vossen and J. J. O'Neill, Jr., RCA Rev. 31, 276 (1970).
9. A. G. Blachman, Met. Trans. 2, 699 (1971).
10. J. L. Vossen, J. Vac. Sci. Tech. 8, S12 (1971); contains a critical review of the RF sputtering literature through 1971.
11. W. D. Westwood and P. S. Wilcox, J. Appl. Phys. 42, 4055 (1971).
12. A. G. Blachman, J. Vac. Sci. Tech. 10, 299 (1973).
13. P. Petroff, T. T. Sheng, A. K. Sinha, G. A. Rozgonyi, and F. B. Alexander, J. Appl. Phys. 44, 2545 (1973).
14. M. J. McCulley, G. W. Neudeck, and G. L. Leidl, J. Vac. Sci. Tech. 10, 391 (1973).
15. W. Hoffmeister and M. Zeugel, Thin Solid Films 3, 35 (1969).
16. G. C. Schwartz and R. E. Jones, IBM J. Res. Develop. 14, 52 (1970).
17. A. Devenyi, C. Rusu, M. Rusu, A. Barna, and P. B. Barna, Proc. International Conference on Semiconductor Heterojunctions and

Layered Structures 4, 105 (1970).

18. J. P. deNeufville, J. Non-Crystalline Solids 8-10, 85 (1972).

19. H. K. Rockstad and J. P. deNeufville, Proceedings of the Eleventh International Conference on the Physics of Semiconductors, Polish Scientific Publishers, Warsaw, 1972, p.542.

20. T. Takamori, R. Roy, and G. J. McCarthy, Mater. Res. Bull. 5, 529 (1970).

21. E. A. Fagen, Mater. Res. Bull. 7, 279 (1972).

22. R. F. Brebrick, J. Chem. Phys. 41, 1140 (1964).

23. B. Cobic, G. Carter, and J. H. Leck, Brit. J. Appl. Phys. 12, 288 (1961).

24. D. J. Sarrach, M.S. Thesis, Dept. of Metallurgical Engineering, Wayne State Univ., Detroit, Mich., 1973 (unpublished).

25. H. Fritzsche and S. R. Ovshinsky, J. Non-Crystalline Solids 2, 148 (1970).

TABLE 1

CHARACTERISTICS OF BIAS-SPUTTERED SAMPLES
FOR MASS SPECTOMETRY

Run Number	DC Bias (Volts)	Dep'n Rate (nm/min)	Thickness (microns)	Ge Content (atomic pct.)	Argon Content (atomic pct.)
SI-306	-75	21	3.0	38.3	4.02
SI-305	-50	25	3.4	35.2	3.02
SI-304	-25	27	2.8	34.3	1.72
SI-363	0	24	2.9	33.0	1.06
SI-307	+25	30	3.0	32.7	0.67
SI-308	+50	32	2.7	32.7	0.71
SI-364	+75	29	3.3	32.1	0.78
SI-309	+75	30	0.45	-	0.77
SI-416	0	24	0.41	-	0.94
SI-417	0	28	1.2	-	1.03
SI-418	0	29	3.0	32.9	0.99
SI-419	0	24	8.0	-	1.05
SI-420	0	27	24.0	-	0.86

TABLE 2 ELECTRICAL PROPERTIES OF BIAS-SPUTTERED SAMPLES

Run Number	DC Bias (Volts)	Virgin σ $(\Omega\text{-cm})^{-1}$	Virgin ΔE (eV)	Annealed σ $(\Omega\text{-cm}^{-1})$	Annealed ΔE (eV)	T_x (deg C)
SI-300	-75	2.8×10^{-5}	.438	9.8×10^{-7}	.563	222
SI-306	-75	9.5×10^{-6}	.447	-	-	214
SI-305	-50	7.9×10^{-6}	.495	3.6×10^{-7}	.596	216
SI-304	-25	7.2×10^{-6}	.537	2.7×10^{-7}	.614	228
SI-363	0	7.4×10^{-6}	.471	2.1×10^{-7}	.611	222
SI-418	0	4.0×10^{-6}	.502	1.1×10^{-7}	.582	237
SI-307	+25	7.0×10^{-6}	.545	2.1×10^{-7}	.640	234
SI-308	+50	8.0×10^{-6}	.491	3.4×10^{-7}	.615	234
SI-364	+75	4.9×10^{-6}	.506	2.5×10^{-7}	.605	223
SI-309	+75	4.8×10^{-6}	.495	2.4×10^{-7}	.597	213

FIGURE CAPTIONS

Fig. 1. (a) Actual germanium content of bias-sputtered films of nominal composition $GeTe_2$, as determined by electron microprobe analysis. (b) Total argon content of bias-sputtered films, as determined by mass spectrometry. See text for further explanation.

Fig. 2. Correlation of actual germanium content with total argon content of bias-sputtered films, from data of Fig. 1. The best-fit straight line through the points has a slope of 0.63.

Fig. 3. Argon partial pressure vs. oven temperature for seven bias-sputtered films of similar thickness. Label on curve gives DC bias in volts. Successive curves have been offset one decade for clarity; the ordinate is correct for the uppermost curve. Mean specimen mass for this sequence: 22 mg. Mean heating rate: 8.5 deg/min. See text for further experimental details and interpretation.

Fig. 4. (Inset) Protypical argon release curve, showing approximate division into four different regimes of release mechanism. See text for further explanation. (Main figure) Decomposition of total argon content [Fig. 1(b)] into partial contributions from each regime.

Fig. 5. Argon partial pressure vs. oven temperature for five zero-bias films varying in thickness. Label on curve gives thickness in micrometers. Successive curves have been offset one decade for clarity; the ordinate is correct for the uppermost curve. Mean specimen mass

for this sequence: 4.4 mg. Mean heating rate: 8.5 deg/min. See text for further explanation.

Fig. 6. Prototypical plot of conductivity vs. reciprocal temperature for zero-bias films, showing directions of traversal and manner of evaluating conductivities, apparent activation energies, and crystallization temperature. See text for further explanation.

Fig. 7. (a) Correlation of room temperature conductivity of virgin (solid circles) and annealed (solid squares) bias-sputtered films with actual composition. (b) Correlation of apparent conductivity activation energy at room temperature with composition, for the same sequence of bias-sputtered films. Open circles and squares represent averaged data from Rockstad and deNeufville, Ref. 19, for unbiased sputtered films of the nominal composition shown.

Fig. 8. (a) Correlation of room temperature conductivity of virgin (solid circles) and annealed (solid squares) bias sputtered films with total argon content. (b) Correlation of apparent conductivity activation energy at room temperature with total argon content, for the same sequence of bias-sputtered films.

Fig. 9. Morphology of crystallization of bias-sputtered films used in conductivity measurements. (a) -75 V bias; (b) -50 V bias; (c) -25 V bias; (d) 0 V bias, partially crystallized; (e) 0 V bias, fully crystallized; (f) +75 V bias. No scale is given, but the field of view in every case is 159 x 121 micrometers. The black pits seen in (d) are large argon bubbles.

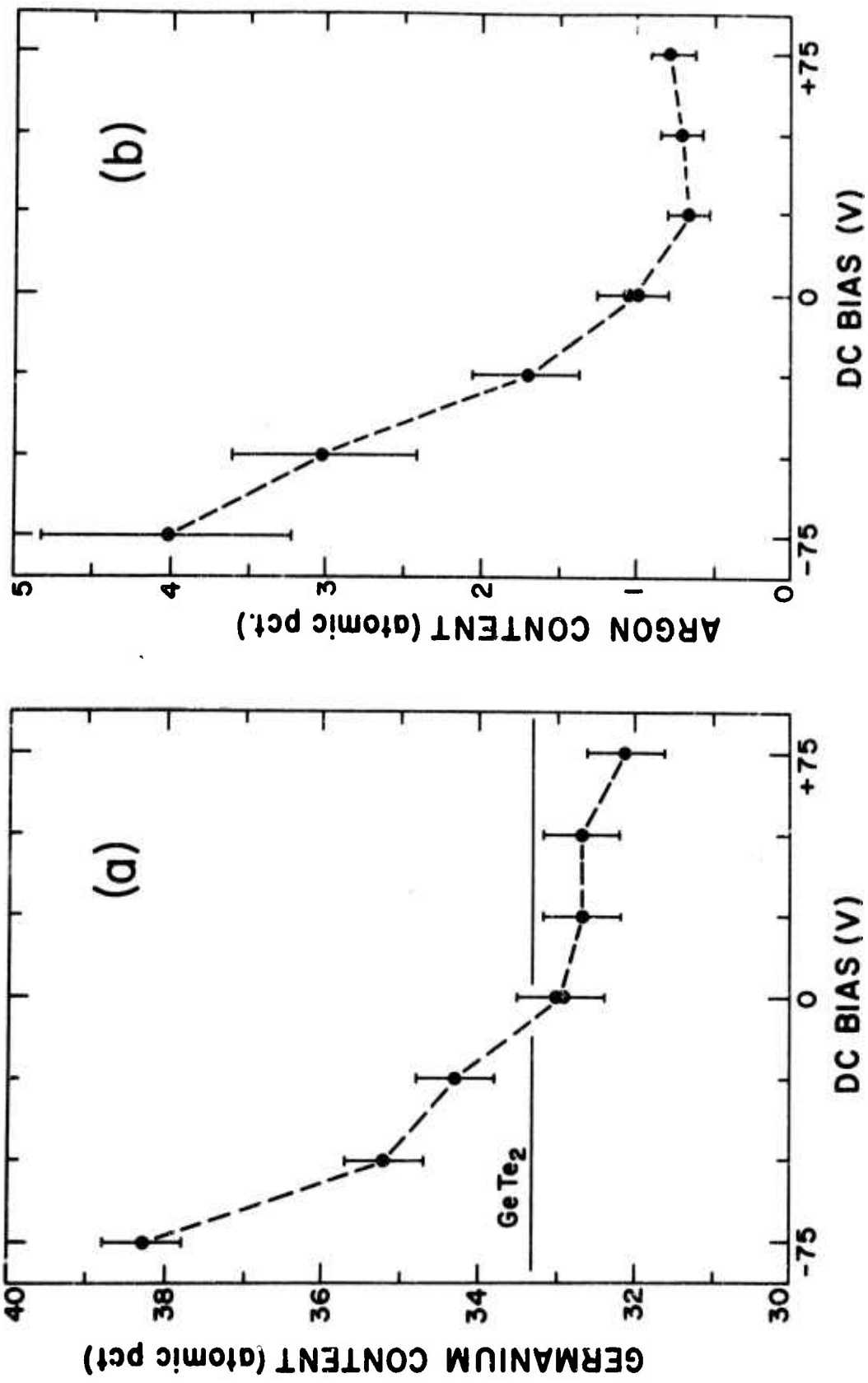
(b)
ARGON CONTENT (atomic pct.)
0
1
2
3
4
5
-75
0
+75
DC BIAS (V)
(a)
GERMANIUM CONTENT (atomic pct)
30
32
34
36
38
40
GeTe2
-75
0
+75
DC BIAS (V)

Fig. 1

ARGON CONTENT (atomic pct.)
5
4
3
2
1
0
GERMANIUM CONTENT (atomic pct.)
32
34
36
38
2 DATA POINTS

Fig. 2

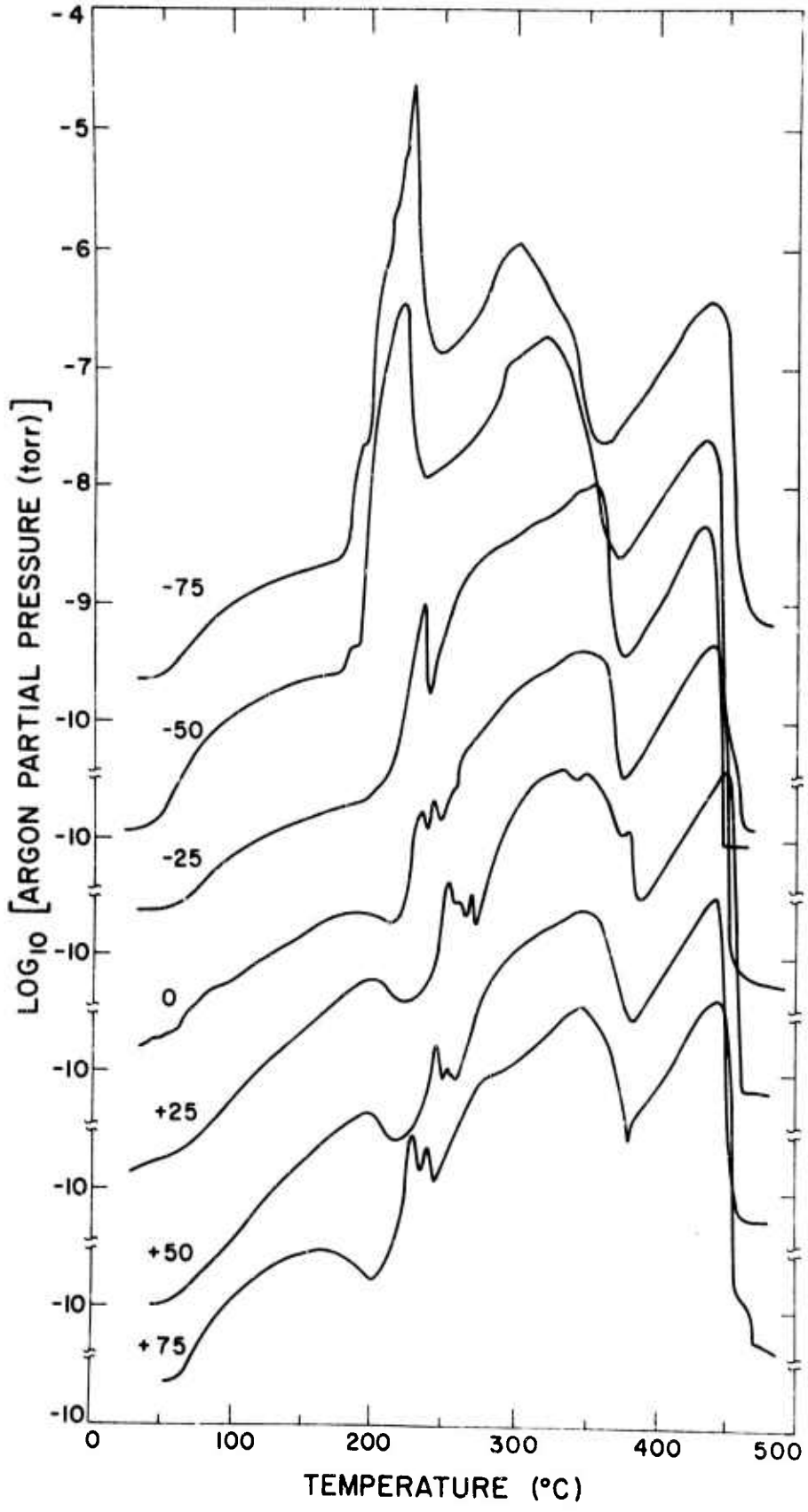
LOG10 [ARGON PARTIAL PRESSURE (torr)]
TEMPERATURE (°C)
-4
-5
-6
-7
-8
-9
-10
0
100
200
300
400
500
-75
-50
-25
0
+25
+50
+75

Fig. 3

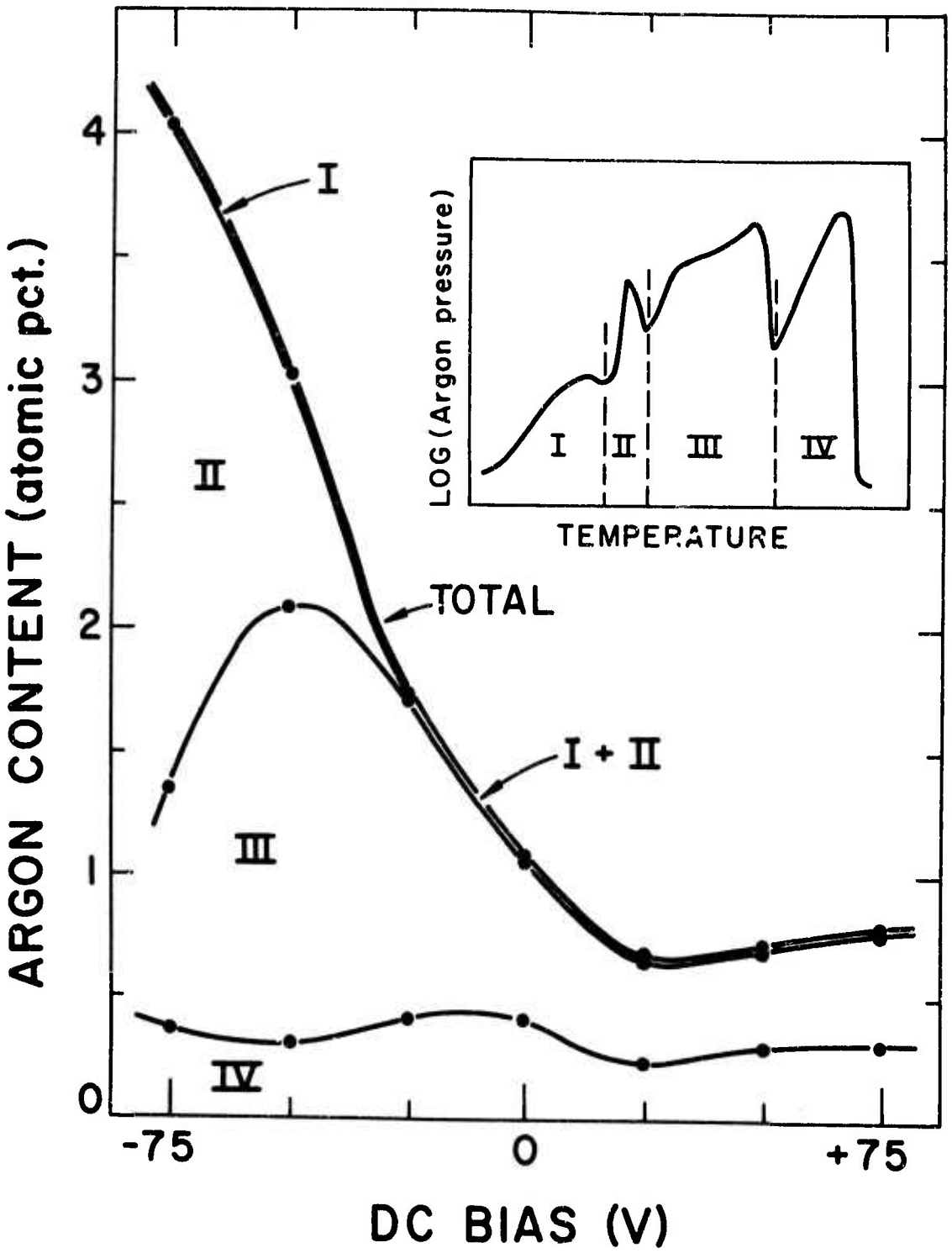
ARGON CONTENT (atomic pct.)
4
3
2
1
0
I
II
III
IV
TOTAL
I + II
LOG (Argon pressure)
I
II
III
IV
TEMPERATURE
-75
0
+75
DC BIAS (V)

Fig. 4

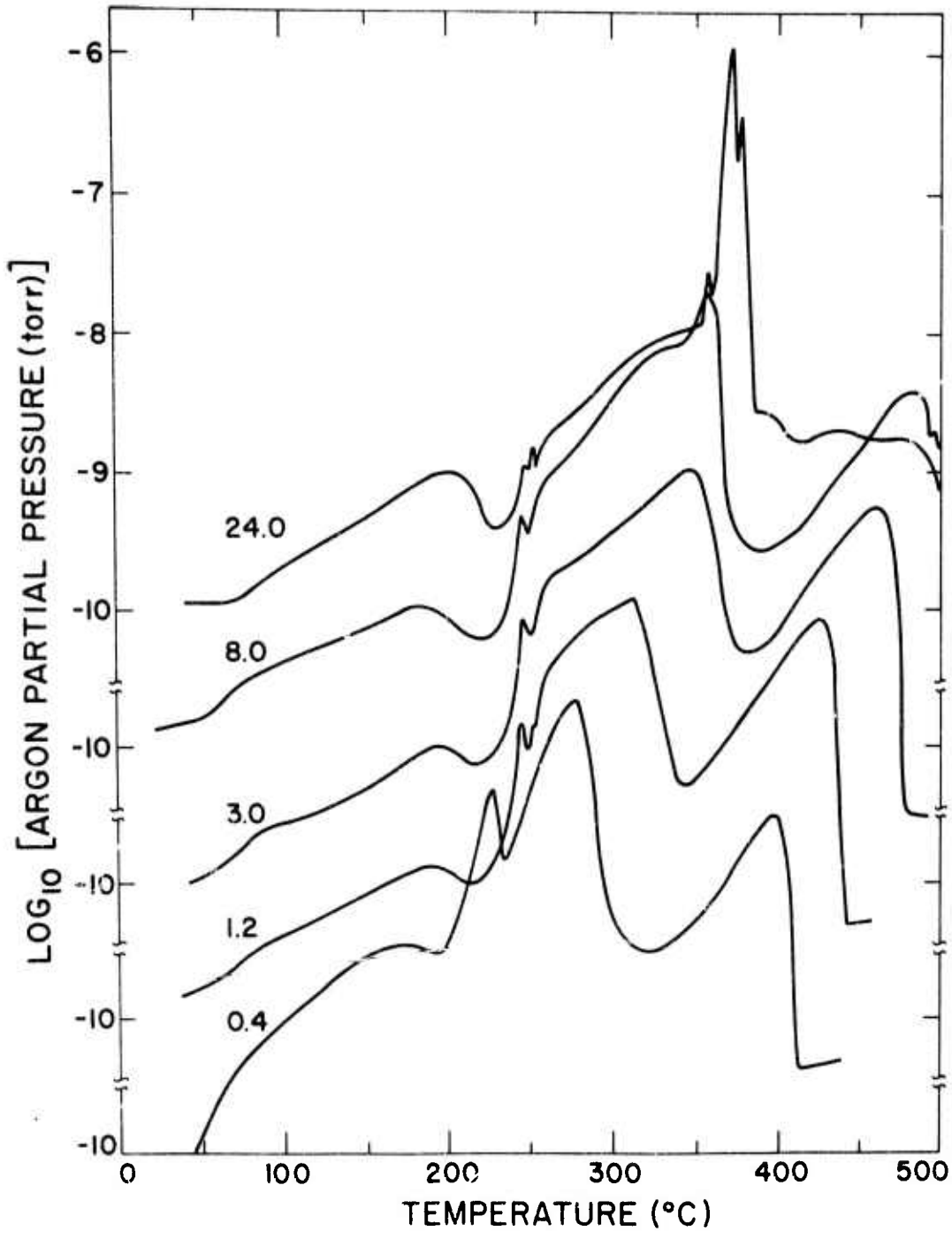
-6
-7
-8
-9
-10
-10
-10
-10
-10
24.0
8.0
3.0
1.2
0.4
LOG10 [ARGON PARTIAL PRESSURE (torr)]
0
100
200
300
400
500
TEMPERATURE (°C)

Fig. 5

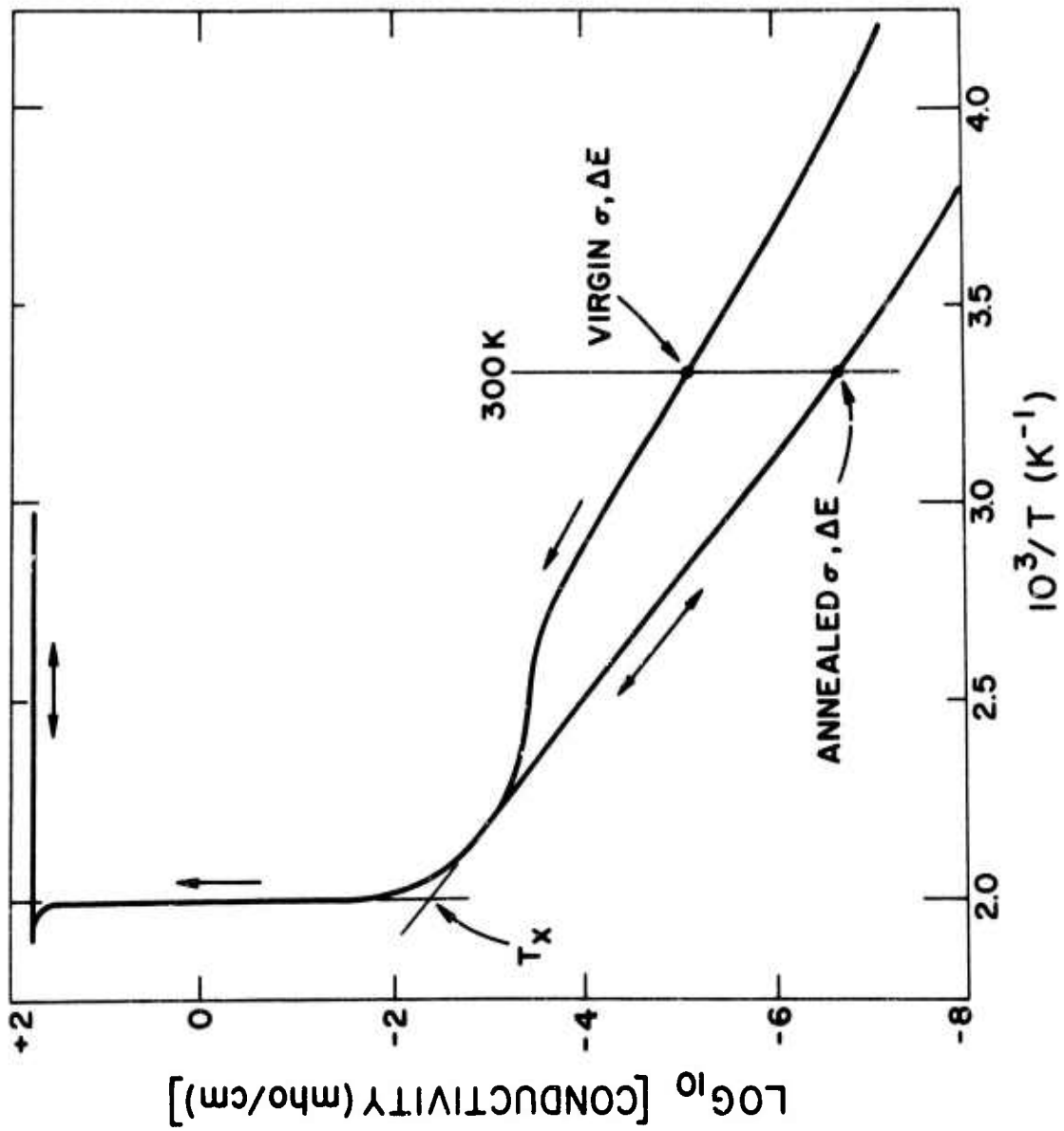
LOG10 [CONDUCTIVITY (mho/cm)]
+2
0
-2
-4
-6
-8
2.0
2.5
3.0
3.5
4.0
10^3/T (K^-1)
300 K
VIRGIN σ, ΔE
ANNEALED σ, ΔE
Tx

Fig. 6

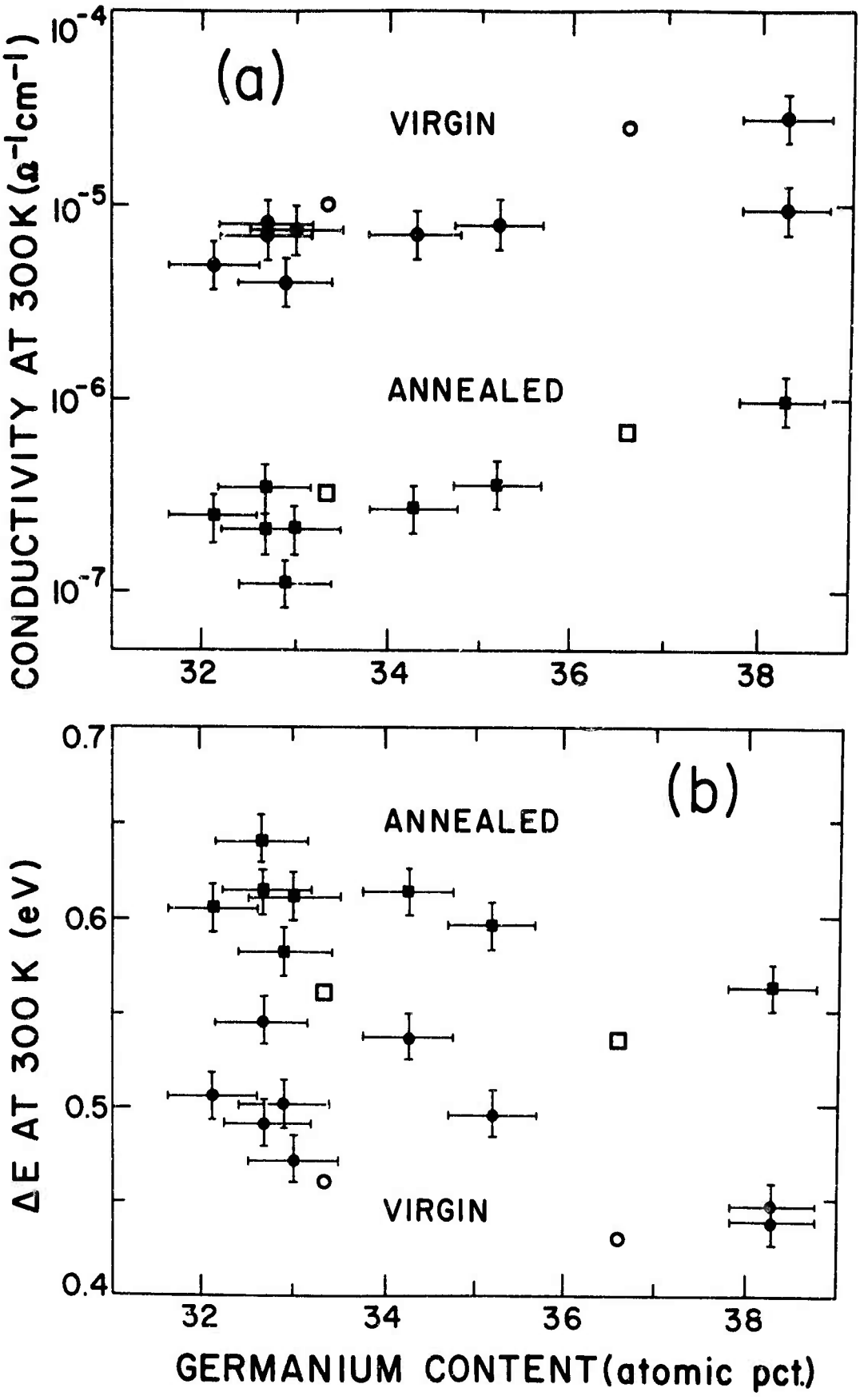
(a)
VIRGIN
ANNEALED
CONDUCTIVITY AT 300K ($\Omega^{-1}cm^{-1}$)
10^{-4}
10^{-5}
10^{-6}
10^{-7}
32
34
36
38
(b)
ANNEALED
VIRGIN
ΔE AT 300 K (eV)
0.7
0.6
0.5
0.4
32
34
36
38
GERMANIUM CONTENT (atomic pct.)

Fig. 7

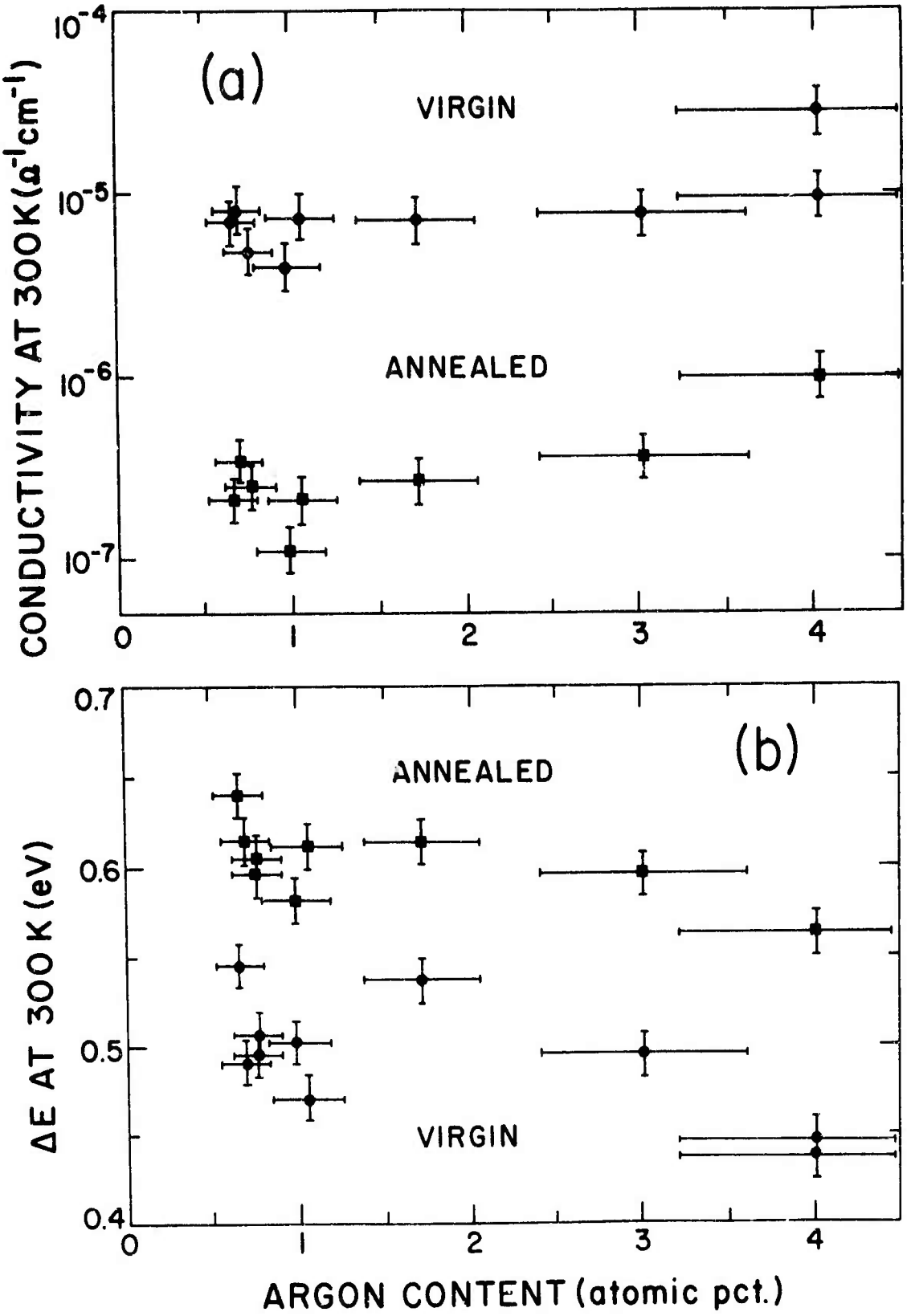
(a)
VIRGIN
ANNEALED
CONDUCTIVITY AT 300K (Ω⁻¹cm⁻¹)
10⁻⁴
10⁻⁵
10⁻⁶
10⁻⁷
0
1
2
3
4
(b)
ANNEALED
VIRGIN
ΔE AT 300 K (eV)
0.7
0.6
0.5
0.4
ARGON CONTENT (atomic pct.)

Fig. 8

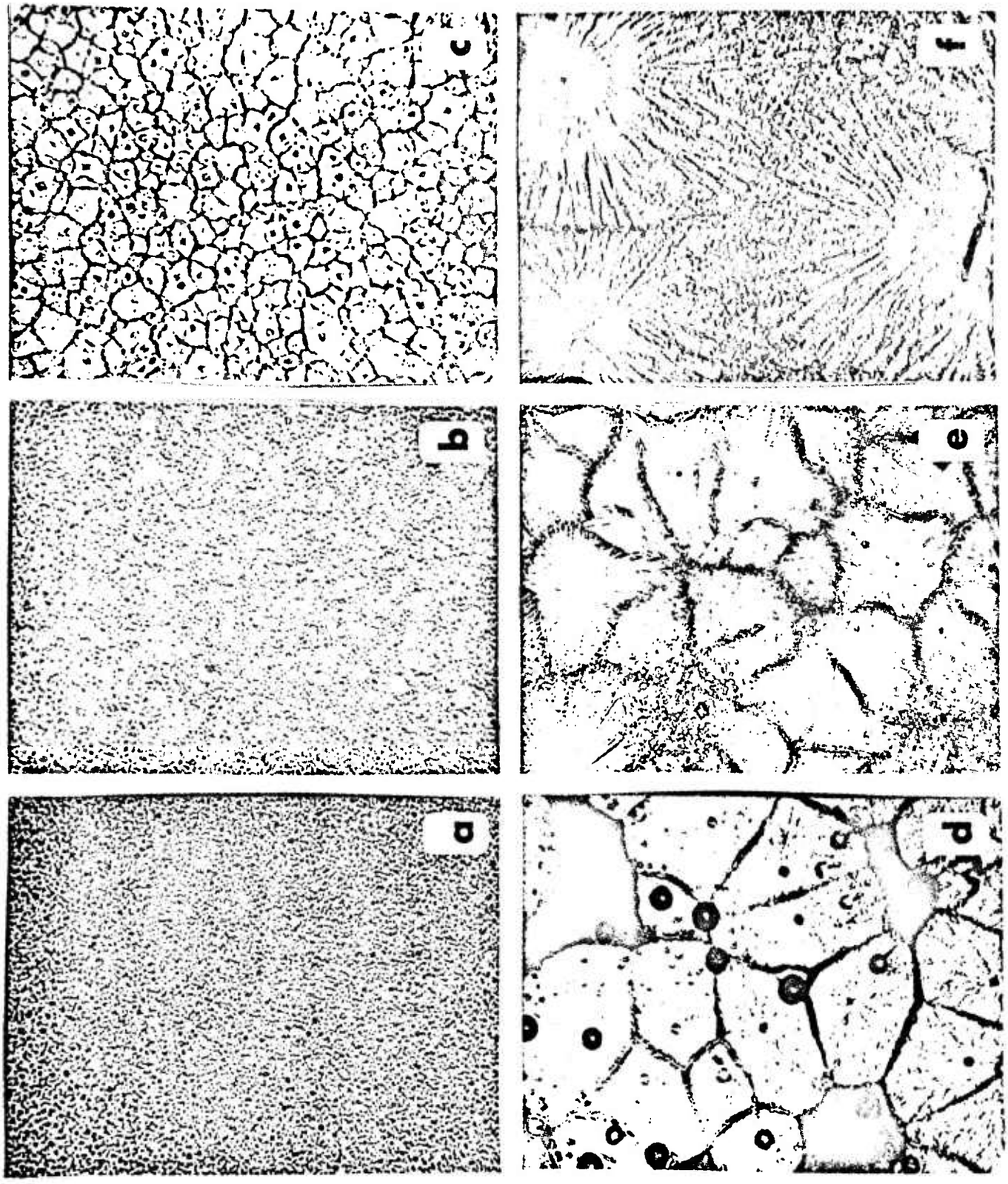

Fig. 9

The Role of Connectedness in the Relationship between Optical Gap and Glass Transition Temperature for Amorphous Semiconductors

J. P. deNEUFVILLE and H. K. ROCKSTAD

Energy Conversion Devices, Inc., Troy, Michigan, U.S.A.

ABSTRACT

We have measured the glass transition temperature T_g and an arbitrarily defined optical gap energy E_{O4} of a wide variety of amorphous semiconducting materials, including many which can be prepared only by evaporation or r.f. sputtering. T_g provides an index of atomic mobility and E_{O4} an index of the covalent bond strength. In a plot of E_{O4} versus T_g, materials tend to be grouped according to the average number $\bar{N}$ of outer electrons per atom, or network connectedness $C = 8 - \bar{N}$. For $C = 2$, T_g is nearly constant, while for $C = 2.4$, 2.66, and 3, $T_g = T_g^{\circ} + \beta E_{O4}$. T_g° is 340 ±20 K, approximately the same as T_g for the $C = 2$ alloys. β is proportional to $C - 2$, the number of covalent bonds per atom which must be broken to create a 2-connected atom. We postulate that this configuration is required for diffusive motion or viscous flow, and interpret the $T_g - E_{O4}$ correlation in terms of a proposed fluidity equation for covalent liquids with $2 < C \leq 4$.

§1. INTRODUCTION

The relationship between chemical bonding and the glass transition temperature of amorphous semiconducting (A.S.) alloys is an essential feature of any comprehensive theory relating structure and properties for these materials. Several such relationships have been proposed which effectively correlate T_g with certain other properties among narrow classes of A.S. alloys. These include a $T_g - \Delta E_o$ correlation, where $2\Delta E_o$ is the electrical band gap, for Si-As-Te glasses (Numoshita et al. 1972), and a $T_g - E_A$ correlation, where E_A is the atomization energy of telluride glasses (Felz et al. 1972). The latter correlation is less successful when extended to sulfide and selenide glasses, even if the ordering energy contribution to E_A is included.

The T_g-band gap correlation, however, is especially appealing because both parameters are easily measured and their correlation hints at the underlying relationship between bond strength and the glass transition. However, if the T_g-band gap correlation is extended beyond a single narrow family of materials, it clearly breaks down, for example: Se, As_2Se_3 and GeAsSe all have roughly the same optical band gaps E_g but their T_g's vary from 35 to 420°C. We have discovered that if the alloys are grouped according to their average number of outer electrons $\bar{N}$, then within each group the $T_g - E_g$ correlation is relatively good. A similar procedure was successfully used by Kastner (1973) to correlate E_g and the melting temperature T_m for numerous crystalline semiconductors,

grouped by $\bar{N}$. It is convenient to introduce the concept of connectedness in order to clarify the relationship between $\bar{N}$ and the E_g vs. T_g correlation for amorphous materials. Average connectedness C, defined by $C = 8 - \bar{N}$, is the average coordination number for covalently bonded materials.

In this paper we exhibit the T_g vs. E_g correlation for several fixed values of C (or $\bar{N}$) and indicate the possible origin of various discrepancies. The origins of the T_g vs. E_g correlation are examined in terms of a simplified model for viscous flow, which leads to predictions of the temperature dependence of viscosity for A.S. liquids based only upon a knowledge of E_g and $\bar{N}$.

§ 2. EXPERIMENTAL

All the T_g data were collected in our laboratories on bulk or r.f. sputtered thin film amorphous samples. T_g was taken as the temperature at which C_p attains a value midway between that in the glass and that in the liquid, as measured by scanning calorimetry at a scan rate of 20 deg/min. T_g for a few materials was measured on both bulk and thin film samples, and the results were in relatively good agreement (±10 deg).

For E_g we have used the arbitrary quantity E_{O4}, defined as the photon energy at which the optical absorption coefficient has the value 10^4 cm^{-1}. All samples were annealed at or near T_g prior to the optical measurement. No optical measurements were performed on the bulk samples.

§ 3. RESULTS

The values of E_{O4} and T_g obtained on a wide variety of chalcogens and chalcogenide alloys are listed in Table 1, grouped according to common values of $\bar{N}$ or C. The alloys with C = 2, 3, 4 and 2.66 fall along five separate E_{O4} vs. T_g lines as plotted in Figure 1. For C = 2, $\bar{N}$ = 6, T_g is roughly constant as fitted by line (a).

The C = 2.4, $\bar{N}$ = 5.6 alloys are exemplified by locally two-dimensional polymers like As_2S_3 which form layered crystals and highly viscous liquids. The T_g vs. E_{O4} data for the alloys examined in this category lie reasonably close ($\Delta T = \pm 10$ deg) to line (b) whose intercept is 328 K and whose slope is 68 deg/eV, with the exception of Sb_2S_3 whose T_g is 25 deg above this line. All the examples of the C = 2.4 alloys correspond to "chalcogen saturated" (deNeufville 1972) compound compositions of the sort A_2B_3 where B is a chalcogen (Group VI) and A is a Group V element. The glassy alloys, if they are chemically ordered by analogy to their crystalline counterparts, contain only A - B nearest-neighbor covalent bonds.

The alloys with C = 2.66, $\bar{N}$ = 5.33, are stoichiometric analogues of SiO_2, containing one Group IV atom and two chalcogen atoms per formula unit. T_g vs. E_{O4} is well fitted ($\Delta T = \pm 10$ deg) by line (c) having an intercept of 318 K, and a slope of 157 deg/eV. These alloys are also chalcogen saturated and contain only IV-chalcogen bonds, to the extent that they are fully ordered. A small group of two component (e.g. $GeSe_2$ and $GeTe_2$) and three component examples (e.g. $(GeSe_2)_x(GeTe_2)_{1-x}$) is

TABLE 1 Optical gaps, E_{O4}, and glass transition temperatures, T_g of various A.S. alloys, grouped according to $\bar{N}$, the average number of outer electrons per atom.

$\bar{N}$	Material	Form*	T_g (K)	E_{O4} (eV)
6	SeTe	f	330	1.307
	Se_3Te	b	338	1.59
	Se	b,f	318	2.05
5.6	As_2Te_3	b	468	1.92
	$As_4Se_3Te_3$	b	417	1.31
	As_2Se_3	b	468	1.92
	Sb_2S_3	f	505	2.06
	As_2S_3	b,f	478	2.55
5.33	$GeTe_2$	f	503	1.20
	Ge_5SeTe_9	f	515	1.22
	$Ge_5Se_3Te_7$	b	533	1.36
	GeSeTe	b	565	1.58
	$Ge_5Se_7Te_3$	b	599	1.77
	Ge_5Se_9Te	b	661	2.12
	$GeSe_2$	b	695	2.41
5.0	Ge_2SeTe	f	545	1.24
	GeSe	f	597	1.71
	GeSbTe	f	522	0.88
	GeSbSe	f	574	1.14
	Ge_2AsTe_2	f	597	1.24

TABLE 1 (CONT.)

$\bar{N}$	Material	Form	T_g (K)	E_{O4} (eV)
	GeAsTe	f	607	1.32
	$Ge_3As_4Te_3$	f	608	1.34
	As	f	616	1.39
	Ge_2As_2SeTe	b	615	1.52
	GeAsSe	b	677	1.67

* f ≡ film, b ≡ bulk, calorimetric specimen

included in this plot.

For the case of C = 3, $\bar{N} = 5$, two separate branches of T_g vs. E_{O4} are observed: line (d), comprising only the two points GeSe and Ge_2SeTe, lying parallel to but above the $GeSe_2$-$GeTe_2$ C = 2.66 curve, with an intercept of 365 K and a slope of 144 deg/eV; and a higher line (e) with a lower intercept of 350 K and a higher slope of 195 deg/eV, comprising many compositions including pure As and many ternary alloys such as GeTeSb, GeTeAs, GeSeAs, etc.

No T_g or E_{O4} data are available for the elemental alloys such as amorphous Si and Ge, which appear to crystallize below T_g. Thus not only is T_c experimentally inaccessible, but E_{O4} is as well, because the films cannot be fully annealed prior to crystallization.

§ 4. DISCUSSION

We note in Fig. 1 that both T_g at a given E_{O4} and $\partial T_g / \partial E_{O4}$ increase with increasing coordination. These trends have a simple explanation. The materials represented in curves (b) through (e) all have 3-dimensional bonding. For these materials the coordination number indicates the number of bonds per atom which must be broken to obtain fluidity. For a given bond strength, which is related to E_{O4}, we thus expect T_g to increase with coordination number. These considerations also account for the increase of $\partial T_g / \partial E_{O4}$ with increasing coordination number. For the two-fold coordination materials represented by curve (a), T_g is

substantially independent of E_{O4} because T_g is associated with the breaking of weak van der Waals bonds between chains and rings, whereas E_{O4} is related to the covalent bond strength.

In order to understand the origin of these correlations in greater depth, including their apparent linearity and common intercept of $\simeq$ 325 - 365 K, it is necessary to examine the glass transition phenomenon and its relationship to the fluidity (reciprocal viscosity) equation. Since T_g measures the onset of diffusive motions, it closely corresponds to a fixed value of viscosity. The simplest form of the fluidity equation which describes the fluidity behavior for a wide variety of glass-forming liquids is the Fulcher equation (Fulcher 1925)

$$\Phi = \Phi_o \exp[-A/(T-T_o)] \qquad (1)$$

where Φ_o, A and T_o are adjustable fitting constants. In an attempt to correlate A with covalent bond strengths, we will write $A = \alpha E_{O4}/k$ where α is a suitable constant for each material which we shall later determine in terms of C.

Then

$$\Phi = \Phi_o \exp[-\alpha E_{O4}/k(T - T_o)]. \qquad (2)$$

Taking $\Phi (T_g) = 10^{-12}$ poise^{-1}, as appropriate for T_g as measured herein, and $\Phi_o = 10^2$ poise^{-1}, typical of many liquids, we can evaluate α as

$$\alpha = 32.2\ k\ (T_g - T_o)/E_{O4} \qquad (3)$$

From Fig. 1 we note that $T_g = T_g^{\,o} + \beta\ E_{O4}$ or

$$\beta = (T_g - T_g^{\,o})/E_{O4} \qquad (4)$$

where $T_g^{\,o} \approx 340$ K and β depends on C. By identifying T_o in (3) with $T_g^{\,o}$ in (4) we obtain

$$\alpha = 32.2\ \beta k \qquad (5)$$

$T_g^{\,o}$ corresponds to the value of T_g in the limit when $C \rightarrow 2$ or $E_{O4} \rightarrow O$, e.g., in the absence of three dimensional covalent bonding. For these same limits, $\phi(T_o) = O$, so T_o is somewhat less than $T_g^{\,o}$ (Angell, 1968). However we shall use the approximation $T_g^{\,o} = T_o$ for $C > 2$ liquids in the absence of extensive $\phi(T)$ data for these materials. In any case it is clear that alloys whose fluidities obey Eq. (2) will have the $T_g - E_{O4}$ relationship of Eq. (4).

We have applied Eq. 5 to the data in Fig. 1 to derive the values of α for each C listed in Table 2a. We postulate that $\alpha = \delta(C-2)$ for C = 2.4 to 4, where δ is independent of C. The ratio $\delta = \alpha/(C-2)$ varies from 0.47 to 0.65 over the observed range of C with an average value of 0.55. Thus we postulate that the fluidity of A.S. alloys can be approximately expressed as

$$\phi = \phi_o \exp[\delta(C-2)E_{O4}/k(T-T_o)] \qquad (6)$$

for $C > 2$, where δ is about 0.55. For these alloys T_o can be taken as approximately 325 K for C = 2.4 and 2.67 and 355 K for C = 3.

TABLE 2

a. List of constants in assumed fluidity equations versus connectedness C.

C	α	C-2	$\frac{\alpha}{C-2} = \delta$
4		2	
3	0.541*	1	0.541
2.67	0.436	.67	0.654
2.4	0.187	.4	0.468
2	0	0	-

* Slope taken from upper branch of $\bar{N} = 5$ data.

b. Comparison of α values from Table 2a with values calculated using a fixed value of δ, chosen as 0.55, versus connectedness C.

δ	C	α calc	α
0.55	4	1.11	
	3	.554	0.541
	2.67	.370	0.436
	2.4	.222	0.187

By assuming $\delta = 0.55$, hypothetical values of α can be calculated from $\alpha = \delta\ (C-2)$ for any $C > 2$, e.g. $C = 4$. The results for specific values of C are tabulated in Table 2b and compared with the empirical values of α from Table 2a. On the basis of α calculated for $C = 4$, and by assuming a value for $T_o \approx 350$ K the line for $C = 4$ in Fig. 1 is obtained. For amorphous Ge, using $E_{O4} \approx 1.1$ eV, a T_g of the order of 755 K is thus predicted. Amorphous Ge usually crystallizes below 755 K, presumably without diffusive motion, precluding verification of this calculated value of T_g.

The empirical success of our postulated relation between $C - 2$ and α may indicate that the activated configuration for viscous flow is a two-connected atom. In the limit $C = 2$, no thermal activation of covalent bonds is required. When T_g scales with E_{O4} for alloys with a given value of $\bar{N}$, we conclude that these alloys share a common network topology. For example, we suppose that GeAsSe and the other ternary alloys plotting on line (e) have 3-fold coordination similar to the amorphous As structure (Krebs and Steffen 1964). Conversely, we suppose that GeSe and Ge_2SeTe, which plot on line (d), have a 2-fold chalcogen, 4-fold Ge network structure.

The equation for fluidity which we have postulated to account for the $T_g - E_{O4}$ correlation cannot be verified for most of these materials, because the amorphous phase tends to crystallize just below T_g, while above T_m the semiconductor liquid has usually transformed, via an

increase in coordination number, to a metallic or nearly metallic liquid, thereby invalidating the assumptions of the covalent fluidity curve. However in the case of As_2Se_3, where neither of these circumstances interferes significantly, Eq. (3), using $\alpha \approx 0.189$ derived from Fig. 1, is in excellent agreement (within one decade) with published data throughout the entire fluidity range from 10^{0} to 10^{-16} poise^{-1} (Nemilov 1964, Kolomiets 1964).

It is well known that fitting of fluidity data for glass forming liquids to Eq. (1) requires $T_o \approx 0.85\ T_g$ for van der Waals bonded molecular and linear polymer liquids (Angell 1968) and a $T_o \approx 0$ K for heavily cross-linked network liquids such as SiO_2 (Hetherington et al. 1964). Indeed, Angell has identified the glasses with $T_o \rightarrow T_g$ as "ideal" in the sense that their configurational entropy at T_g approaches zero as T_o approaches T_g. Eq. (6) represents a successful effort to describe the transition between these two cases for $2 < C \leq 3$ and with varying values of E_{O4}. Interestingly, the value of T_o remains nearly fixed as E_{O4} and C increase. However, as E_{O4} is changed substantially by the inclusion of oxide (and sulfide) liquids into the T_g - E_{O4} plots, T_g increases sub-linearly with E_{O4}, presumably as a result of a concomitant decrease of T_g^{o}.

We acknowledge the support of ARPA Contract DAHC15-70-C-0187.

REFERENCES

ANGELL, C. A., 1968, J. Amer. Ceram. Soc., 51, 117.

deNEUFVILLE, J. P., 1972, J. Non-Crystalline Solids, 8-10, 85.

FELZ, A., BÜTTNER, H. J., LIPPMANN, F. J., and MAUL, W., 1972, J. Non-Crystalline Solids, 8-10, 64.

FULCHER, G. S., 1925, J. Amer. Ceram. Soc., 6, 339.

HETHERINGTON, G., JACK, K. H., and KENNEDY, J. C., 1964, Phys. and Chem. Glasses, 5, 130.

KASTNER, M., 1972, Phys. Rev. Letters, 28, 355.

KOLOMIETS, B. T., 1964, Phys. Stat. Sol., 7, 359.

KREBS, H., and STEFFEN, R., 1964, Z. Anorg. Allg. Chem., 327, 224.

NEMILOV, S. V., 1964, Soviet Physics - Solid State, G, 1075.

NUMOSHITA, M., and ARAI, H., 1972, Solid State Commun., 11, 213.

FIGURE CAPTIONS

Figure 1. Glass transition temperature of amorphous semiconducting liquids plotted as a function of E_{O4}, the photon energy at which $\alpha = 10^4 cm^{-1}$. The points correspond to the data in Table 1, and are fitted to lines of constant connectedness $C = 8 - \bar{N}$ where $\bar{N}$ is the average number of outer electrons per atom.

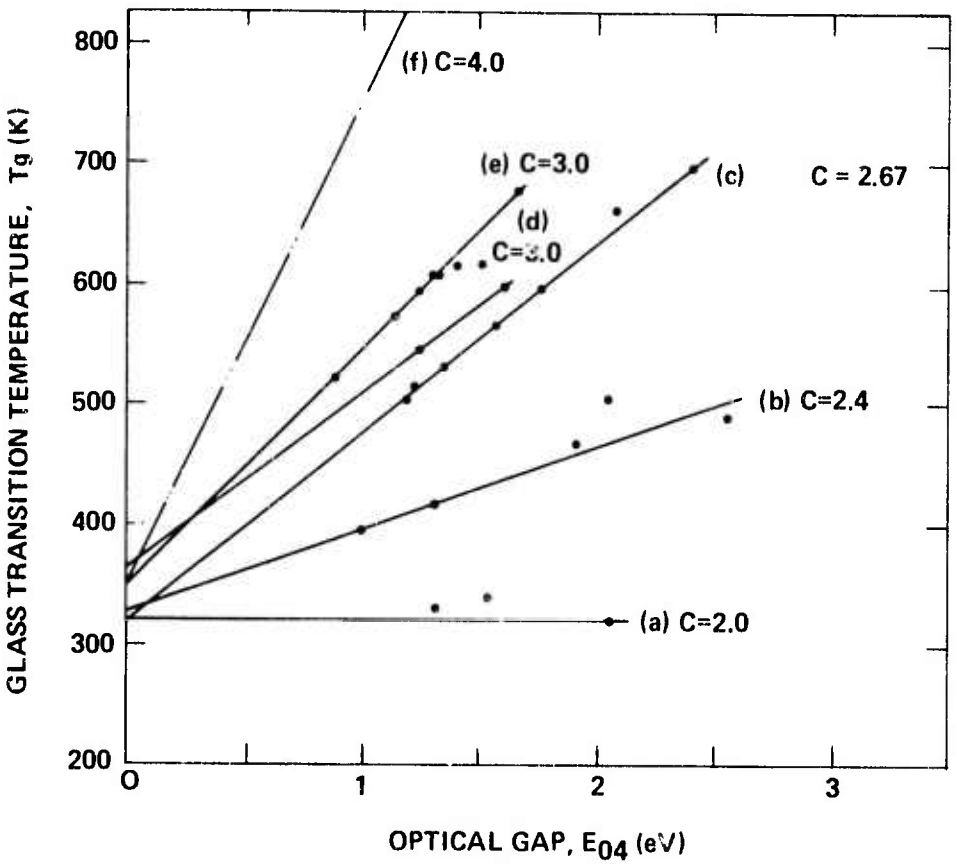
800
700
600
500
400
300
200
0
1
2
3
(f) C=4.0
(e) C=3.0
(c)
C = 2.67
(d)
C=3.0
(b) C=2.4
(a) C=2.0
GLASS TRANSITION TEMPERATURE, Tg (K)
OPTICAL GAP, E04 (eV)

Fig. 1

THE THERMAL CONDUCTIVITY OF SOME CHALCOGENIDE GLASSES*

Richard Flasck and Howard K. Rockstad
Energy Conversion Devices, Inc.
1675 West Maple Road
Troy, Michigan 48084

The temperature-dependent thermal conductivities of several chalcogenide glasses were determined above 300°K. At 300°K, the thermal conductivity for most of these glasses is about 3 mW/cm-deg.

*Work supported by the Advanced Research Projects Agency under Contract No. DAHC 15-70-C-0187.

The thermal conductivities above 300°K for a number of chalcogenide glasses are given in this paper. Materials included in this study, and their approximate glass transition temperatures, are:

$As_2Te_3Tl_2Se$	70°C
As_2Se_3	180
As_2S_3	205
$(GeTe_2)_{30}$ $(GeSe_2)_{70}$	325
GeTeSe	287
$Ge_{15}Te_{81}Sb_2S_2$	135
$Ge_{17}Te_{83}$	146
$Ge_{16}As_{35}Te_{28}S_{21}$	200
$Te_{48}As_{30}Si_{12}Ge_{10}$	220
$Te_{40}As_{35}Si_{18}Ge_7$	305

The glasses were formed from high purity (>99.99%) elements which were melted and homogenized in sealed silica glass ampoules followed by quenching in a water or mercury bath.[1/]

Thermal conductivity values were determined by a steady state comparative technique.[2/] Low thermal impedances at the interfaces in the sample holder were assured by use of a thermal conduction grease.[3/] A heat shield was employed to minimize radiation losses. Temperatures were measured with three mil copper-constantan thermocouples. Pyrex Code 7740 glass was used as the reference, and thermal conductivity values from the literature[4/] were used for this material. The absolute thermal

conductivity of our reference material had an uncertainty of about ±10%, due to variations in the thermal conductivities of different batches of Pyrex 7740 and possible error in the literature values employed. It was estimated that radiation effects gave less than 10% error at 500°K. The relative uncertainty in our measured values was usually less than 5%; this depended on the degree of thermal equilibrium attained, and scatter in some of our data is due to imperfect equilibrium.

The results are plotted in Fig. 1. For comparison, thermal conductivities from the literature are plotted for Pyrex 7740,[4] As_2S_3,[5,6] and As_2Se_3.[6,7] It is noteworthy that our thermal conductivity curves for most of the chalcogenide materials lie within a fairly narrow range. The thermal conductivity of the chalcogenide glasses examined ranged between 2.5 and 4 mW/cm-deg at 300°K. The thermal conductivity increased with increasing temperature and was typically between 4 and 10 mW/cm-deg at 500°K, although our data for many of the materials did not extend to that temperature. It may also be noted that at 300°K most of the chalcogenide alloys exhibit a thermal conductivity about one fourth that of oxide-based glasses such as Pyrex 7740 and vitreous SiO_2. As might be expected, for As_2S_3 vs. As_2Se_3 and $(GeTe_2)_{30}(GeSe_2)_{70}$ vs. $(GeTe_2)_{50}$-$(GeSe_2)_{50}$ the more weakly bonded material (or the material having the larger mean atomic weight) in each of the two pairs exhibits the smaller thermal conductivity.

Thomas and Fray[8] obtained temperature independent thermal conductivities between 120 and 400°K for two multicomponent chalcogenide

glasses. One of these glass compositions, $Te_{48}As_{30}Si_{12}Ge_{10}$, was also included in our study, and yielded a distinct temperature dependence. Although we offer no explanation for Thomas and Fray's results, our own results indicate that temperature independent thermal conductivities for those glasses are unlikely. Uphoff and Healy's data for As_2S_3, As_2Se_3, and $As_2(S\text{-}Se\text{-}Te)_3$ alloys near room temperature agree very well with our data.[2] Thermal conductivity values for As_2S_3 and As_2Se_3 by Kolomiets, et al. and Stourac, et al. at 300°K are about twice as large as our results for the same materials.[6] Data of Rozov, et al. for As-Se and As_2Te_3-As_2Se_3 alloys are in better agreement with our results, although their values are generally smaller than ours.[7] An estimated curve for As_2Se_3 from their data for the As-Se system is also included in Fig. 1(a), since their study included compositions bracketing but not including As_2Se_3. Earlier results[5] for As_2S_3 are about 50% smaller than our results for that material. A portion of the discrepancy between our data and other workers' data for As_2S_3 may be due to sample differences. Most of the discrepancies must be due to differences in the absolute calibration of the various apparatus. The uncertainty in the absolute values of our results is less than the above discrepancies, if the absolute accuracy of the values for our reference material is accepted as better than 10%.

An extensive description of the thermal conductivity and specific heat of noncrystalline solids has been given by Zeller and Pohl.[9] They note the similarity of thermal conductivities for a great variety of materials

including polymers, varnishes, Se, GeO_2, and SiO_2-based glasses. Although their discussion emphasizes the similarity of the low temperature properties of these materials, the thermal conductivities of those materials above $100^{\circ}K$ are also all within about one decade of each other. A portion of Fig. 3 of Ref. 9, obtained from Refs. 10-13, is included in Fig. 1(b) for comparison with our data, showing that at $300^{\circ}K$ our chalcogenide data are in the middle of the range of data for those other noncrystalline solids. The curves in Fig. 1(b) for SiO_2 and Pyrex 7740 are the recommended values from Ref. 4, and are similar to the curves shown by Zeller and Pohl for the same materials. Many of the chalcogenide glasses in our study showed stronger temperature dependences than do the other noncrystalline solids in the vicinity of $300^{\circ}K$.

Acknowledgement

The authors are grateful to Dr. J. P. de Neufville and J. Tyler for furnishing glass samples for this study.

Figure Caption

Figure 1 Thermal conductivity vs. temperature for a number of chalcogenide glasses as determined in this study. Data for As_2S_3 and As_2Se_3 by other workers are included for comparison: b, Ref. 5; c, Ref. 6, Kolomiets, et al.; d, Ref. 6, Stourac, et al.; and e, estimated from Ref. 7. Also included for comparison are data for Pyrex® 7740 and vitreous silica from the National Standard Reference Series (a, Ref. 4), and several other noncrystalline solids as summarized by Zeller and Pohl (Ref. 9): f, Ref. 10; g, Ref. 11; h, Ref. 12; and i, Ref. 13.

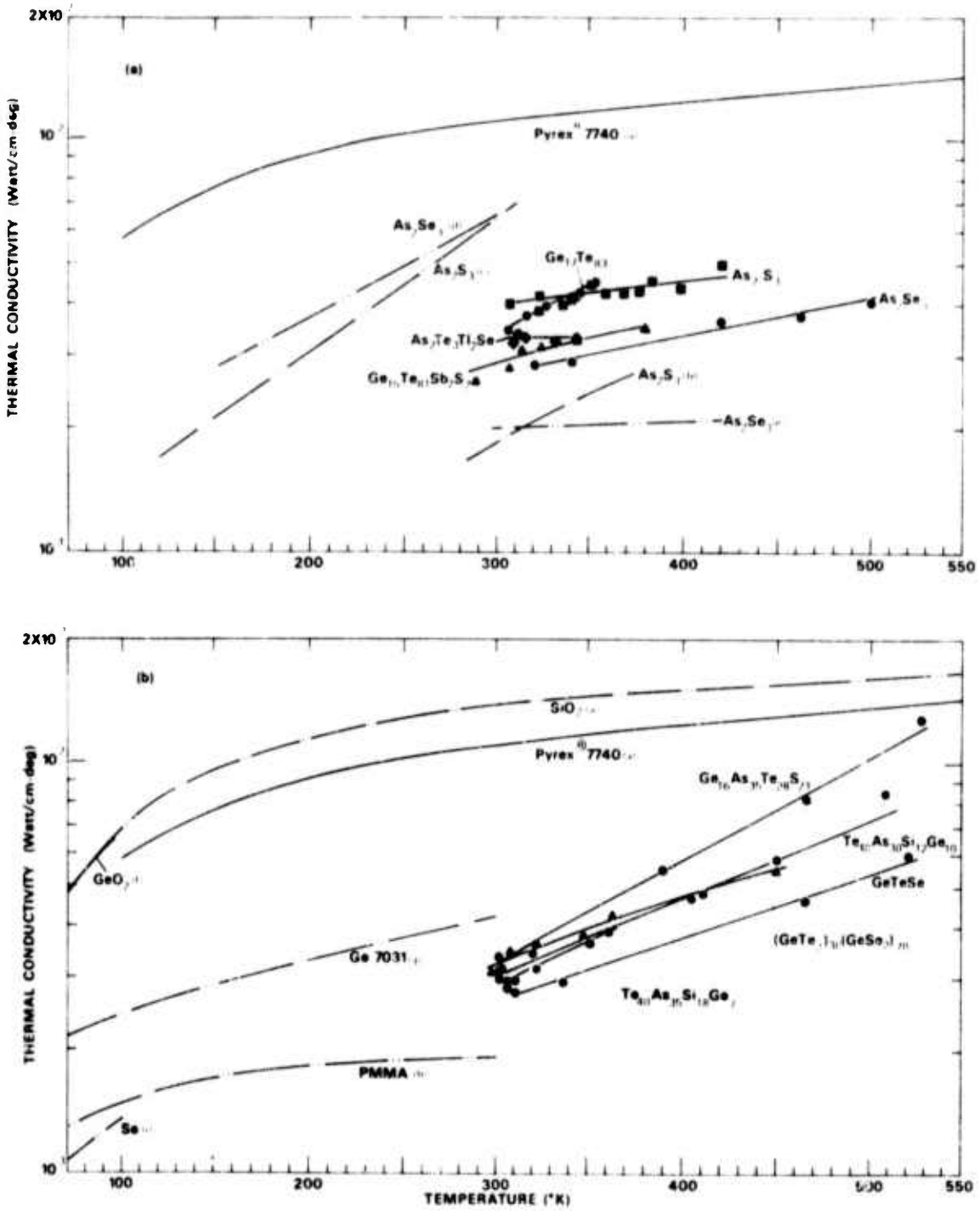
(a)
THERMAL CONDUCTIVITY (Watt/cm deg)
Pyrex 7740
As2Se3
As2S3
Ge15Te81
As2S3
As2Se3
As2Te3Tl2Se
Ge15Te81Sb2S4
As2S3
As2Se3
100
200
300
400
500
550
(b)
THERMAL CONDUCTIVITY (Watt/cm deg)
SiO
Pyrex 7740
GeO2
Ge 7031
PMMA
Se
Ge16As35Te48S1
Te81As15Si3Ge1
GeTeSe
(GeTe)1/2(GeSe)1/2
Te81As15Si3Ge1
100
200
300
400
500
550
TEMPERATURE (°K)

Fig. 1

References

1. J. P. de Neufville, J. Non-Crystalline Solids 8-10 (1972) 85.

2. cf., H. L. Uphoff and J. H. Healy, J. Appl. Phys. 32 (1961) 950.

3. G. C. Electronics, Rockford, Illinois, Z-5 transistor silicone compound No. 8101.

4. R. W. Powell, C. Y. Ho, and P. E. Liley, "Thermal Conductivity of Selected Materials," National Standard Reference Data Series - National Bureau of Standards - 8, (U.S. Government Printing Office, Washington, 1966).

5. American Institute of Physics Handbook, (McGraw Hill, New York, 1957), p. 4-76.

6. B. T. Kolomiets, L. Payasova, and L. Stourach, Sov. Phys. - Solid State 7 (1965) 1285;
L. Stourac, B. T. Kolomiets, and V. P. Silo, Czech. J. Phys. B 18 (1968) 92.

7. I. A. Rozov, A. F. Chudnovskii, and V. F. Kokorina, Sov. Phys. - Semicond. 1 (1968) 969.

8. C. B. Thomas and A. F. Fray, Royal Radar Establishment, England, to be published.

9. R. C. Zeller and R. O. Pohl, Phys. Rev. B 4 (1972) 2029.

10. K. Guckelsberger and J - C Lasjaunias, Compt. Rend. 270 (1970) B 1427.

11. J. H. McTaggart and G. A. Slack, Cryogenics 9 (1969) 384.

12. K. Biermann and K. H. Hellwege, J. Polymer Science 57 (1962) 99;
C. L. Choy, G. L. Salinger, and Y. C. Chang, J. Appl. Phys. 41 (1970) 597.

13. G. K. White, S. B. Woods, and M. T. Elford, Phys. Rev. 112 (1958) 111.

Transport and Optical Properties of Amorphous $(GeTe_2)_{1-x}(GeSe_2)_x$ Alloy Films*

Howard K. Rockstad and Richard Flasck
Energy Conversion Devices, Inc., Troy, Michigan 48084

Electrical, thermoelectric, and optical measurements were made on sputtered amorphous alloys covering the $(GeTe_2)_{1-x}(GeSe_2)_x$ pseudobinary system. The structure of annealed alloys is believed analogous to the chemically ordered but random network structure of SiO_2 glasses. Optical absorption gaps and electrical activation energies increase with increasing Se:Te ratio. Annealing of the films increases both the optical gaps and electrical activation energies. The thermopower is positive for unannealed films, but for annealed films with significant Se content ($x > 0.45$) the thermopower is negative. These data represent the first observations of negative thermopowers in amorphous chalcogenide alloys.

I. INTRODUCTION

Comprehensive measurements of electrical, thermoelectric, and optical properties of amorphous alloys in the entire $(GeTe_2)$-$(GeSe_2)$ system yield a number of interesting observations which can be employed to give a much better understanding of the electronic structure of these materials than would be possible if similar measurements were performed only on individual compositions. Bulk glasses cannot be made of Te-rich materials in this system; however, using a sputtering technique, amorphous films were prepared for representative compositions extending from $GeTe_2$ to $GeSe_2$. Even though glasses cannot be readily obtained from quenching the liquid phases for some of the alloys [$GeTe_2$ to $(GeTe_2)_{70}(GeSe_2)_{30}$], calorimetric studies on sputtered films show that glass transition temperatures exist for all the alloys. DeNeufville[1] discussed optical properties, electrical activation energies, thermal properties and densities for these films. He observed that the optical gap, electrical activation energy and glass transition temperature increase with increasing Se:Te ratio while the electrical conductivity at a given temperature, $\sigma(T)$, decreases. Also, the density decreases with increasing Se:Te ratio. In this paper we extend the description of the optical and electrical properties and we also describe thermopower behavior for these amorphous alloys, including these properties for both unannealed and annealed alloys. In contrast to previous observations that the thermopower for amorphous

chalcogenides is always positive, we have found negative thermopowers for $GeSe_2$-rich materials in this alloy system. We found that for any given composition in this system containing some Se, the material before anneal has a positive thermopower but annealing tends to make the thermopower negative (i.e., by either bringing about a reduction in the positive thermopower in spite of an increase in the conductivity activation energy, or by bringing about a negative thermopower in the annealed state).

The structure of annealed films in this alloy system probably is a network containing almost entirely Ge-Te and Ge-Se bonds with Ge in 4-fold and Te and Se in 2-fold coordination, as discussed by deNeufville[1] and Rockstad and deNeufville,[2] in analogy with the network of Si-O bonds in vitreous SiO_2.[3] This suggestion is supported by extrema in various physical properties relating to bond strength at the GeX_2 stoichiometric composition for $Ge_{1-y}X_y$ alloys, for X = Te, Se, and $Te_{0.5}Se_{0.5}$.[1,2,4] In this structure for $GeTe_2$, for example, the Te-Ge-Te tetrahedral bond angles are preserved, with Ge atoms at the centers of the tetrahedra; the Ge-Te-Ge bond angles are variable. Even though there is probably nearly complete chemical ordering, the germanium-tellurium tetrahedra are assembled in a random network structure,[3] as exemplified, for example, by the Evans-King model. In this model, various-membered rings of atom-pairs (mostly five and six) are present. Within the Ge-Te-Se ternary, the $GeTe_2$-$GeSe_2$

pseudobinary is particularly interesting because of this structural analogy with vitreous silica and because of the extrema in various physical properties that occur on this pseudobinary line.

DeNeufville[1] showed that the glass transition temperature T_g rose smoothly from about 230°C for $GeTe_2$ to 420°C for $GeSe_2$. The rate of change of T_g (as well as the optical gap) with composition was significantly greater near $GeSe_2$ than near $GeTe_2$, suggesting that the addition of a small concentration of the weaker Ge-Te bonds to the network made up of Ge-Se bonds had a relatively large effect on reducing the glass transition temperature (and optical gap). DeNeufville also reasoned that the films were homogeneous on a fine scale both before and after annealing at T_g.

Electrical conductivities for these materials are thermally activated, although there are slight curvatures in the log σ vs. 1/T plots. The electrical activation energies are near one half of the optical gap,[1] as is the case for many other amorphous chalcogenides. As discussed by a number of people, amorphous chalcogenide semiconductors are believed to have bands of extended states through which transport takes place, although with a relatively low mobility of the order of 1 to 10 $cm^2/V\text{-}sec$.[5,6] It is also believed that such materials have localized states lying between the valence and conduction bands due to the inherent disorder of the amorphous lattices.[5,6,7] The dc conductivities for the $(GeTe_2)_{1-x}(GeSe_2)_x$ films are apparently due to

the extended states, with the Fermi level located in the general vicinity of the center of the gap between the valence and conduction bands. Localized states play no more than a minor role in the transport properties described in this paper, except that the localized states may be important in determining the location of the Fermi level,[8] or except to the degree that a "soft" mobility edge is important.

It is, of course, desirable to evaluate optical gaps for any amorphous material. Unfortunately, because of exponential (or other) tails in the fundamental optical absorption edge, optical gaps are somewhat ambiguous. The high absorption coefficient regimes for many amorphous semiconductors fit a relation $\alpha\hbar\omega = B(\hbar\omega - E_o)^2$ where α is the absorption coefficient, $\hbar\omega$ is the photon energy, and E_o and B are constants; this relation can be derived by assuming parabolic bands.[9] Thus E_o is a suitable parameter for an optical gap. Another parameter often used is the photon energy for which α takes on a certain value. In this paper we shall choose to use the photon energy for which $\alpha = 10^4\ cm^{-1}$ and we designate this energy as E_{O4}.

X-ray spectra of both unannealed and annealed films used in this study confirmed their amorphous state. Although the sputtered films contained argon, we believe this argon did not affect the physical properties described in this paper. Fagen also concluded that the changes of electrical properties upon annealing are not related to the

argon content.[10]

II. EXPERIMENTAL

Films were sputtered onto Corning 7059 glass substrates or, in the case of thermopower samples, sapphire substrates, with coplanar molybdenum electrodes. Substrates were held near room temperature during deposition; however, experience with crystallization and annealing effects suggests that the effective film deposition temperatures were as high as 70 or 80°C. Sputtering cathodes were prepared as described by deNeufville.[1] Microprobe analysis showed that the Ge, Te, and Se contents of the films were within two atomic per cent of the original cathode compositions.

Thermopower measurements were performed in a vacuum chamber. The sapphire substrate was placed between two low-thermal mass heating elements. Each thermopower data point was obtained from the slope of a ΔV vs. ΔT line, where ΔV and ΔT were the voltage and temperature differences at the molybdenum - chalcogen junctions. Typically, ΔT extended from -2 to 2 degrees. The absolute thermopower of molybdenum was negligible compared to that of the chalcogen ide. Annealing of the thermopower sample was performed in the same apparatus by raising the sample temperature to the quoted annealing temperature for a few minutes. Since annealing effects are both time and temperature dependent the quoted annealing temperatures do not

have an absolute meaning. However, it is our experience, that for a given annealing temperature a major fraction of any annealing effect took place in the short interval used here. Conductivities were measured on the thermopower samples in situ.

Optical samples were annealed in a furnace flushed with dry nitrogen for a time of about one-half hour. The annealing temperatures were between the temperature at which annealing effects saturated and T_g for each alloy. Conductivity measurements were also made on these samples in this furnace, and agreed with the conductivity measurements on the thermopower samples.

III. OPTICAL SPECTRA

Optical absorption spectra at room temperature for unannealed films of various alloys from $GeTe_2$ to $GeSe_2$ were described by deNeufville.[1] Absorption spectra at room temperature for annealed films are shown in Fig. 1. These latter spectra are similar to the spectra for unannealed films but the curves are shifted to higher energies. No significant changes in slopes were noted except for $GeSe_2$, for which the absorption edge slope increased upon annealing. A direct comparison of spectra for unannealed and annealed films of $GeTe_2$ is given in Fig. 4 of Ref. 1. In Fig. 2 the compositional dependences of E_{04} at room temperature for unannealed and annealed films are shown. This figure, reproduced from Ref. 1 but corrected

at x = 1.0, also includes conductivity activation energies evaluated at 25°C. The data of Fig. 1 for representative compositions are replotted in Fig. 3 as $\sqrt{(\alpha h\omega)}$ vs. $h\omega$, showing the linearity of such a plot for high absorption coefficients. Fig. 3 also includes plots for unannealed films for x = 0.3 and 0.7.

Let us define $\Gamma = \partial \ln(\alpha/\alpha_o)/\partial h\omega$ and evaluate Γ at $\alpha = 10^3$ cm^{-1}. Table I lists values of E_{04}, E_o, $B\Gamma$, and Γ^{-1} for various annealed alloys. For annealed films B ranges from 3.5×10^5 to 7.6×10^5 cm^{-1} eV^{-1}. The slopes of the absorption edges for the annealed alloys shown in Fig. 1 progressively decrease as the optical gap increases, with the exception of those for $GeSe_2$ and GeTeSe. In fact, all curves except that for $GeSe_2$ can be nearly collapsed into one curve by scaling the energy axes. The decrease of slope with increasing gap is borne out by the decrease in both B and Γ in Table I, with the exception of $GeSe_2$. The absorption edge for $GeSe_2$ is shallower than that for $GeTe_2$, while alloying $GeTe_2$ and $GeSe_2$ gives absorption edges which are shallower than that of either $GeTe_2$ or $GeSe_2$.

The values of B in Table 1 are comparable with the values tabulated by Mott and Davis[6] for a few other amorphous semiconductors. The values of Γ^{-1} range from 0.07 to 0.11 eV. The corresponding values of Γ range from 9 to 14 eV^{-1}. These latter values are smaller than values of Γ (15 to 22 eV^{-1}) tabulated by Mott and Davis for a number of other amorphous semiconductors. A small portion of the difference can be

attributed to the fact that Mott and Davis' values for Γ were obtained from exponential portions of the absorption curves whereas our values were evaluated at $\alpha = 10^3$ cm^{-1}, where the plots in Fig. 1 still show some curvature. Nevertheless, evaluation of Γ at lower absorption coefficients for x = 0.1 and 1.0 in Fig. 1, for example, yields 16 and 11.5 eV^{-1}, respectively; these values are only 6 to 15% larger than the values listed in Table I for the same materials. Thus, at least the Se-rich materials in the $(GeTe_2)_{1-x}(GeSe_2)_x$ system have values of Γ about one-half as large as the Γ values for some amorphous chalcogenides such as As_2Se_3.[6] This is significant since, in attempting to understand the source of the exponential absorption edge in amorphous semiconductors, the narrow range of Γ values for various materials has usually been noted by other workers.

The temperature dependence β of E_{O4} was measured between 300 and 400°K with the following results:

$GeTe_2$	6.7 (±0.2) x 10^{-4} eV/deg
GeTeSe	6.1 (±0.6) x 10^{-4}
$(GeTe_2)_{30}(GeSe_2)_{70}$	5.8 (±1) x 10^{-4}
$GeSe_2$	6.8 (±0.7) x 10^{-4}

Thus, the temperature dependence of E_{O4} is relatively invariant with composition, with a value of 6 to 7 x 10^{-4} eV/deg.

TABLE I

OPTICAL PARAMETERS FOR $(GeTe_2)_{1-x}(GeSe_2)_x$ FILMS

	x	E_{04} (eV)	E_o (eV)	B ($\times 10^5 cm^{-1} eV^{-1}$)	Γ at 10^3 cm^{-1} (eV^{-1})	Γ^{-1} at $10^3 cm^{-1}$ (eV)
$GeTe_2$	0	1.20	1.07	5.6	13.8	0.07
	0.1	1.22			13.8	0.07
	0.3	1.36	1.23	5.2	9.7	0.10
GeTeSe	0.5	1.59	1.43	4.9	10.7	0.09
	0.7	1.77	1.56	3.5	9.1	0.11
	0.9	2.09			9.1	0.11
$GeSe_2$	1.0	2.42	2.24	7.6	10.8	0.09

IV. ELECTRICAL AND THERMOELECTRIC PROPERTIES

For all the alloys examined in this system, annealing of films at temperatures between the substrate deposition temperature and the appropriate glass transition temperature brought about decreases in the electrical conductivity, increases in the conductivity activation energy, and increases in the optical gap. The annealing effects on the conductivity are shown in Fig. 4(a) and (b) where the electrical conductivity and conductivity activation energy ΔE_o at 96°C are plotted vs. annealing temperature for a number of alloys. Arrows are also included to show the glass transition temperatures. For most of the alloys, the effects of annealing on the electrical properties saturated 15 or more degrees below T_g. Higher annealing temperatures gave no further changes in the conductivity until the crystallization temperature was reached, whereupon the conductivity increased by several orders of magnitude. However, slight changes were found in the Seebeck coefficient even in the vicinity of T_g.

The temperature dependence of the electrical conductivity and Seebeck coefficient for amorphous $GeTe_2$ are shown in Fig. 5(a) and (b) at different annealing temperatures. The electrical conductivity is apparently thermally activated; however, there is slight curvature in the log σ vs. 1/T plots. For convenience, we define the parameter $\Delta E_o = -\partial \ln\sigma / \partial(1/kT)$ evaluated at 96°C. The high temperature portions of the S vs. 1/T plots are linear, within experimental error. It is

possible, nevertheless, that a curvature corresponding to the small curvatures in the log σ vs. 1/T curves can be present in the S vs. 1/T curves. We define the slope $\Delta E_s/e = dS/d(10^3/T)$. The annealing behavior illustrated in Fig. 5(a) and (b) shows that ΔE_o increases, $\sigma(T)$ decreases, and ΔE_s increases with annealing.

The temperature dependences of σ and S for a $(GeTe_2)_{30}(GeSe_2)_{70}$ film are shown in Fig. 6(a) and (b). The annealing effects on σ are qualitatively similar to the annealing effects for $GeTe_2$. The annealing effects on S are drastically different, however. Virgin films of $(GeTe_2)_{30}$ $(GeSe_2)_{70}$ yield positive linear S vs. 1/T plots with a positive slope, as did $GeTe_2$ films. But annealing decreases S until it becomes about -1.0 mV/^{o}K, and the slope ΔE_s also is negative. Also, for the annealing interval from 188 to 268^{o}C, in which the pronounced change in S from positive to negative takes place, the change in electrical conductivity is only about a factor of 2. Since the conductivity change is so small for this drastic change in S, it is tempting to suggest that this annealing step involved a slight change in position of the Fermi level from the valence band side to the conduction band side of the gap, and that the electron and hole conductivity mobilities are comparable. Of course, this is not the only possible interpretation but it is the simplest.

Results for GeTeSe were qualitatively very similar to those shown in Fig. 6 for x = 0.7. In this case, a change in S from a positive value to about -0.7 mV/^{o}K took place between the 195 and 273^{o}C annealing

steps; the conductivity decrease in this annealing interval was about a factor of 4 to 5. Upon further annealing at 336°C (above T_g of 290°C) S remains negative but its magnitude is reduced to about 0.4 mV/°K as shown in Fig. 7.

Figure 8 shows σ and S vs. 1/T for a $(GeTe_2)_{70}(GeSe_2)_{30}$ film (x = 0.3). The results for S are intermediate to the results shown in Figs. 5 and 6 for x = 0 and 0.7, respectiveiy. For x = 0.3, S progressively decreases with annealing but does not reach a state that is clearly indicative of n-type conduction. After annealing at 250 and 271°C, S exhibits a minimum which is indicative of mixed conduction but with the predominant transport species changing with temperature. At low temperature p-type conduction probably predominates slightly for those most-annealed states.

The compositional dependences of σ and ΔE_c measured at 96°C are shown in Fig. 9 for virgin and well-annealed films. Figure 7(a) and (b) summarize the temperature dependences of S for various compositions of films in the virgin and well-annealed amorphous states. Figure 7 shows that in unannealed films both S and ΔE_s increase as Te is replaced by Se, coupled with the increase in ΔE_o, as would be expected if the dominant transport took place in a band of states well below the Fermi level and with the separation of those states and the Fermi level increasing with increasing Se content. However, for the annealed amorphous state S decreases progressively with X in the same range

of x, whereas ΔE_o still increases with X. Fig. 10 shows the annealing dependence of S and ΔE_s evaluated at 96°C for various compositions. The decrease in S with increasing annealing temperature is seen for compositions from x = 0 to 0.5.

For unannealed films with x = 0, 0.1, 0.3 and 0.5, approximate differences $\Delta E_o - \Delta E_s$ are 0.03, 0, 0.03, and 0.01 eV respectively. These differences are all small and can be readily accounted for by a very slightly temperature dependent mobility. ΔE_s could not be determined for larger values of x because of the films' high resistivities.

For annealed $GeTe_2$ (x = 0), $\Delta E_o - \Delta E_s$ was about 0.04 to 0.05 eV, and is probably accounted for by a slight temperature dependence of the mobility and/or slightly mixed conduction. For strongly annealed $(GeTe_2)_{0.9}(GeSe_2)_{0.1}$ films (x = 0.1), ΔE_s is only 0.28 eV whereas ΔE_o is about 0.63 eV. The fact that both S and ΔE_s are significantly lower for these films than for $GeTe_2$ even though ΔE_o is slightly larger, coupled with the enormity of $\Delta E_o - \Delta E_s = 0.35$ eV, clearly suggests that there are significant contributions to the transport from carriers in bands of states both above and below the Fermi level for the x = 0.1 material. A reduction in both S and ΔE_s is expected for two-carrier transport, as shown by the equations in Table 2 of Rockstad, et al.[11] Also, in view of the general trend towards negative thermopower as the Se:Te ratio is increased, it is evident that $\Delta E_o - \Delta E_s$ for x = 0.1

is primarily due to mixed conduction rather than a temperature dependent mobility. It is, perhaps, surprising that S vs. 1/T is, nevertheless, linear. Linearity, even in the presence of two-carrier transport, can of course result if the relative location of the Fermi level with respect to the valence and conduction band edges is independent of T.

The structure of S vs. 1/T for annealed films with x = 0.3 and 0.4, in particular, shows evidence of mixed conduction, as discussed earlier, and the existence of the minimum near 500°K suggests a transition from the predominance of one band to the other as the temperature is changed. Films with greater amounts of Se, such as x = 0.5 and 0.7, also indicate this behavior but their large magnitude of S and the predominance of the negative slopes imply predominant transport in a conduction band above the Fermi level. Unfortunately, for the latter alloys, because of their high resistivities, the temperature ranges for Seebeck coefficient measurements were severely limited. A direct comparison of ΔE_o and ΔE_s cannot profitably be made for the latter alloys because of these restricted temperature ranges.

Figure 11 shows S vs. composition at specified temperatures. Curve (a) for unannealed films shows the increase of S with increasing Se:Te ratio, while curve (b) for annealed films shows a nearly progressive decrease of S with increasing Se:Te ratio and a change in

sign from positive to negative in the vicinity of x = 0.45.

V. DISCUSSION

The s^2p^4 outer electron configuration for Group VI elements such as Se and Te leads to a filled lone pair band lying between the bonding and antibonding bands for Group VI solids, if hybridization between the s and p states is negligible.[12,13] This lone pair band is then the valence band. For materials like $GeTe_2$, with Ge in four-fold coordination and Te in two-fold coordination, the valence band should also be a non-bonding or lone pair band.

Hence, a measure of optical gaps or pseudogaps is not a measure of the gap between bonding and antibonding states. We expect, nevertheless, that the lone pair band will be more or less similarly located between the bonding and antibonding bands for different compositions in this pseudobinary system. Thus, as the composition and effective bond strength are changed, the energy difference between the peaks of the valence and conduction band densities of states should follow the effective bond strength. Whether the valence band is a bonding band or a lone pair band then has little effect on the ensuing discussion.

Although many amorphous semiconductors exhibit linear log σ vs 1/T plots, the films discussed here all have slightly curved log σ vs 1/T plots, though the conduction still appears to be thermally activated.

Either a temperature dependent mobility or a temperature dependence of the Fermi level might account for the curvature. Another possibility is a "soft" mobility edge, where the mobility increases with increasing density of states in the band tail, giving rise to curvature while still maintaining a thermally activated character. Such behavior is discussed in detail by Redfield[14] and also illustrated analytically by Rockstad.[15]

For the remaining discussion it is convenient to separately discuss the annealing behavior of these alloys and the compositional dependence of various physical properties.

A. Annealing

Annealing of these alloys at temperatures below T_g brought about increases in the optical absorption edge energy and the conductivity activation energy and also marked changes in the thermopower. The temperature range in which annealing took place was relatively independent of composition, even though T_g increased significantly with increasing Se:Te ratio. Measurements of conductivity as a function of film thickness show that the annealing effects are volume distributed effects,[1] in contrast with the surface effects described by Johnson and Quinn.[16] Concomitant with the annealing effects on the electrical and optical properties described here, deNeufville[17] found enthalpy changes and small changes in the X-ray diffraction patterns. For $GeTe_2$ films, for example, the enthalpy decrease during annealing was 0.3 kcal/gm-atom. The X-ray diffraction patterns indicated amorphous

structures for both unannealed and annealed films.

The density of states pseudogap, as indicated by the optical absorption edge, increases with annealing for the alloys described here. Several possible explanations of this increase should be considered.[18] Annealing is expected to reduce defects and voids, although we do not expect dangling bonds in these chalcogenides. Such a reduction could sharpen the tails of the density of states spectra and thereby increase the optical gap. The optical absorption edge slopes do not change significantly upon annealing (see Fig. 4 of Ref. 1) except for the case of $GeSe_2$, and so they do not indicate a sharpening of the density states tails. It is possible, however, according to the theory of Dow and Redfield,[19] that the optical absorption edge slope is not directly connected to the density of states slope, in which case the density of states tails may have sharpened even though the optical absorption edges did not.

For unannealed films, significant fluctuations in bond lengths and bond angles might be expected. These fluctuations may then be reduced by annealing. Thus the unannealed films would possess many weaker bonds than do the annealed films, leading to a smaller gap in the unannealed films.

Another important possibility is that the annealing effects involve changes in bonding, towards a more ordered structure having only Ge-X bonds and no Ge-Ge or X-X bonds, with X = Te, Se. If the unannealed

materials contain Ge-Ge and X-X bonds as well as Ge-X bonds, as is certainly plausible, but the annealed materials contain only Ge-X bonds, then the effective bond strength and especially the density of states pseudogap should increase with annealing, as was observed. However, sufficient atomic motion for a gross rearrangement of atoms on the short time scale of a few minutes cannot take place as far below T_g as the observed annealing temperatures. Annealing begins around 100°C but T_g is 230°C or more. Viscosities have not been measured for these alloys, but it is reasonable to assume that the activation energy for the viscosity is at least 1.5 eV. In this case, the viscosity at 100°C is more than five decades higher than the viscosity at T_g so that gross atomic motion at 100°C is not possible. It may be, nevertheless, that only slight atomic motions are required to provide the necessary bonding rearrangements. Furthermore, the estimate given above for the viscosity at 100°C applies only to the annealed states. The unannealed material may have a lower viscosity at 100°C than would an annealed material. Perhaps the most important factor is the degree of freedom of the Te or Se bonds, in contrast with the rigidity of the tetrahedral bonds of Ge. Each tellurium atom forms two bonds, at approximately right angles, and also has two lone-pair (non-bonding) p-state electrons. Thus, only two of six equivalent possible bonding directions are used in any given bonding arrangement. Slight atomic displacements during annealing could make

it favorable for a Te bond to change direction completely so that Te-Te and Ge-Ge bonds can be replaced by Ge-Te bonds without gross motion of individual atoms. Intuitively, one feels the sputter deposition on substrates held at room temperature should result in a great number of Ge-Ge and/or X-X bonds, and we believe that the bonding in annealed films of $GeTe_2$ in particular must be made up almost entirely of Ge-Te bonds. Extrema in various physical properties such as the optical gap at the GeX_2 composition in the Ge-X binary alloy system support this contention.[2,4] Hence we feel bond rearrangement (chemical ordering) is a likely contribution to the annealing effects observed in this work.

Quantitative discussion of this interpretation can also be made. The difference in bond energy between like-atom bonds and unlike-atom bonds can be estimated from $23(X_A-X_B)^2$ kcal/mole, where X_A and X_B are obtained from Pauling's electronegativity scale.[30] In this formula mole refers to a mole of bonds, as opposed to a mole of material. For $GeTe_2$ and $GeSe_2$, respectively, these differences are 2.1 and 8.3 kcal/mole of bonds or 0.09 and 0.36 eV/bond. At and below 10^4 cm^{-1} the absorption edges for $GeTe_2$ and $GeSe_2$ shifted about 0.07 and 0.16 eV, respectively. If only a few per cent of the bonds are weaker in the unannealed materials by energies of order 0.09 and 0.36 respectively for $GeTe_2$ and $GeSe_2$, the observed shifts in the absorption tails can probably be accounted for. For $GeTe_2$, using 4 as the average

number of bonds per $GeTe_2$ molecule, the measured enthalpy change of 0.3 kcal/gm-atom can be accounted for by changing only 11% of the bonds from like-atom bonds to unlike-atom bonds. It is quite plausible that this small percentage of like-atom bonds are created in the as-deposited sputtered films.

For unannealed films, significant fluctuations in bond lengths and bond angles might be expected. These flucutations may then be reduced by annealing. Thus the unannealed films would possess many weaker bonds than do the annealed films, leading to a smaller gap for the unannealed films. However, because of the freedom of orientation of the Te and Se bonds, bond distortions in these alloys should not be as pronounced as bond distortions in Group IV amorphous semiconductors having purely tetrahedral bonding.[21] Hence, although relief of bond distortions likely contributes to the observed annealing effects, this effect is probably not as important as chemical ordering for these GeX_2 alloys.

In addition to bringing about an increase of the density of states pseudogap, annealing of these materials changes the predominant p-type behavior of the unannealed films to mixed n-p or even strong n-type behavior in annealed films. Such a change could be interpreted as due to a shift in the Fermi level location away from the valence band or by an increase in the ratio of electron to hole mobility. We feel that the first explanation is more likely. As described in detail in a separate

paper,[22] the data suggest that the Fermi level for unannealed materials is displaced significantly from the center of the pseudogap or mobility gap but that annealing brings the Fermi level near the center of the gap. As well as E_{O4}, ΔE_o also increases with annealing, and, as noted by deNeufville,[1] the percentage increase in ΔE_o is greater than the percentage increase in E_{O4}. Thus, the ratio $\Delta E_o/E_{O4}$ increases upon annealing, suggesting that the Fermi level is displaced further from the nearest band edge in annealed than unannealed materials.

Either of two alternatives could explain the shift of the Fermi level. If the defect structure in the unannealed films causes a peak in the density of states as illustrated by Davis and Mott,[23] then this peak could locate the Fermi level below the gap center. Annealing then reduces this defect structure or changes the location of the peak. Alternatively, in the absence of such a peak, a valence band tail which is steeper than the conduction band tail could cause the Fermi level to be closer to the valence band mobility edge in the unannealed materials. A sharpening of the conduction band tail could then bring the Fermi level relatively closer to the conduction band in the annealed materials. We favor the latter alternative since the occurrence of such a peak in the density of states for these materials seems unlikely.

Devenyi, et al.[22] suggest that the annealing effects on the electrical conductivity of sputtered Ge-Te films were partially the result of desorption of argon which was included during the sputtering process.

Fagen[10] made detailed studies of annealing effects on the argon desorption with mass spectrometric analyses for sputtered $GeTe_2$ films, and found that most of the argon escapes at temperatures above the temperatures where the annealing effects on the electrical conductivity take place. He thus concluded that argon desorption was not responsible for the annealing effects on the electrical conductivity.

B. Compositional Dependence

As expected, the optical gap or density of states pseudogap increases with increasing Se:Te ratio. This increase follows the expected increase in bond strength. This optical gap is not linear with Se-content, but, as discussed by deNeufville[1] and in the introduction, the greatest rate of change of gap with composition occurs at the $GeSe_2$ end of the $GeTe_2$-$GeSe_2$ binary.

Although annealed films are closest in detailed structure to genuine glasses, the unannealed films are of interest in their own right. Firstly, unannealed films come closer to a completely disordered structure, since we believe annealed films really have ordered chemical bonding even though they are amorphous with an otherwise random network structure. Secondly, our thermopower results for unannealed films indicate a strong similarity of behavior for the different compositions. At a given temperature, for example, S increases uniformly with increasing Se:Te ratio, in accordance with the increase in ΔE_o and ΔE_s (see Fig. 11).

In contrast, for annealed films the thermopower at a given temperature drops rapidly from positive to negative values as the Se:Te ratio is increased beyond 0.5 (i.e., x is increased beyond 0.3).

DeNeufville[1] noted that the percentage increase in ΔE_o due to annealing increased considerably with increasing Se:Te ratio, even though the percentage increase in E_{O4} due to annealing changed only slightly with changing Se:Te ratio. Correlating this observation with the thermopower observation, a self-consistent picture is obtained if it is supposed that 1) all unannealed films in this system have a Fermi level considerably below the pseudogap center; 2) annealing brings the Fermi level closer to the gap center for $GeTe_2$-rich alloys but it is still on the valence band side; 3) annealing raises the Fermi level above the gap center, towards the conduction band, for $GeSe_2$-rich materials.

The negative thermopowers observed for $x > 0.3$ represent the first observations of negative thermopowers in amorphous chalcogenides,[25] to the best of our knowledge, with the exception of observations of small negative thermopowers in amorphous Se.[26] It has often been noted in the past that amorphous chalcogenides invariably yield positive thermopowers.[27] We also found a change in thermopower from positive to negative as Te is replaced by Se in annealed films of two other pseudobinary systems, the GeTe-GeSe and GeTeAs-GeSeAs alloy systems. The effect is analogous to the results of self-compensation in wide

band gap crystalline semiconductors such as those II-VI crystals which can be fabricated only p-type or only n-type.[28] The direction of the trend from Te to Se is also the same as the trend in II-VI crystals.

C. Comparison of Chalcogenide and Group IV Semiconductors

Finally, a comparison of the slopes of the optical absorption edges of amorphous chalcogenides and amorphous Group IV semiconductors is of interest. With the exception of absorption measurements by Donovan, et al.[29] and Chopra and Bahl,[30] absorption edges for amorphous Ge films are generally significantly shallower than the edges for chalcogenide films having similar optical gaps. Typical values of Γ^{-1} for amorphous Ge[31] are 0.14 to 0.16 eV compared to about 0.07 eV for $GeTe_2$ and 0.06 eV for As_2Te_3.[32] The steep absorption edges described by Donovan et al. and Knotek and Donovan[29] may be an occupation effect at the Fermi level rather than the result of a steep density of states edge.[33] Based on the optical absorption results, the density of states tails for amorphous Ge are also probably significantly shallower than for amorphous chalcogenides. This is apparently a result of bond distortions. As illustrated by the Polk model, large bond distortions are required for a random network structure of tetrahedrally bonded atoms, with the angle of distortion varying up to 20^{o}.[21] These gross bond distortions stand in stark contrast to a random network structure of $GeTe_2$, which can come about with very little

distortion of the tetrahedral bonds about the Ge atoms. Experimental results for the analogous glass SiO_2 show that the tetrahedral bond angles for silicon are preserved.[3] Any necessary bond angle fluctuations are apparently absorbed by the oxygen bonds. We expect the structure of $GeTe_2$ to be similar to that of SiO_2, with any necessary bond angle fluctuations absorbed by the Te bonds, which are not as rigid as the Group IV tetrahedral bonds, and hence such fluctuations do not involve as much energy as do fluctuations in Ge tetrahedral bond angles. Furthermore, amorphous Ge may involve fluctuations in bond lengths as well, whereas amorphous $GeTe_2$ probably does not. These bond distortions as well as numerous unsatisfied bonds in amorphous Ge likely cause the shallow density of states tails, which in turn lead to a much higher density of states at the Fermi level for amorphous Ge than for amorphous chalcogenides having a comparable band separation. Other multicomponent chalcogenides, other than GeX_2 materials treated in this pape. probably also have relatively steep density of states tails compared to Ge due to the flexibility of the chalcogen bonds, even if the composition is relatively complex.

SUMMARY

Annealing of alloys in the $GeTe_2$-$GeSe_2$ system brings about increases in the optical gaps and the electrical activation energies. The thermopower is positive for all unannealed alloys but is negative for

the $GeSe_2$-rich annealed alloys. The Fermi level is below the gap center for all the unannealed alloys, but is relatively close to the gap center for annealed alloys. The unannealed alloys probably possess a significant degree of chemical bonding disorder which is reduced by annealing, as was demonstrated by Ferrier, et al.[34] for amorphous Te-Tl alloys. As the disorder is reduced through annealing, the tendency is for the Fermi level to shift to higher energies. This same major tendency appears to also take place in tetrahedrally bonded amorphous films such as GaAs and GaSb.[35]

These observations of negative thermopowers represent the first negative thermopowers observed for amorphous chalcogenides,[25] although negative thermopowers have also been reported for tetrahedral glasses such as $CdGeAs_2$[34] and Group IV[2,35,36] and III-V[35] amorphous films.

Amorphous chalcogenides such as $GeTe_2$ have steeper density of states tails than purely tetrahedrally bonded amorphous Ge because of the bonding flexibility allowed by the two-fold coordinated chalcogen atoms. Thus, the chalcogenides also have lower densities of localized states through the gap between extended states than does amorphous Ge.

ACKNOWLEDGEMENTS

The authors are grateful to D. E. Sarrach and R. Nowicki for sample preparation and to R. Seguin for much of the optical data. We are grateful to J. P. deNeufville, E. A. Fagen and H. Fritzsche for numerous discussions and suggestions. We thank S. R. Ovshinsky for his encouragement and support of this program.

FOOTNOTES

*Work supported by the Advanced Research Projects Agency under Contract No. DAHC 15-70-C-0187.

1. J. P. deNeufville, J. Non-Crystalline Solids 8-10, 85 (1972).

2. H. K. Rockstad and J. P. deNeufville, Proceedings of the Eleventh International Conference on the Physics of Semiconductors (Polish Scientific Publishers, Warsaw, 1972), p. 542.

3. D. L. Evans and S. V. King, Nature 212, 1353 (1966); W. H. Zachariasen, J. Am. Chem. Soc. 54, 3841 (1932).

4. H. K. Rockstad, R. Flasck, and J. P. deNeufville, Bull. Am. Soc. 18, 454 (1973); unpublished data.

5. L. Banyai, Physique des Semi-Conducteurs (Dunod, Paris, 1964); A. I. Gubanov, Quantum Electron Theory of Amorphous Conductors (Consultants Bureau, New York, 1965); N. F. Mott, Advan. Phys. 16, 49 (1967); M. H. Cohen, H. Fritzsche, and S. R. Ovshinsky, Phys. Rev. Letters 22, 1065 (1969).

6. N. F. Mott and E. A. Davis, Electronic Processes in Non-Crystalline Materials (Oxford, London, 1971).

7. H. Fritzsche, in Electronic and Structural Properties of Amorphous Semiconductors, (Academic Press, in press).

8. cf. H. K. Rockstad, J. Non-Crystalline Solids 8-10, 621 (1972).

9. J. Tauc, in Optical Properties of Solids, Ed. F. Abeles, (North Holland, Amsterdam, 1970).

10. E. A. Fagen, to be published.

11. H. K. Rockstad, R. Flasck, and S. Iwasa, J. Non-Crystalline Solids 8-10, 326 (1972).

12. E. Mooser and W. B. Pearson, Progress in Semiconductors (Heywood and Company L.T.D., London, 1960), Vol. 5, p. 104.

13. M. Kastner, Phys. Rev. Letters 28, 355 (1972).

14. D. Redfield, Phys. Rev. Letters 27, 730 (1971).

15. Refer to σ_2 in Fig. 4(b) of Ref. 5d and replace $[1-f(E)]\, g(E)$ in Eq. 1 of that reference with $\mu(E)$, where $\mu(E)dE$ is the differential mobility; for the case of Fig. 4(b), $\mu(E)$ increases approximately exponentially as $\exp (E-E_F)/0.04eV)$.

16. R. T. Johnson, Jr. and R. K. Quinn, Solid State Commun. 9, 393 (1971).

17. J. P. deNeufville, unpublished.

18. Second Semi-Annual Technical Report prepared by Energy Conversion Devices, Inc. for the Advanced Research Projects Agency under Contract DAHC15-70-C-0187, p. 18.

19. J. D. Dow and D. Redfield, Phys. Rev. B 5, 584 (1972).

20. L. Pauling, The Nature of the Chemical Bond (Cornell University Press, Ithaca, 1960).

21. D. E. Polk, J. Non-Crystalline Solids 5, 365 (1971); D. E. Polk and D. S. Boudreaux, Phys. Rev. Letters 31, 92 (1973).

22. H. K. Rockstad, following paper.

23. E. A. Davis and N. F. Mott, Phil. Mag. 22, 903 (1970).

24. A. Devenyi, C. Rusu, M. Rusu, A. Barna, and P. B. Barna, Proceedings of the International Conference on the Physics and Chemistry of Semiconductor Heterojunctions and Layered Structures 4, 105 (1970).

25. H. K. Rockstad and R. Flasck, Bull. Am. Phys. Soc. 17, 116 (1972); Third Semi-Annual Technical Report prepared by Energy Conversion Devices, Inc., for the Advanced Research Projects Agency under Contract DAHC15-70-C-0187, pp. 48ff.

26. Y. I. Dutchak, V. Y. Prokhorenko, and I. P. Klyus, Sov. Phys. - Semicon. 2, 625 (1968).

27. See, for example, Ref 6, p. 329.

28. See, for example, M. Aven and J. S. Prener, Physics and Chemistry of II-VI Compounds (Interscience, New York, 1967).

29. T. M. Donovan, W. E. Spicer, J. M. Bennett, and E. J. Ashley, Phys. Rev. B 2, 397 (1970); M. L. Knotek and T. M. Donovan, Phys. Rev. Letters 30 652 (1973).

30. K. L. Chopra and S. K. Bahl, Phys. Rev. B 1, 2545 (1970).

31. A. H. Clark, Phys. Rev. 154, 750 (1967); R. C. Chittick, J. Non-Crystalline Solids 3, 255 (1970); G. A. N. Connell and A. Lewis, submitted for publication, and references contained therein.

32. H. K. Rockstad, J. Non-Crystalline Solids 2, 192 (1970).

33. H. K. Rockstad, "Sharp absorption edges and shallow density of states tails for amorphous germanium," in preparation.

34. R. P. Ferrier, J. M. Prado, and M. R. Anseau, J. Non-Crystalline Solids 8-10, 798 (1972).

35. W. Beyer and J. Stuke, J. Non-Crystalline Solids 8-10, 321 (1972); J. Stuke, Proceedings of the Second International Conference on Conduction in Low-Mobility Materials, Eilat, Israel (Taylor and Francis, London, 1971) pp. 193ff.

36. R. Grigorovici, N. Croitoru, and A. Devenyi, Rev. Romanian Phys. 11, 869 (1966).

37. R. Callaerts, M. Denayer, F. H. Hashmi, and P. Nagels, Discussions of the Faraday Soc. 50, 27 (1970); J. Tauc, L. Stourac, V. Vorlicek, and M. Zavetova, Proceedings of the Ninth International Conference on the Physics of Semiconductors, Moscow, (Nauka, Leningrad, 1968), Vol. 2, p. 1251.

FIGURE CAPTIONS

Figure 1. Spectral dependence of the absorption coefficient for annealed amorphous $(GeTe_2)_{1-x}(GeSe_2)_x$ alloys at room temperature. Also included is the curve for unannealed $GeSe_2$.

Figure 2. Variation with composition of the optical gap and the conductivity activation energy. After J. P. deNeufville, J. Non-Crystalline Solids 8-10, 85 (1972).

Figure 3. Optical absorption for selected unannealed and annealed amorphous $(GeTe_2)_{1-x}(GeSe_2)_x$ alloys at room temperature, plotted vs $\sqrt{(\alpha h\omega)}$ vs photon energy.

Figure 4. The electrical conductivity σ and conductivity activation energy $\Delta E_o = -\partial \ln\sigma/\partial(1/kT)$ vs annealing temperature for various alloys. Both parameters were evaluated at 96°C. Glass transition temperatures T_g are indicated by arrows.

Figure 5. Temperature dependence of the thermoelectric power S and the electrical conductivity σ for amorphous $GeTe_2$ at various stages of annealment.

Figure 6. Temperature dependence of the Seebeck coefficient S and the electrical conductivity σ for amorphous $(GeTe_2)_{30}(GeSe_2)_{70}$ at various stages of annealment.

Figure 7. Temperature dependence of the Seebeck coefficient S for various amorphous $(GeTe_2)_{1-x}(GeSe_2)_x$ alloys in the unannealed states. Annealed states shown are those obtained near or below T_g.

For $x = 0.5$, data for a higher temperature anneal ($336^{\circ}C$) is also shown.

Figure 8. Seebeck coefficient S and the Seebeck coefficient activation energy $edS/d(10^3/T)$ vs annealing temperature for various amorphous $(GeTe_2)_{1-x}(GeSe_2)_x$ alloys, evaluated at $96^{\circ}C$.

Figure 9. Temperature dependence of the Seebeck coefficient S and the electrical conductivity σ for amorphous $(GeTe_2)_{70}(GeSe_2)_{30}$ at various stages of annealment.

Figure 10. Seebeck coefficient vs composition at $60^{\circ}C$ for unannealed alloys and at $96^{\circ}C$ for fully annealed alloys.

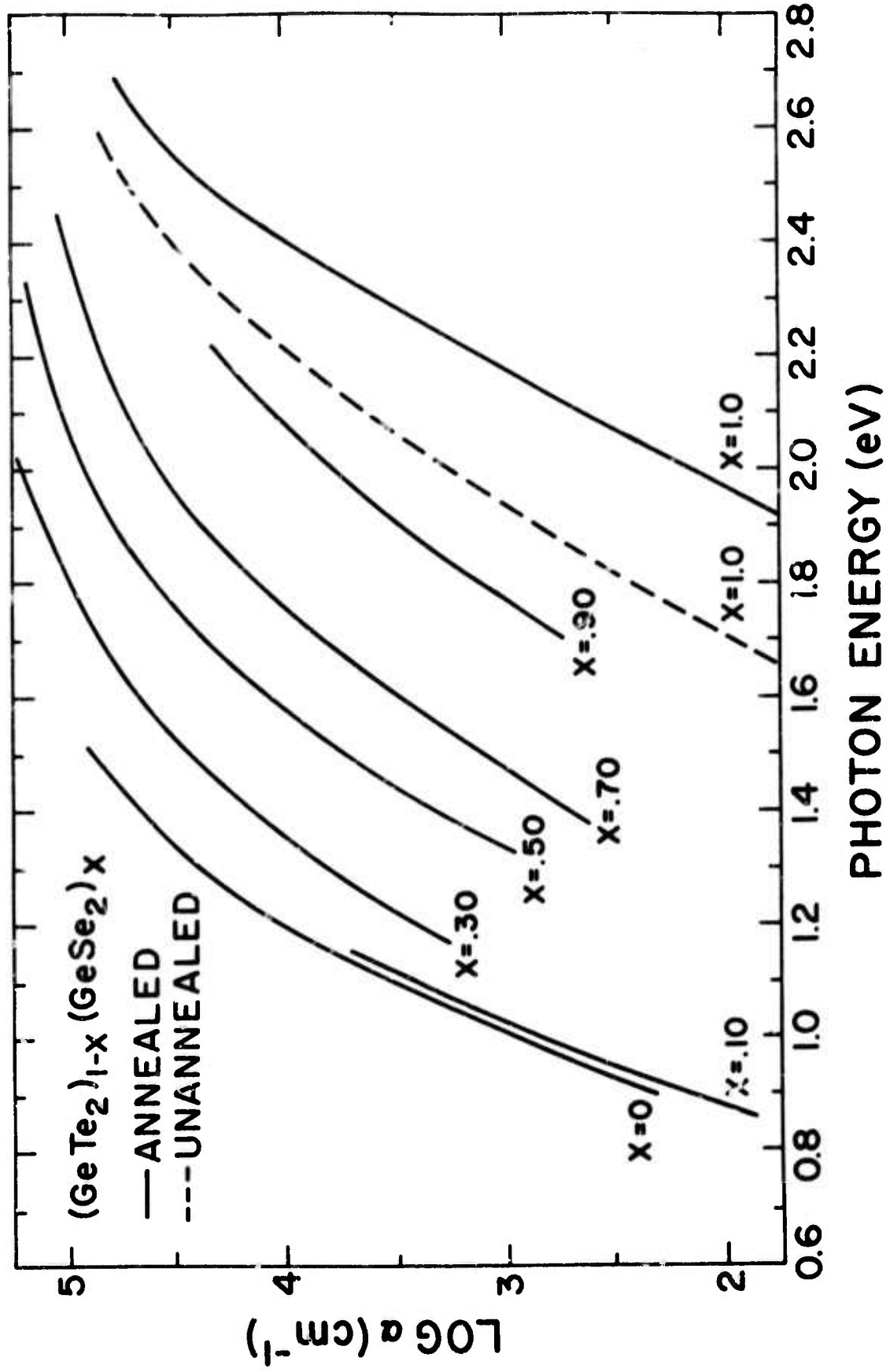
LOG α (cm⁻¹)
PHOTON ENERGY (eV)
(GeTe2)1-x (GeSe2)x
—ANNEALED
---UNANNEALED
X=0
X=.10
X=.30
X=.50
X=.70
X=.90
X=1.0
X=1.0
5
4
3
2
0.6
0.8
1.0
1.2
1.4
1.6
1.8
2.0
2.2
2.4
2.6
2.8

Fig. 1

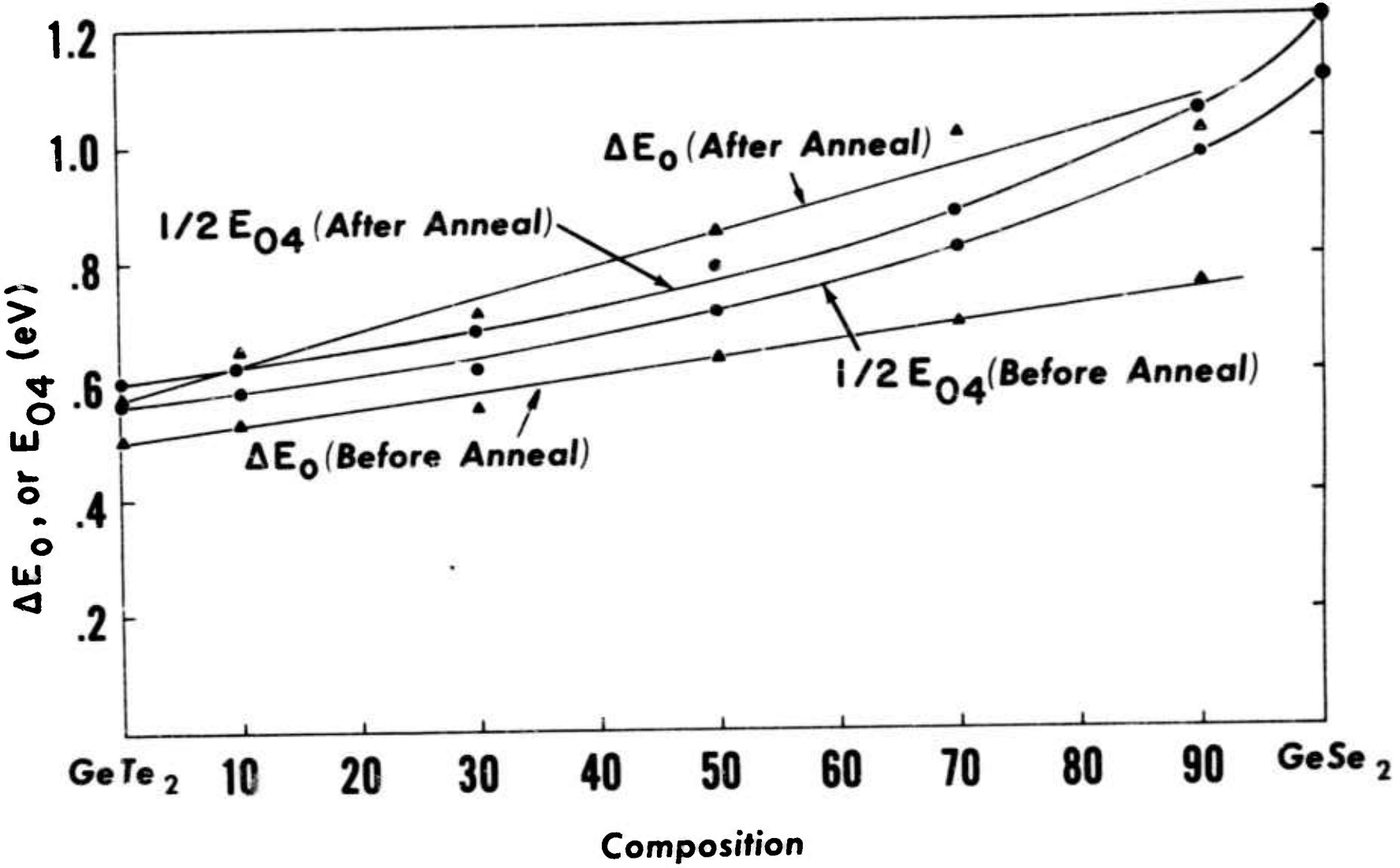
1.2
1.0
.8
.6
.4
.2
ΔE₀, or E₀₄ (eV)
ΔE₀ (After Anneal)
1/2 E₀₄ (After Anneal)
1/2 E₀₄ (Before Anneal)
ΔE₀ (Before Anneal)
GeTe₂
10
20
30
40
50
60
70
80
90
GeSe₂
Composition

Fig. 2

$\sqrt{\alpha\hbar\omega}$ (cm^{-1}eV)$^{1/2}$
PHOTON ENERGY (eV)
$(GeTe_2)_{1-x}(GeSe_2)_x$
— ANNEALED
--- UNANNEALED
X=0
X=.30
X=.30
X=.50
X=.70
X=.70
X=.90
X=1.0
X=1.0
0
100
200
300
400
500
600
700
1.0
1.2
1.4
1.6
1.8
2.0
2.2
2.4
2.6

Fig. 3

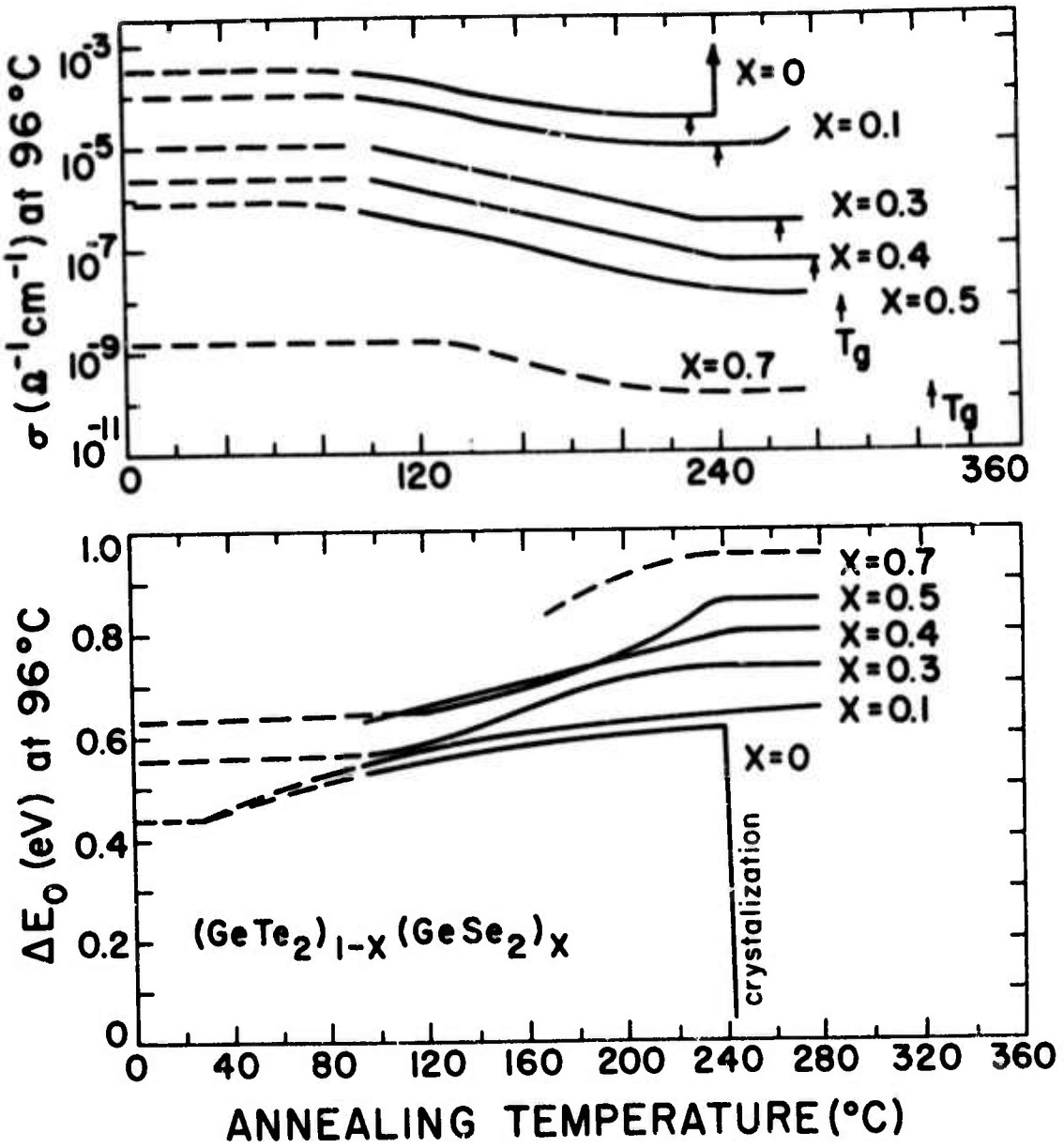
σ (Ω⁻¹cm⁻¹) at 96°C
10⁻³
10⁻⁵
10⁻⁷
10⁻⁹
10⁻¹¹
X=0
X=0.1
X=0.3
X=0.4
X=0.5
X=0.7
Tg
Tg
0
120
240
360
ΔE₀ (eV) at 96°C
1.0
0.8
0.6
0.4
0.2
0
X=0.7
X=0.5
X=0.4
X=0.3
X=0.1
X=0
crystalization
(GeTe₂)₁₋X (GeSe₂)X
0
40
80
120
160
200
240
280
320
360
ANNEALING TEMPERATURE (°C)

Fig. 4

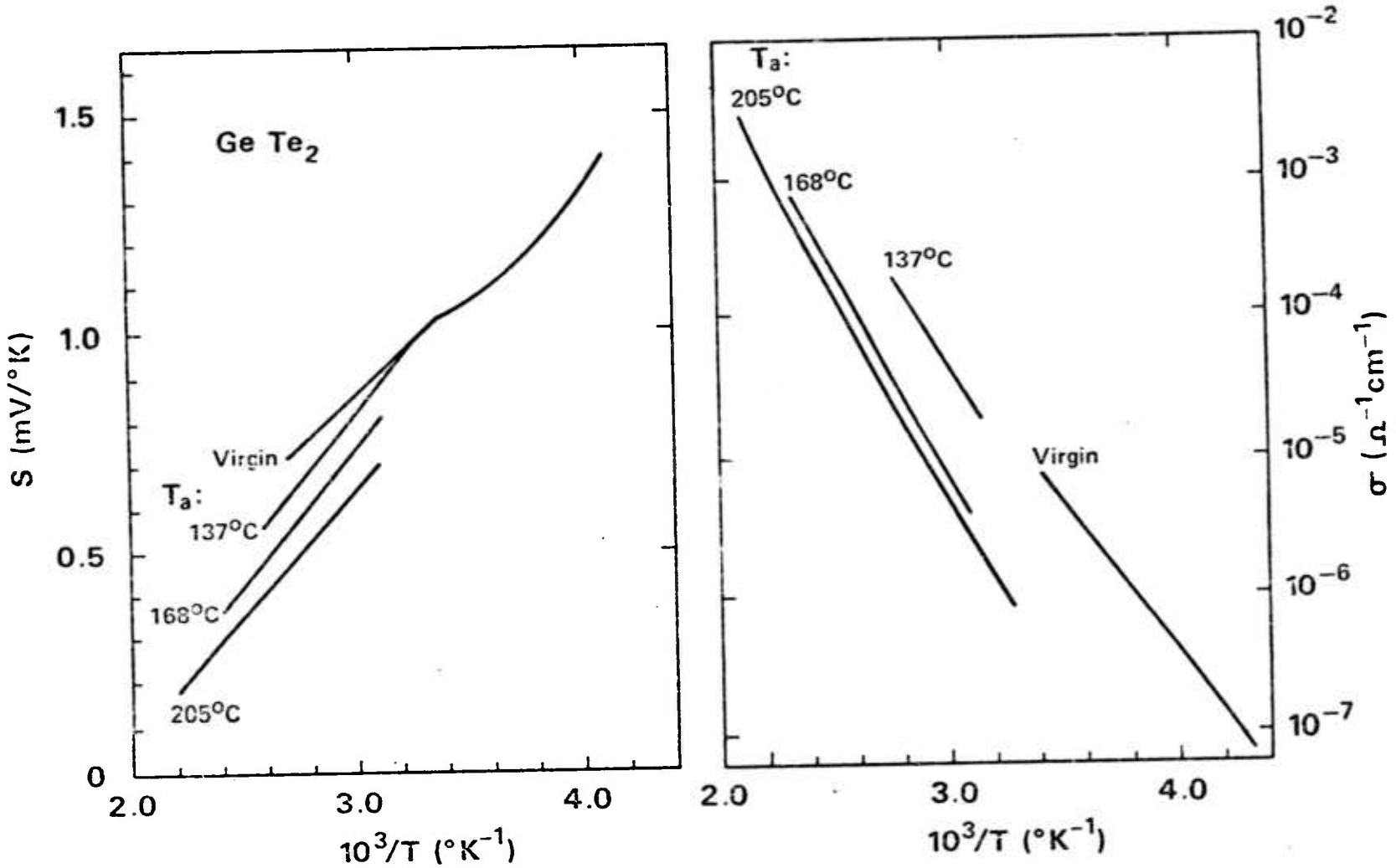
Ge Te2
S (mV/°K)
1.5
1.0
0.5
0
Virgin
Ta:
137°C
168°C
205°C
2.0
3.0
4.0
10³/T (°K⁻¹)
Ta:
205°C
168°C
137°C
Virgin
10⁻²
10⁻³
10⁻⁴
10⁻⁵
10⁻⁶
10⁻⁷
σ (Ω⁻¹cm⁻¹)
2.0
3.0
4.0
10³/T (°K⁻¹)

Fig. 5

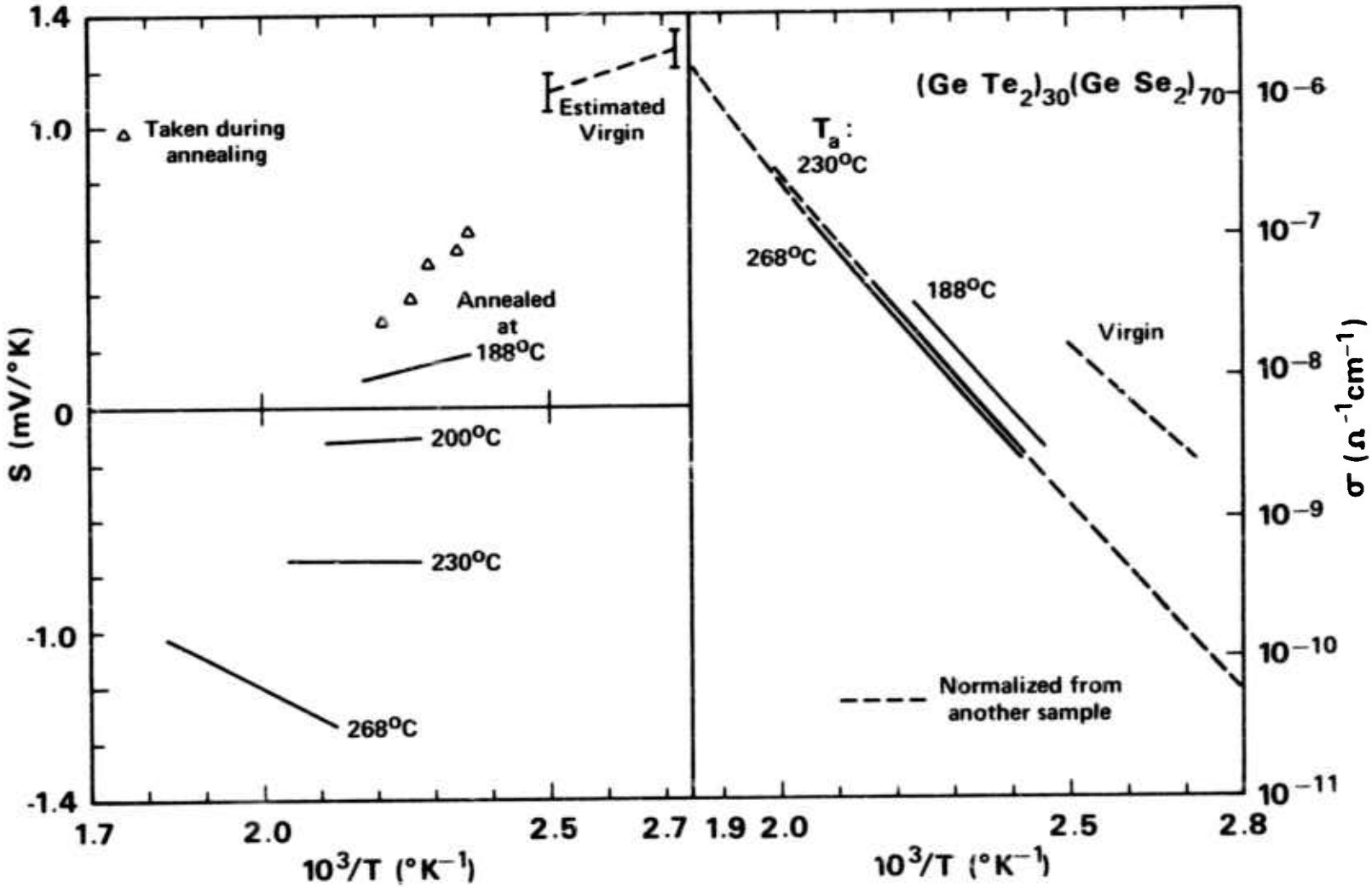
1.4
1.0
0
-1.0
-1.4
S (mV/°K)
Taken during annealing
Estimated Virgin
Annealed at 188°C
200°C
230°C
268°C
1.7
2.0
2.5
2.7
10³/T (°K⁻¹)
(Ge Te₂)₃₀(Ge Se₂)₇₀
Tₐ:
230°C
268°C
188°C
Virgin
Normalized from another sample
10⁻⁶
10⁻⁷
10⁻⁸
10⁻⁹
10⁻¹⁰
10⁻¹¹
σ (Ω⁻¹cm⁻¹)
1.9
2.0
2.5
2.8
10³/T (°K⁻¹)

Fig. 6

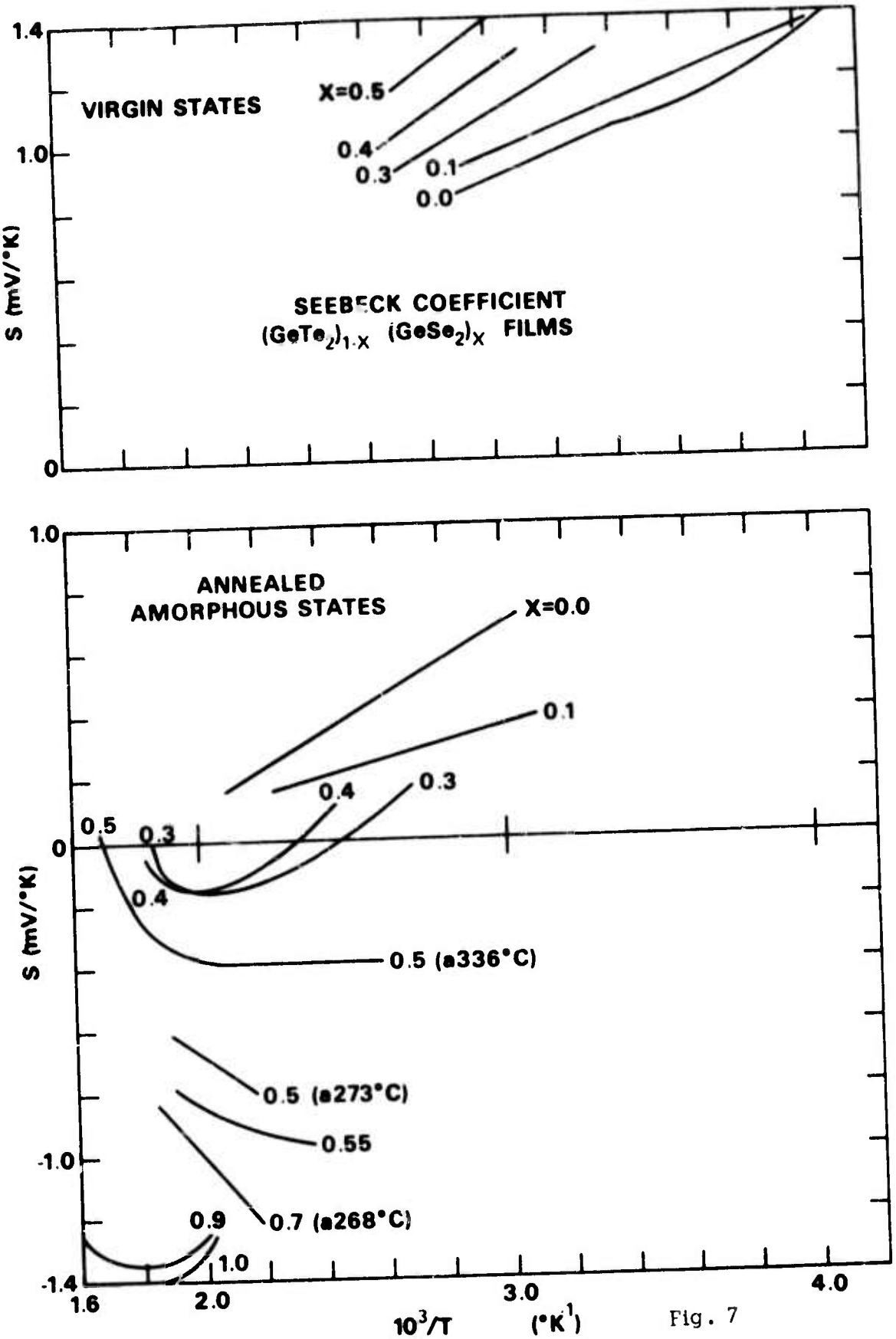
1.4
1.0
0
VIRGIN STATES
X=0.5
0.4
0.3
0.1
0.0
S (mV/°K)
SEEBECK COEFFICIENT
(GeTe2)1-X (GeSe2)X FILMS
1.0
0
-1.0
-1.4
ANNEALED
AMORPHOUS STATES
X=0.0
0.1
0.4
0.3
0.5
0.3
0.4
0.5 (a336°C)
0.5 (a273°C)
0.55
0.9
0.7 (a268°C)
1.0
1.6
2.0
3.0
4.0
10³/T (°K⁻¹)

Fig. 7

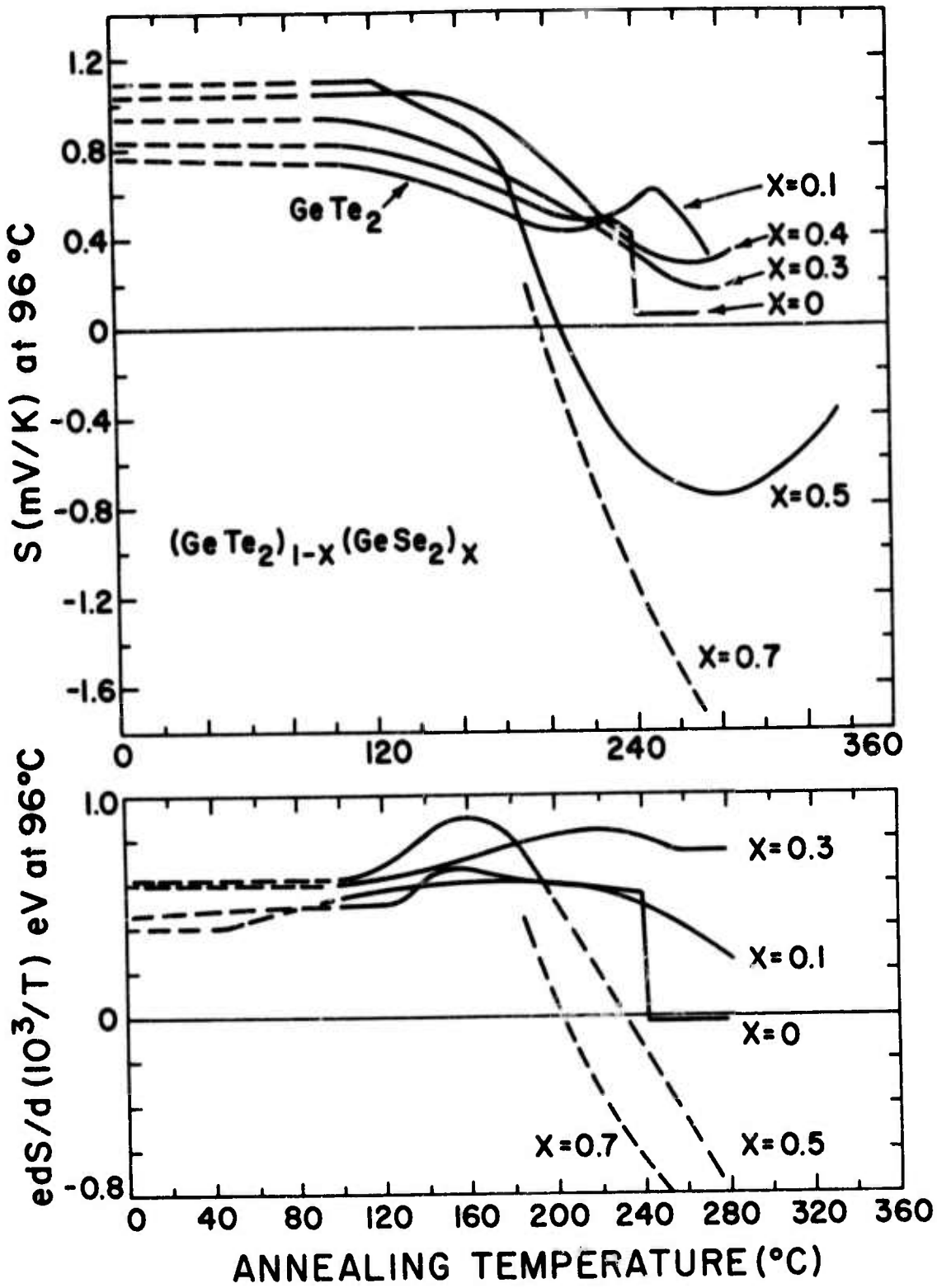
S (mV/K) at 96°C
1.2
0.8
0.4
0
-0.4
-0.8
-1.2
-1.6
GeTe2
X=0.1
X=0.4
X=0.3
X=0
X=0.5
X=0.7
(GeTe2)1-X(GeSe2)X
0
120
240
360
edS/d(10³/T) eV at 96°C
1.0
0
-0.8
X=0.3
X=0.1
X=0
X=0.7
X=0.5
0
40
80
120
160
200
240
280
320
360
ANNEALING TEMPERATURE (°C)

Fig. 8

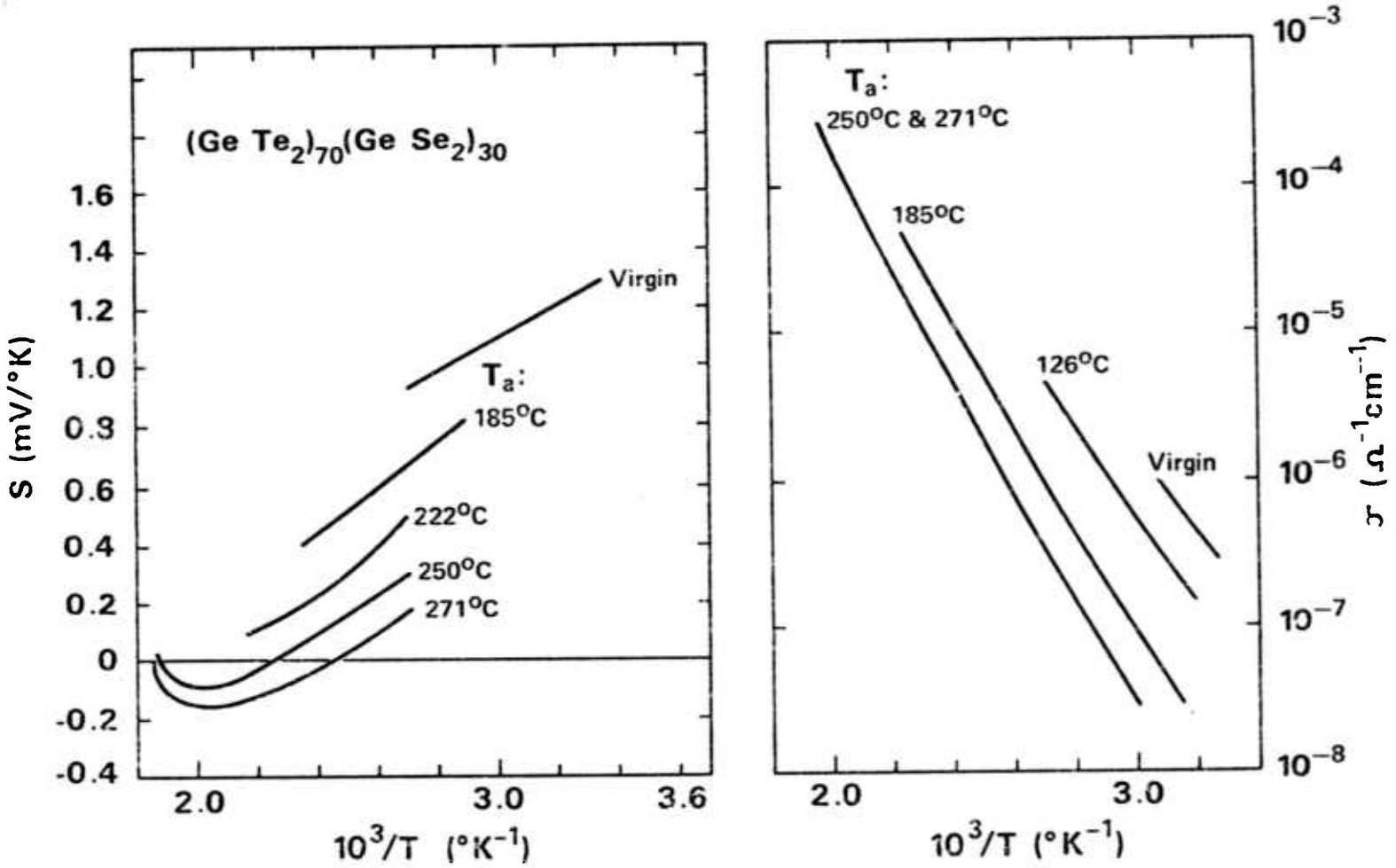
(Ge Te2)70(Ge Se2)30
S (mV/°K)
1.6
1.4
1.2
1.0
0.3
0.6
0.4
0.2
0
-0.2
-0.4
Virgin
Ta:
185°C
222°C
250°C
271°C
2.0
3.0
3.6
10³/T (°K⁻¹)
Ta:
250°C & 271°C
185°C
126°C
Virgin
10⁻³
10⁻⁴
10⁻⁵
10⁻⁶
10⁻⁷
10⁻⁸
σ (Ω⁻¹cm⁻¹)
2.0
3.0
10³/T (°K⁻¹)

Fig. 9

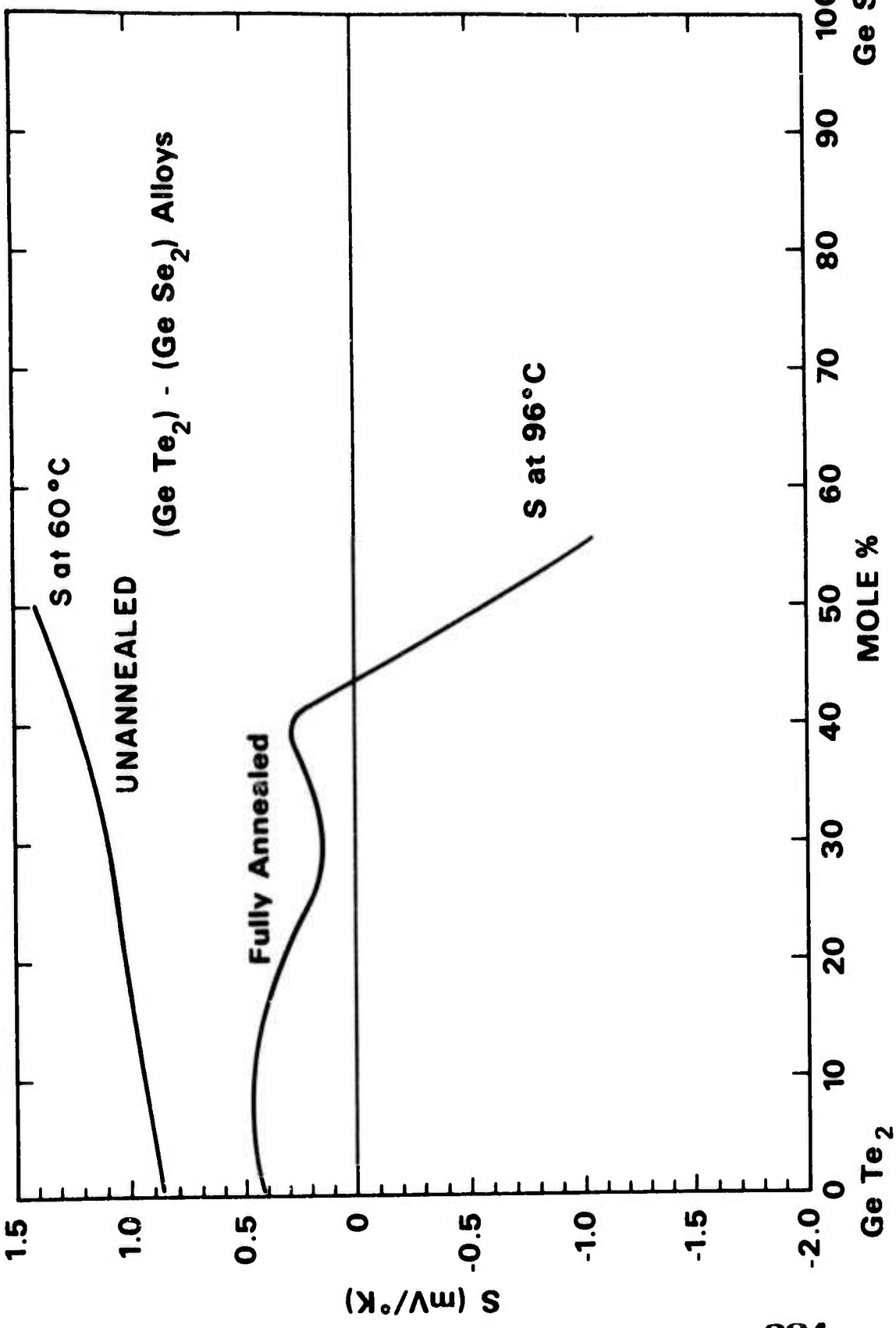
(Ge Te2) - (Ge Se2) Alloys
S at 60°C
UNANNEALED
Fully Annealed
S at 96°C
S (mV/°K)
1.5
1.0
0.5
0
-0.5
-1.0
-1.5
-2.0
0
10
20
30
40
50
60
70
80
90
100
MOLE %
Ge Te2
Ge Se2

Fig. 10

Band Level Diagram for Amorphous $(GeTe_2)_{1-x}(GeSe_2)_x$ Alloys*

Howard K. Rockstad

Energy Conversion Devices, Inc., Troy, Michigan 48084

Comparison of 'optical gaps' and 'electrical gaps' for amorphous chalcogenides is discussed. By analysis based on the observation of both n- and p-type thermoelectric powers in the $GeTe_2$ - $GeSe_2$ pseudobinary system, the position of the Fermi level with respect to valence and conduction band edges is estimated.

INTRODUCTION

Numerous comparisons have been made of so-called optical gaps and electrical conductivity activation energies for various amorphous semiconductors.[1-4] It is usually noted for amorphous chalcogenides that the conductivity is thermally activated with an activation energy of the order of one-half of an optical gap. However, definitions of optical absorption gaps in amorphous chalcogenides are somewhat arbitrary, and their relationships to a gap between extended states are unknown. Nor can the separation of the Fermi level from either of the band edges be determined precisely from the conductivity activation energy because of an unknown temperature dependence of that separation and also because of a possible temperature dependence of the mobility. Hence it has not been possible to precisely define a band level diagram for amorphous chalcogenides, nor has it been possible to state whether or not the Fermi level is in the center of a gap between extended states. It might be supposed that the Fermi level would necessarily be centrally located between valence and conduction bands at moderately high temperatures, but such a relationship may be prevented because of large densities of localized states located between those bands, particularly because of tailing of the density of states band edges for amorphous semiconductors.

Nevertheless, it is generally assumed that the Fermi level must be roughly in the center of a gap between extended states. In fact,

for the lack of a better relation, many models used for discussing other types of data assume a symmetrical density of states with the Fermi level in the precise center between valence and conduction bands.[4,5] In contrast, it will be shown below that for certain amorphous materials the Fermi level is a significant distance from a mobility gap center or a density of states pseudogap center, even at room temperature or 100 degrees above room temperature, thus assuring the predominance of one carrier over the other during thermal equilibrium. The same conclusion was reached by the author on a quite different basis for amorphous As_2Te_3 films.[6] Also, several authors have stated for certain materials that the 'conductivity gap' is more (or less) than the 'optical gap'.[1,2,4] In these relationships the conductivity gap is assumed to be twice the conductivity activation energy. Because of the ambiguities in both the 'conductivity gap' and the 'optical gap', such relationships are extremely crude. Since a shift of location of the Fermi level by only a few hundredths eV at room temperature will change the electron to hole population ratio in extended states by a factor of ten, it is clearly important to make drastic improvements in the band level relationship.

In this paper the relative location of the Fermi level with respect to extended state valence and conduction band edges is discussed for sputtered amorphous films of $(GeTe_2)_{1-x}(GeSe_2)_x$ alloys. The results represent a considerable improvement over previous generalizations

such as those described in the previous paragraphs, and they accurately describe the qualitative variation of the Fermi level position with composition and with annealing in this alloy system.

Extensive optical absorption, electrical conductivity, and thermoelectric power data have been obtained for both virgin and annealed films in this system. Optical absorption and conductivity activation energy data have been published by deNeufville.[7] DeNeufville noted that the percentage increase in the optical gap upon annealing was everywhere smaller than the percentage increase in the conductivity activation energy, and the absolute change in optical gap upon annealing increased only slightly with increasing Se:Te ratio while the absolute change in the conductivity activation energy increased considerably with increasing Se:Te ratio. The significance of deNeufville's observation in terms of the relative position of the Fermi level and the valence and conduction band edges will be made clear by the band level diagrams in this paper. The photon energy $\hbar\omega(10^4 cm^{-1})$ at which the absorption coefficient is 10^4 cm^{-1} was taken as a measure of the optical gap; this quantity will be designated E_{O4} in this paper. Since there is no true density of states gap as in crystalline materials, it is convenient to define a density of states pseudogap, and use E_{O4} as a measure of such a pseudogap.[8] The compositional dependences of E_{O4} for virgin and annealed films were given in Refs. 7 and 9, and thermoelectric data have also been given.[9] Although

the conductivity for these materials is thermally activated, there are slight curvatures in the log σ vs 1/T graphs; hence, for the following discussion $\Delta E_o = -\partial \ln\sigma/\partial(1/kT)$ at 96°C has been somewhat arbitrarily chosen as a measure of the conductivity activation energy.[9] Choice of room temperature instead of 96°C would not change the final results significantly except that data at that temperature is unavailable for the widest gap materials because of their high resistivities. Conductivity activation energies vary from 0.47 to about 0.9 eV for annealed films while E_{O4} varies from 1.2 to 2.36 eV, from $GeTe_2$ to $GeSe_2$.[9] Both properties are somewhat smaller for virgin films. Thermoelectric data indicated that all virgin compositions examined are p-type;[10] annealed films with $x \leq 0.1$ are also p-type but annealed films with $x \geq 0.5$ are n-type.[9] S vs 1/T data for annealed films with $x = 0.3$ and 0.4 show transitional behavior between valence and conduction band type of conduction; probably valence band transport dominates the mixed conduction at low temperature and conduction band transport dominates at high temperature.

ANALYSIS AND RESULTS

For this simple binary system where one Group VI element is replaced by another Group VI element, it is reasonable to make the approximation that as x is varied, $E_c - E_v$ is proportional to E_{O4}, where it is assumed that the mobility gap model is appropriate for this system and

E_c and E_v are conduction and valence band mobility edges.[11] Although the applicability of the sharp mobility edge concept is uncertain, it is nevertheless useful to employ band edges as points of reference. These band edges then may represent sharp or soft mobility edges or an energy where the differential conductivity $\sigma(E)dE$ is largest at reasonably high temperatures, say above room temperature.

For simplicity, it will be assumed that the separation of the Fermi level and the nearest edge approximately scales with the empirical parameter ΔE_o as the composition is varied.[12] Then the ratio $(E_F - E_v)/(E_c - E_v)$ or $(E_c - E_f)/(E_c - E_v)$ approximately scales with $\Delta E_o/E_{O4}$. The latter ratio $\Delta E_o/E_{O4}$ is plotted in Fig. 1 for virgin and annealed films. The two salient features of Fig. 1 are that 1) $\Delta E_o/E_{O4}$ is smaller for virgin than for annealed films and 2) the ratio for annealed films peaks at about $x = 0.5$. Furthermore, thermoelectric data indicate that annealed compositions on the $GeSe_2$ side of the peak are n-type whereas those on the $GeTe_2$ side are p-type, although there is a fairly broad range of compositions for which conduction is mixed. It appears that the peak in Fig. 1 for annealed films is a consequence of a Fermi level location which moves with respect to the center of the mobility gap as the composition is varied, passing through the center of the gap in the vicinity of $x = 0.5$.[13]

Since there are so many unknowns in amorphous materials, including namely, the effective densities of states at the mobility edges,

the carrier mobilities, the location of the Fermi level and the temperature dependences of these quantities, several complex alternatives are possible explanations of the peak in Fig. 1 coupled with the n-and p-type thermopower for annealed alloys. For example, it could be assumed that the Fermi level is in the center of the mobility gap for all compositions in the binary. Then, for consistency with the thermopower data it would follow that the mobility-density of states product for holes dominates for $GeTe_2$-rich materials and the mobility-density of states product for electrons dominates for $GeSe_2$-rich materials. The existence of the peak in $\Delta E_o/E_{optical}$ would then necessarily be explained by some appropriate variation of $\beta_{e,h}$ with composition and/or variation of the density of states at the mobility edges. Here, β_h and β_e are the temperature dependences of the separation of the Fermi level and the valence and conduction band edges, respectively. The simplest assumption, however, consistent with and making direct use of the thermopower results coupled with the peak in $\Delta E_o/E_{O4}$, is the assumption that the Fermi level is slightly on one side of the gap center for some materials and slightly on the other side for other materials.

Making the approximation that $D\Delta E_o/E_{O4} = (E_F - E_v)/E_c - E_v)$ or $(E_c - E_F)/(E_c - E_v)$, depending on whether the material is p- or n-type, with D independent of composition and determined at $x = 0.5$, $D = 0.89$ is obtained from Fig. 1. Using this value of D, E_F may then be plotted with respect to E_v and E_c. Such plots are given in Fig. 2(a) and (b) for

virgin and annealed films, respectively, the gap center, $1/2\ (E_c - E_v)$, is also plotted (dotted line) as a basis of reference for the Fermi level (solid line). Since correct values of $E_c - E_v$ are unknown, the vertical scales of Fig. 2 are labeled 'arbitrary units'. However, if eV are used as the units, the curves for the conduction band edges are equivalent to E_{O4}. The particular lines shown for the Fermi levels are based on equal electron and hole mobilities, but unequal mobilities would not change the positions significantly.[13] The essential results shown by Fig. 2(a) and (b) are that the Fermi level is significantly below the gap center for all unannealed alloys, it is relatively close to but below the gap center for annealed $GeTe_2$-rich alloys, and it is above the gap center for annealed $GeSe_2$-rich alloys.

The approximation in the above paragraphs assumes that $\Delta E_o = E_v + \beta_h T$ is proportional to $E_F - E_v$ for $x < 0.5$ (and $\Delta E_o = E_c - E_F + \beta_e T$ is proportional to $E_c - E_F$ for $x > 0.5$), which requires that β_h (β_e) scales with E_F ($E_c - E_F$) as the composition and gap are changed. Such an assumption is not valid and probably introduces an error in our treatment of a few hundredths eV at the endpoints of the $GeTe_2$-$GeSe_2$ binary. An alternative and distinctly different simplifying assumption that can be made is that β_h and β_e are independent of composition. Since β, the temperature dependence of E_{O4}, is nearly independent of composition,[9] this latter assumption may be more reasonable than the assumption of the above paragraph. Taking $\beta_h = \beta_e = 3.5 \times 10^{-4}$ eV/deg, $(\Delta E_o - \beta_{h,e} T)/E_{O4}$ can be plotted for both virgin and annealed materials.

A graph similar to Fig. 1 results. Then $D(\Delta E_o - \beta_{h,e}T)/E_{O4} = (E_F - E_v)/(E_c - E_v)$ or $(E_c - E_F)/(E_c - E_v)$, and the corresponding band level schematics for this assumption can be determined. (D in this case is 1.016.) The results are very similar to the solid lines of Fig. 2(a) and (b), with the Fermi level displaced from 0 to 0.03 eV lower for annealed films, and 0.04 to 0.08 eV lower for virgin films. The broken lines in Fig. 2(a) and (b) represent this second approximation. Note that the solid and broken lines are relatively close so that the location of the Fermi level varies very little with the approximations discussed in this last paragraph, and the qualitative conclusions which will be discussed later are unchanged.

An estimate of the mobility gap can be made for annealed GeTeSe since the Fermi level is in the center of the gap for this alloy, in our interpretation. The temperature dependence of E_{O4} for this material is $\beta = 6.8 \times 10^{-4}$ eV/deg. For those alloys where a reasonable comparison can be made, ΔE_o is close to the thermopower slope ΔE_s, so any temperature dependence of the mobility is small and will be neglected here.[9] In this case, $E_c - E_v = 2\Delta E_o - \beta T = 1.5 \pm .06$ eV at 300°K. This number is in close accord with $E_{O4} = 1.53$ eV at 300°K for that composition. Note that this calculation is independent of other approximations made earlier in this paper. An independent estimate of $E_c - E_v$ can be made from the thermopower slope for annealed $GeTe_2$ coupled with Fig. 2(b). Assuming negligible contribution to the transport in $GeTe_2$ from carriers

above the Fermi level, $E_F - E_v = \Delta E_s - \beta_h T$. Also, from the lower Fermi level position indicated in Fig. 2(b), which was derived based upon assuming β_h and β_e are independent of composition, $E_c - E_v = 2.63(E_F - E_v)$. Using $\Delta E_s = 0.55$ eV and $\beta_h \approx 1/2\ \beta$, $E_c - E_v = 1.18$ eV at 300°K is obtained, in good agreement with $E_{O4} = 1.2$ eV.[14] The good agreement between E_{O4} and the values of $E_c - E_v$ calculated here may be partially fortuitous since uncertainties of perhaps at least ±0.06 eV should be ascribed to $E_c - E_v$ due to unknowns such as motion of the Fermi level with temperature and uncertainties in proper values for the conductivity activation energy.

SUMMARY AND DISCUSSION OF THE PHYSICAL RESULTS EVIDENT IN THE BAND LEVEL DIAGRAMS

It is difficult to locate the Fermi level in the gap for amorphous semiconductors because of the great number of unknowns. Hence it is necessary to make approximations or assumptions. The assumptions made above, although not rigorously valid, are quite helpful in visualizing the location of the Fermi level in the gap for the $GeTe_2$-$GeSe_2$ alloy system.

From Fig. 2 it is seen that for virgin sputtered films the Fermi level is on the valence band side of the gap and is more than 0.1 eV from the gap center for all compositions. For annealed films the Fermi level is generally closer to the gap center than it was for virgin films; and it is below the gap center for $0 < x < 0.4$ but is above the gap center for

$0.6 < x < 1.0$.[15]

As was noted before from optical absorption data,[7,9] the density of states pseudogap increases with annealing of the sputtered films. From Fig. 2(a) and (b), annealing causes the Fermi level to move further away from the valence band for all alloys. This shift is most dramatic for $x > 0.5$, in the sense that it brings about a change in sign of thermopower behavior between the virgin and annealed states.

A model for the change of sign of the thermopower with composition for annealed materials is that even in the annealed state the Fermi level is determined by defects. We assume that the annealed materials are in metastable equilibrium at the glass transition temperature (T_g), and that defects are present in this metastable state. The nature and density of these defects are such as to cause a trend from p- to n-type behavior as the Se:Te ratio is increased. However, for unannealed films, the process of deposition on substrates held considerably below T_g introduces additional defects which completely dominate over the above defects. These additional defects cause the Fermi level to lie considerably below the gap center regardless of the Se:Te ratio.

The trend from p-type behavior to n-type behavior as Te is replaced by Se in annealed films is in the same direction as the trends observed in wide gap crystalline semiconductors, where native defects and self-compensation effects dominate the conduction behavior (i.e., certain

crystalline compounds in thermodynamic equilibrium cannot be doped with donors and others cannot be doped with acceptors).[16] We speculate that such self-compensation effects are also operative in amorphous semiconductors, even though the types of defects present in these amorphous semiconductors must be quite different than the types of defects present in crystalline semiconductors. We have also observed the same trends from p- to n-type thermoelectric power as Te is replaced by Se in annealed films of the GeTe-GeSe and GeTeAs-GeSeAs alloy system. In glasses of the As_2Te_3 - As_2Se_3 system, on the basis of a comparison of optical gaps and electrical activation energies, the Fermi level also appears to move relatively further from the valence band edge with respect to the mobility gap, as Te is replaced by Se. Although thermopower data by one laboratory for the entire system is unavailable, the literature indicates that As_2Te_3 and As_2Se_3 are both p-type[17-19,6] and the ratios $\Delta E_o/E_{optical}$ and $\Delta E_s/E_{optical}$ increase significantly with increasing Se:Te ratio.[18,19] It may well be that the Fermi level is on the valence band side of the gap center for all vitreous As_2Te_3-As_2Se_3 alloys, but that the Fermi level is much further from the gap center for small Se:Te ratios than for As_2Se_3. Thus there appears to be a trend in a variety of amorphous chalcogenides for $(E_F - E_v)/(E_c - E_v)$ to increase as the Se:Te ratio is increased.

Other detailed work on the thermopower and electrical conductivity of various amorphous chalcogenide alloys has been performed by

Seager, et al.[17] Their alternative school of thought takes these latter data as evidence for polaron conduction and avoids the use of the Fermi level and band language that was used in this paper. Nevertheless, the band language employed in this paper must also be consistent with their school of thought.

ACKNOWLEDGEMENT

The author is indebted to Professor H. Fritzsche for suggestions.

FOOTNOTES

* Work supported by the Advanced Research Projects Agency under Contract No. DAHC 15-70-C-0187

1. cf., J. T. Edmund, J. Non-Crystalline Solids 1, 39 (1968); Brit. J. Appl. Phys. 17, 979 (1966);

T. N. Vengel and B. T. Kolomiets, Sov. Phys. - Tech. Phys. 2, 2314 (1957);

J. Stuke, Festkörperprobleme 9, 46 (1969) - a paper presented at a meeting of the German Physical Society, Munich, March 1969;

K. Weiser and M. H. Brodsky, Phys. Rev. B1, 791 (1970).

2. A. E. Owen and J. M. Robertson, J. Non-Crystalline Solids 2, 40 (1970).

3. H. Fritzsche, J. Non-Crystalline Solids 6, 49 (1971).

4. K. W. Böer and R. Haislip, Phys. Letters 24, 230 (1970).

5. K. Weiser, R. Fisher, and M. H. Brodsky, Proceedings of the Tenth International Conference on the Physics of Semiconductors (U.S. Atomic Energy Commission, Oak Ridge, 1970), p. 667;

R. J. Gambino and A. J. Grant, "Photoconductivity in amorphous As_2Te_3 films", paper GC-16 at the Amer. Phys. Soc. meeting, March, 1972;

W. E. Howard and R. Tsu, Phys. Rev. B1, 4709 (1970).

6. H. K. Rockstad, J. Non-Crystalline Solids 8-10, 621 (1972).

7. J. P. de Neufville, J. Non-Crystalline Solids 8-10, 85 (1972).

8. Alternatively, an optical gap or density of states pseudogap can be defined from the extrapolated intercept E_o of $\sqrt{(\alpha\hbar\omega)}$ with the $\hbar\omega$ axis, using absorption coefficient data above about 10^4 or 10^5 cm^{-1}. Such an E_o is smaller in magnitude than E_{O4} for these materials, but the relative variation of the two quantities with composition is approximately the same. In this paper E_{O4} is considered to be preferable since available experimental values for this quantity are more accurate.

9. H. K. Rockstad and R. Flasck, preceeding paper. Also in the third Semi-annual Technical Report for the Advanced Research Projects Agency under Contract DAHC 15-70-C-0187.

10. Because of high resistivities for high Se:Te ratios, thermopower data for $x \geq 0.7$ in the virgin state are not available. However, if we assume all virgin materials in this alloy system are p-type, all the results are self-consistent. The relatively small magnitude of $\Delta E_o/E_{o4}$ for virgin films as shown in Fig. 1 for all x from 0 to 0.9 is consistent with the assumption that the Fermi level is on the valence band side of a band gap for all these films.

11. cf., N. F. Mott and E. A. Davis, Electronic Processes in Non-Crystalline Materials, (Clarendon Press, Oxford, 1971).

12. The thermopower slope ΔE_s cannot be used profitably for this purpose because of mixed conduction in annealed materials for $x \geq 0.1$ and because of a limited temperature range for thermopower measurements for large x.

13. If the electron-hole mobility ratio is unequal to unity, the Fermi level should pass through the gap center somewhat to one side of the peak in Fig. 1. However, a large mobility ratio, such as 10^2, is unlikely because such a mobility ratio should cause a sharp gradient in the ratio plotted in Fig. 1 on one side of the peak.

14. $\Delta E_s = 0.55$ eV was obtained from the same sample and annealing step that gave $\Delta E_o = 0.616$ eV at 96°C, as was used for Figs. 1 and 2(b).

15. Evaluation of $\Delta E_o = -\partial \ln\sigma / \partial(1/kT)$ at 200°C instead of at 96°C would shift the peak in Fig. 1 for annealed materials to smaller x. Somewhat surprisingly, this is consistent with the thermopower data, which indicates that for $x \geq 0.3$ the relative position of the Fermi level with respect to E_v and E_c moves further away from the valence band, towards the conduction band, as the temperature increases, since the temperature dependence of S indicates transitional behavior. Thus a similar band level diagram at 200°C for annealed films would show the Fermi level somewhat higher than that of Fig. 2(b), and quite near the gap center for $x = 0.3$ instead of $x = 0.5$.

16. cf., M. Aven and J. S. Prener, Physics and Chemistry of II-VI Compounds (Interscience, New York, 1967).

17. C. H. Seager, D. Emin, and R. K. Quinn, J. Non-Crystalline Solids 8-10, 341 (1972); D. Emin, C. H. Seager, and R. K. Quinn, Phys. Rev. Letters 28, 813 (1972).

18. H. K. Rockstad, R. Flasck, and S. Iwasa, J. Non-Crystalline Solids 8-10, 326 (1972).

19. B. T. Kolomiets and E. M. Raspopova, Sov. Phys. - Semicond. 5, 1346 (1972) and references contained therein; P. Nagels, R. Callaerts, and M. Denayer, Proceedings of the Eleventh International Conference on the Physics of Semiconductors, (PWN-Polish Scientific Publisher, Warsaw, 1972), p. 549.

FIGURE CAPTIONS

Figure 1. The ratio $\Delta E_o/E_{O4}$ vs x for virgin (unannealed) and annealed $(GeTe_2)_{1-x}(GeSe_2)_x$ films.

Figure 2. Band level diagrams for virgin (unannealed) and annealed amorphous films of $(GeTe_2)_{1-x}(GeSe_2)_x$ showing the relative locations of the valence and conduction band edges and the Fermi level for temperatures in the vicinity of room temperature to 100°C. The Fermi level is indicated for two different assumptions: i) solid line - $\Delta E_o/E_{O4}$ is proportional to the smaller of $(E_c - E_F)/(E_c - E_v)$ or $(E_F - E_v)/(E_c - E_v)$; ii) broken line - β_h and β_e, as defined in in the text, are independent of composition. The curves for the conduction band edges are also equivalent to the measured values of E_{O4} if the unit eV is ascribed to the vertical scales.

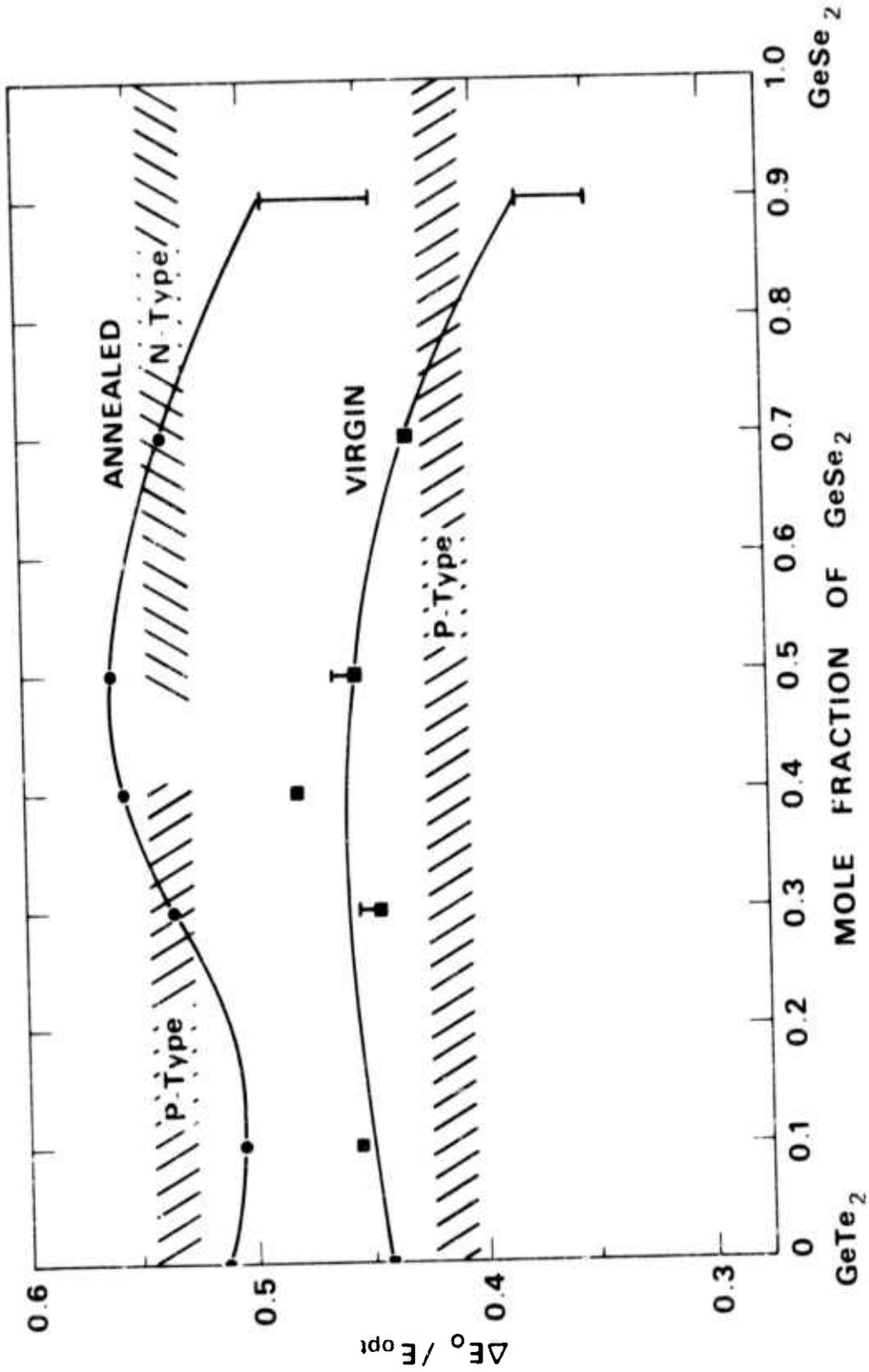
ANNEALED
N-Type
P-Type
VIRGIN
P-Type
0.6
0.5
0.4
0.3
$\Delta E_o / E_{opt}$
0
0.1
0.2
0.3
0.4
0.5
0.6
0.7
0.8
0.9
1.0
$GeTe_2$
MOLE FRACTION OF $GeSe_2$
$GeSe_2$

Fig. 1

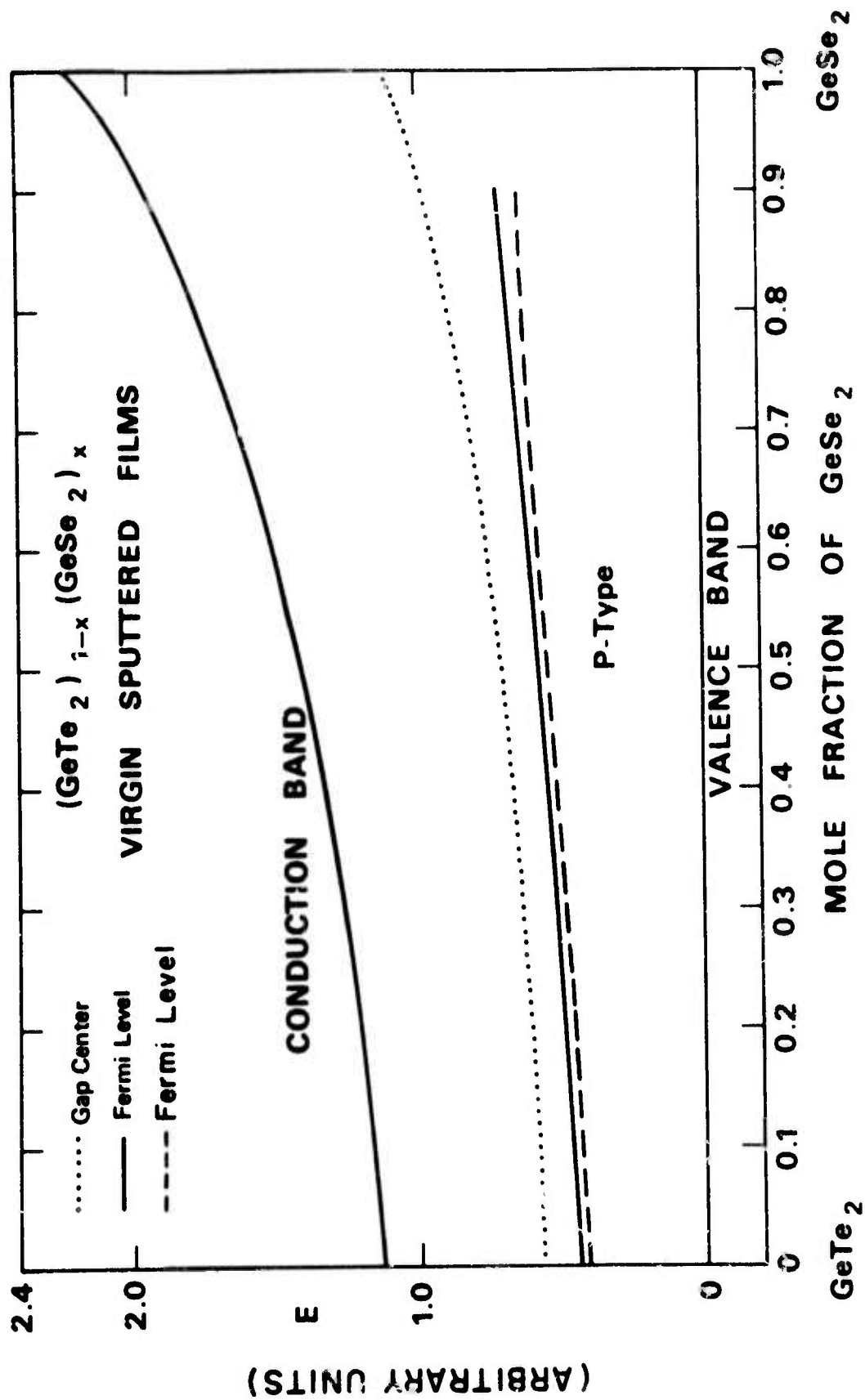
(GeTe2)1-x (GeSe2)x
VIRGIN SPUTTERED FILMS
Gap Center
Fermi Level
Fermi Level
CONDUCTION BAND
P-Type
VALENCE BAND
E
(ARBITRARY UNITS)
2.4
2.0
1.0
0
GeTe2
0 0.1 0.2 0.3 0.4 0.5 0.6 0.7 0.8 0.9 1.0
GeSe2
MOLE FRACTION OF GeSe2

Fig. 2a

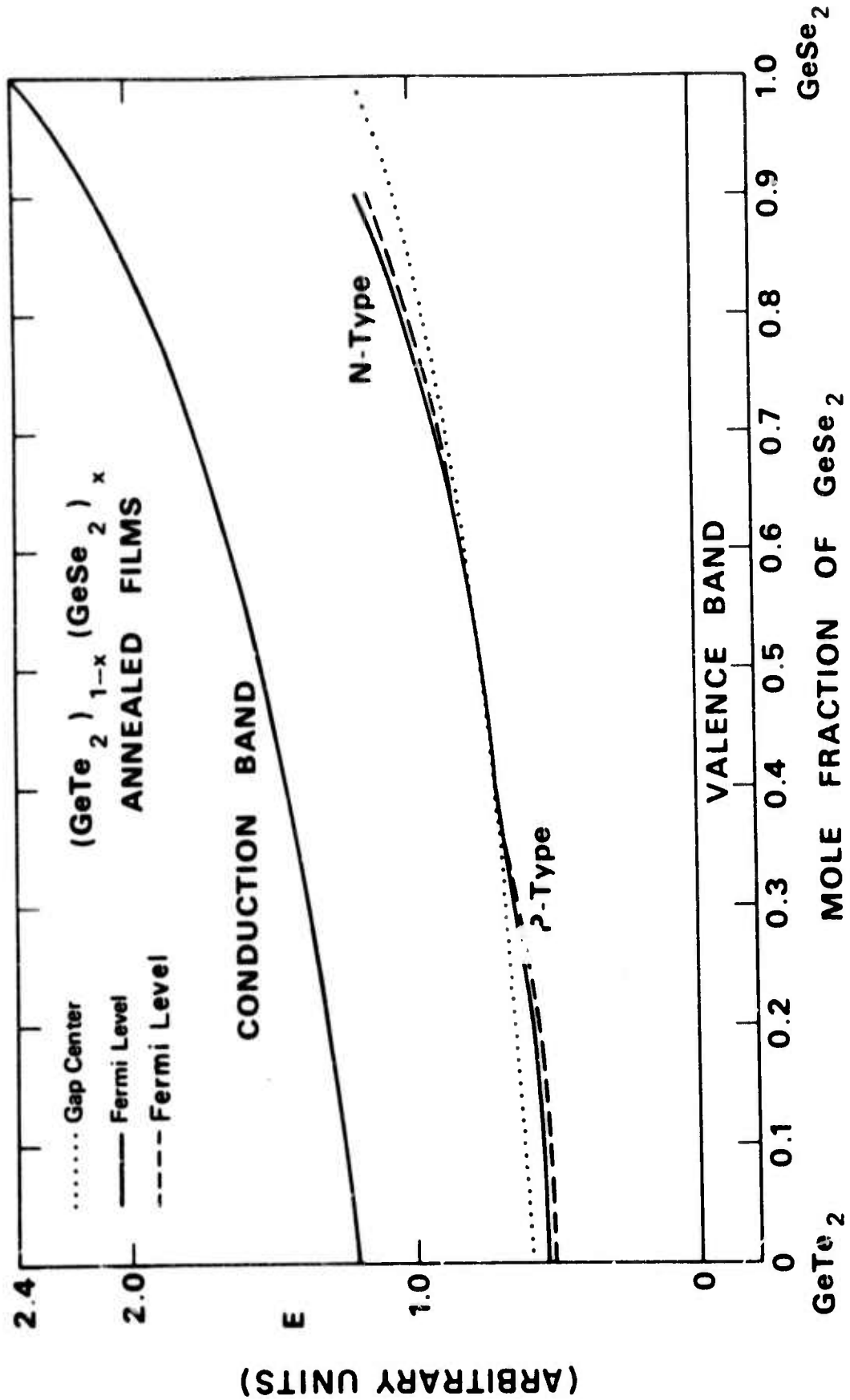
(ARBITRARY UNITS)
E
2.4
2.0
1.0
0
GeTe2
0
0.1
0.2
0.3
0.4
0.5
0.6
0.7
0.8
0.9
1.0
GeSe2
MOLE FRACTION OF GeSe2
CONDUCTION BAND
VALENCE BAND
N-Type
P-Type
(GeTe2)1-x (GeSe2)x
ANNEALED FILMS
Gap Center
Fermi Level
Fermi Level

Fig. 2b